Biofunctionalization of nanoparticles: their putative applications

Thesis submitted to the

University of Pune

For the degree of

Doctorate of Philosophy

In Biotechnology

By

Mrs. Priyanka Murawala

Research Supervisor

B. L. V. Prasad, Ph.D.

National Chemical Laboratory

Pune – 411008, India.

March 2011

Acknowledgement

I take this opportunity to acknowledge and extend my sincere gratitude towards all those people who have been involved, directly or indirectly, to make the research work described in this thesis possible.

This is not customary to write but firstly, I would like to express my immense love and warmth to my little angel, my daughter Rhythm for her tolerance and understanding whenever I leave her and go for my work. She is (2 yrs now) very little to understand but yet she understood. You have always brought love, warmth and a big smile on my face whenever I have seen you coming to me……. A feeling that I have never felt before……☺☺I love you a lot Ridddoooo…

I am indebted to my guide, Dr. B. L. V. Prasad for introducing me to the field of Nanotechnology. This thesis would not have been possible without his constant inspiration, invaluable guidance and continuous support. His initiation and thoughtfulness has shaped this thesis. I thank him whole heartedly for all his support.

I would also like to thank Dr. S. Sivaram, former Director, NCL and Dr. Sourav Pal, Director, NCL, for allowing me to carry out research at this Institute and providing with the required facilities. I am thankful to CSIR, Govt. of India, for the research fellowship.

Most part of the work presented in this thesis has been carried out in different laboratories both in NCL and outside of it. I would take this opportunity to thank all my collaborators. I would like to thank Dr. Sree Kumar and his student Sreekuttan, NCL, Pune for cyclic voltammetry studies presented in chapter 2. Dr. Souvik Maiti, IGIB, New Delhi is greatly acknowledged for the CD spectra studies. I also thank Mrs. Suguna Adhayantaya, NCL for her help in TGA measurements and lab related matters. I would also like to extend my sincere thanks to Dr. Mala Rao, NCL, Pune, for her elderly advice irrespective of my work commitments, thinking about my betterment always.

I would like to present my sincere thanks to Dr. R. R. Bhonde and Ms. Smruti Phadnis from the National Centre for Cell Science, Pune, for cell culture work presented in Chapter 3. I especially thank Dr. Anjali Shiras and Siva also from the National Centre for Cell Science, Pune, for cell culture work presented in Chapters 5. I would like to thank Dr. Jomon Joseph and his entire group from the National Centre for Cell Science, Pune, for their enormous support regarding reagents and work assistance during emergencies. I would like to thank Dr. Jomon Joseph once again for his valuable suggestions during the course of my

PhD and for being a member of the work evaluation committee. I would like to extend my sincere thanks to Dr. Varsha Pokharkar and Vishal Mali from Poona College of Pharmacy for animal studies. I am indebted to all those rats who sacrificed their lives for my in vitro toxicity studies presented in chapter 6.

I express my gratitude towards my former and current lab-mates for their constant support and encouragement. I thank Dr. Vijaykumar, Dr. Vipul Bansal, Dr. Amit Singh, Dr. Atul Bharde, Dr. Hrushikesh Joshi, Dr. Ambrish Sanyal, Dr. Akhilesh Rai, Dr. Sourabh Shukla, Dr. Sanjay Singh, Dr. Prathap Chandran, Dr. Sonali, Deepti, Manasi, Sudarsan, Sheetal, Swarna, Vilas, Ravi, Anal, Ajay, Prakash, Neeraj, Balanagulu, Agnimitra and Rinki for making lab-work a good experience. Agni had spent a very little time with us but had made a great impact on our mind. His bubbly nature and desire to excel always gave an impression of passionate researcher. Lots of love Agni....

I also thank Umesh, Ramya, Raja, Adhish, Priya Mary for their time, help and small yet meaningful gestures. I would also like to acknowledge my project students Shabir and Amruta who have helped me in my project work, especially Amruta from whom I have learnt a lot of cell culture and molecular biology work.

I thank Mr. Deepak, Mr. Punekar and Mr. Pardesi from the Physical Chemistry division office for their extensive help in all official matters and administrative work. I would also like to thank the NCL Library staff, administrative staff, SAC staff and technical staff at CMC for their assistance in the administrative issues during this time.

Friends are those who always make you feel happy even if you think about them and their presence near you surrounds you with love and warmth. I am lucky to have Maggie, Umesh and Pankhuri as my friends. You three have always been there for me. I take this opportunity to let them know that I treasure their friendship. We have shared real good times whether it is playing badminton, going trekking, freaking out at Abhimaan or NCL complex or at any khopchas where we have been 'us' together and laughed our tensions out. Maggie and Umesh.... you two mean a lot to me... ☺

This thesis has become possible due to the strong faith and constant encouragement from my family. I thank my father in law Chandrakumar Murawala and mother in law Rashmika Murawala from the bottom of my heart for their words of wisdom, trust, blessings and unfailing love. I am blessed to have them as my parents. I could not have made it through without them being there for me at all times. "Sushi Baa" tussii great ho!!!! I'd like to thank Bhaiya and Bhabhi and my sweet Priti Didi for their constant moral boost ups.

I would like to thank my father late Rakesh Prakash Singh and mother Sheela Singh for giving me such a beautiful life. Papa, you have taught me the first lessons of my life and that had laid the foundation of this thesis. My brothers Sumit, Raghav and Rahul and sister Sanjana have always encouraged me and made me smile whenever I felt low. Ishaan... you will always remain in my heart and the time that you have spent with us is very very special for me. Miss you a lot bhai.

No journey seems tough when you have a great companion. Prayag, in you I have found a true friend who has always held my hands and have shown me the right path whenever I was confused. You have always been there whenever I needed you and your presence has always relieved me from my tensions. You have taught me completely a new way to take things in life positively. I am happy to have you in my life and cherish your unconditional love and support.

Thank you everyone who has directly or indirectly helped me and shared a smile during this journey☺

With love

Priyanka

☺

Chapter 1

Introduction

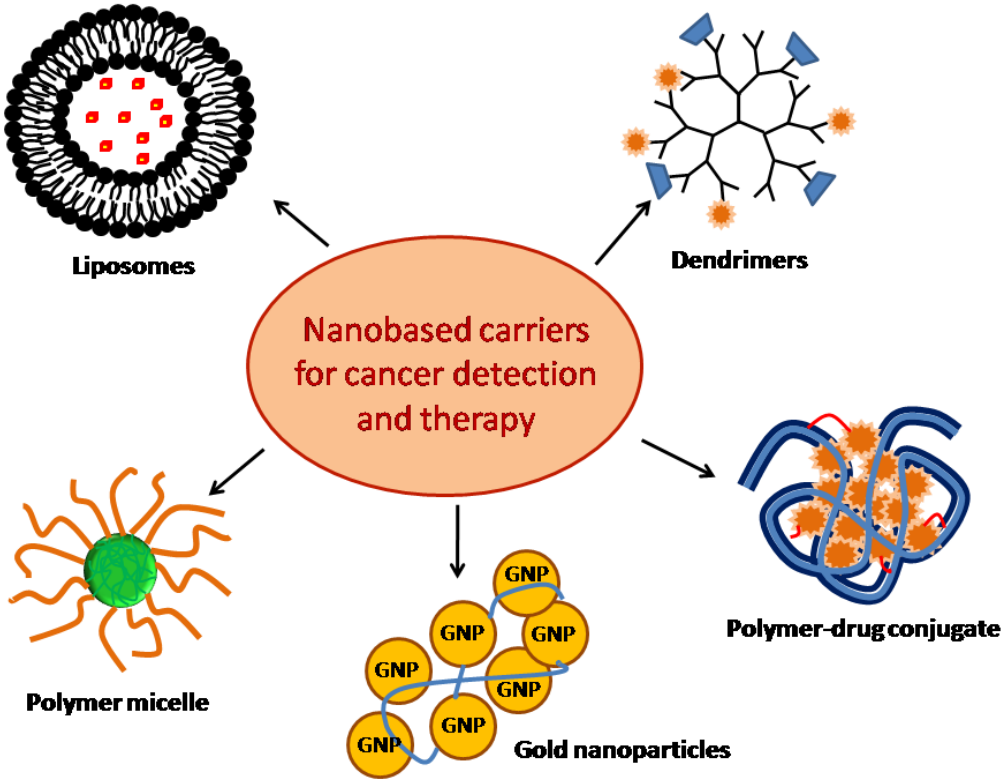

This chapter is an introduction to the thesis and briefly describes various drug delivery systems involving nanoparticles as delivery vehicles. It also emphasizes on the selection of gold nanoparticles as a drug delivery agent above others. Finally a brief outline of the thesis is laid-out.

1.1 Introduction:

An ideal drug delivery technology is the so called "magic bullet", proposed by Paul Ehrlich at the beginning of the 20th century, in which the drug is precisely targeted to the exact site of action[1, 2]. The advent of nanotechnology makes this goal a bit closer, to deliver the drug in the right place at the right time. Nanoscience and nanotechnology are two terms that involve systems/devices at the nanometer scale. It is a multidisciplinary scientific field undergoing explosive development. A part of this field is the development of nano-scaled drug delivery devices. Nanoparticles provide enormous advantages regarding drug targeting, delivery and release and, with their additional potential to combine diagnosis and therapy, emerge as one of the major tools in medicine. Nanoparticles and nano-formulations have already been applied as drug delivery systems with great success in anti-tumor therapy, gene therapy, AIDS therapy, radiotherapy, in the delivery of proteins, antibiotics, virostatics and vaccines[3, 4]. Because of their size, nanometric systems/particles have been proposed to cross blood brain barrier[2,4-9].

Cancer remains one of the world's most devastating diseases; with more than 10 million new cases every year[10, 11]. Current cancer treatments include surgical intervention, radiation and chemotherapeutic drugs, which often also kill healthy cells and cause toxicity to the patient. It would therefore be desirable to develop chemotherapeutics that can either passively or actively target cancerous cells[12]. For anticancer drugs to be effective in cancer treatment they should meet two important criteria; first, after administration, they should ideally be able to reach the desired tumor tissues through the penetration of barriers in the body with minimal loss of their volume or activity in the blood circulation. Second, after reaching the tumor tissue, drugs should have the ability to selectively kill tumor cells without affecting normal cells with a controlled release mechanism of the active drug. These two basic strategies also lead to the improvements in patient survival and quality of life by increasing the intracellular concentration of drugs and reducing dose-limiting toxicities simultaneously. Interestingly, nanoparticles seem to have the potential to satisfy both of these requirements for effective drug carrier systems.

The method by which a drug is delivered can have a significant effect on its efficacy. Conventional chemotherapeutic agents are distributed nonspecifically in the body where they affect both cancerous and normal cells, thereby limiting the dose

achievable within the tumor and also resulting in suboptimal treatment due to excessive toxicities. Some drugs have an optimum concentration range within which maximum benefit is derived, and concentrations above or below this range can be toxic or produce no therapeutic benefit at all. On the other hand, the very slow progress in the efficacy of the treatment of this disease clearly suggests a growing need for a multidisciplinary approach to the delivery of therapeutics to targets in tissues. From this, new ideas on controlling the pharmacokinetics, pharmacodynamics, non-specific toxicity, immunogenicity, biorecognition, and efficacy of drugs are generated. These new strategies, often called drug delivery systems (DDS), are based on interdisciplinary approaches that combine polymer science, pharmaceutics, bioconjugate chemistry, molecular biology and nanotechnology. One of the earliest examples of applying nanotechnology to solving problems in biology was the use of liposomes as drug delivery vehicles[13]. From the viewpoint of biological compatibility, liposomes are ideal drug carriers. They are constructed from natural lipids. Therefore, they are nontoxic, do not elicit undesirable immune responses, and are biodegradable. However, the situation with therapeutic application of liposomes is not as simple as desired. Liposomes are not stable enough in blood and are rapidly eliminated from circulation by reticuloendothelial system of cells[14]. However, the novelty of this method caught the attention of many researchers and had laid foundation for the development of various other DDS.

Cancer nanotherapeutics are rapidly progressing and are being implemented to solve several limitations of conventional drug delivery systems such as nonspecific biodistribution and targeting, lack of water solubility, poor oral bioavailability, and low therapeutic indices (Table 1). To improve the biodistribution of cancer drugs, different types/classes of nanoparticle based drug carriers have been designed for optimal size and surface characteristics to increase their circulation time in the bloodstream. Nanocarriers are nanosized materials (diameter 1–100 nm) that can carry multiple drugs and/or imaging agents. Owing to their high surface area to volume ratio, it is possible to achieve high ligand density on the surface for targeting purposes. Nanocarriers can also be used to increase local drug concentration by carrying the drug within and control releasing it when bound to the targets. They are also able to carry their loaded active drugs to cancer cells by selectively using the

Table 1: *Table illustrates examples of problems exhibited by free drugs that can be ameliorated by the use of drug delivery systems*[15].

Problem	Implication	Effect of DDS
Solubility	In a convenient pharmaceutical format is difficult to achieve, as hydrophobic drugs may precipitate in aqueous media.	DDS such as lipid micelles or liposomes provide both hydrophilic and hydrophobic environments, enhancing drug solubility.
Tissue damage on Extravasation	Inadvertent extravasation of cytotoxic drugs leads to tissue damage, e.g., tissue necrosis with free doxorubicin.	Regulated drug release from the DDS can reduce or eliminate tissue damage on accidental extravasation.
Rapid breakdown of the drug in vivo	Loss of activity of the drug follows administration, e.g., loss of activity of camptothecins at physiological pH.	DDS protects the drug from premature degradation and functions as a sustained release system. Lower doses of drug are required.
Unfavorable pharmacokinetics	Drug is cleared too rapidly, by the kidney, for example, requiring high doses or continuous infusion.	DDS can substantially alter the pharmacokinetics of the drug and reduce clearance. Rapid renal clearance of small molecules is avoided.
Poor biodistribution	Drugs that have widespread distribution in the body can affect normal tissues, resulting in dose-limiting side effects, such as the cardiac toxicity of doxorubicin.	The particulate nature of DDS lowers the volume of distribution and helps to reduce side effects in sensitive, non target tissues.
Lack of selectivity for target tissues	Distribution of the drug to normal tissues leads to side effects that restrict the amount of drug that can be administered. Low concentrations of drugs in target tissues will result in suboptimal therapeutic effects.	DDS can increase drug concentrations in diseased tissues such as tumors by the EPR effect. Ligand-mediated targeting of the DDS can further improve drug specificity.

unique pathophysiology of tumors, such as their enhanced permeability and retention effect and the tumor microenvironment. In addition to this passive targeting mechanism, active targeting strategies using ligands or antibodies directed against selected tumor targets amplify their specificity. Drug resistance, another obstacle that

impedes the efficacy of both molecularly targeted and conventional chemotherapeutic agents, might also be overcome, or at least reduced, using nanoparticles. Nanoparticles have the ability to accumulate in cells without being recognized by P-glycoprotein, one of the main mediators of multidrug resistance, resulting in the increased intracellular concentration of drugs.

In this chapter, we will address, first, the characteristics of nanoparticles required for drug delivery; second, how nanoparticles are being used as drug delivery systems to kill cancer cells more effectively and also to reduce or overcome drug resistance; and lastly types of nanoparticles used for drug delivery system (Scheme 1).

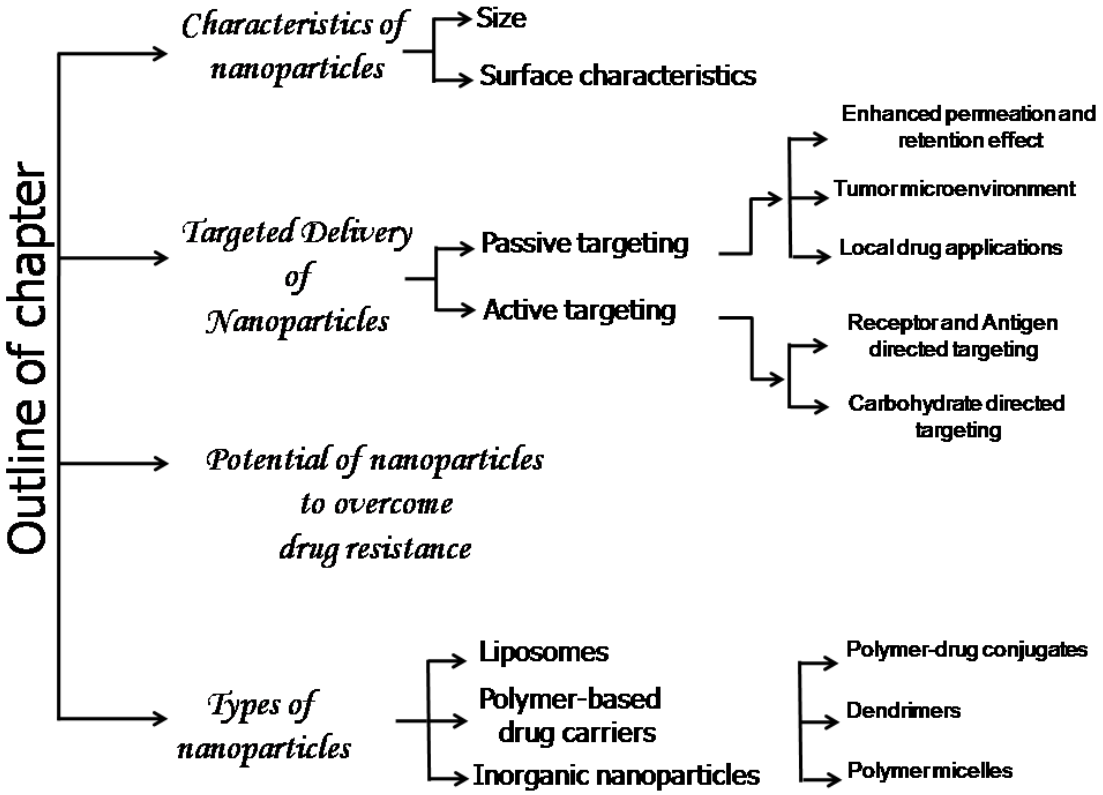

Scheme 1: *Schematic representation of outline of chapter.*

1) Characteristics of nanoparticles:

To effectively deliver drug to the targeted tumor tissue, nanoparticles must have the ability to remain in the bloodstream for a considerable time without being eliminated. The fate of injected nanoparticles can be controlled by adjusting their size and surface characteristics.

A) Size:

One of the advantages of nanoparticles is that their size is tunable. The size of nanoparticles used in a drug delivery system should be large enough to prevent their rapid leakage into blood capillaries but small enough to escape capture by fixed macrophages that are lodged in the reticuloendothelial system, such as the liver and spleen. The size of the sinusoid in the spleen and fenestra of the Kupffer cells in the liver varies from 150 to 200 nm[16] and the size of gap junction between endothelial cells of the leaky tumor vasculature may vary from 100 to 600 nm[17]. Consequently, the size of nanoparticles should be below 100 nm to reach tumor tissues by passing through these two particular vascular structures.

B) Surface characteristics:

In addition to their size, the surface characteristics of nanoparticles are also an important factor determining their life span and fate during circulation relating to their capture by macrophages. Nanoparticles should ideally have a hydrophilic surface to escape macrophage capture[18]. This can be achieved in two ways: coating the surface of nanoparticles with a hydrophilic polymer, such as PEG that protects them from opsonization by repelling plasma proteins. Alternatively, nanoparticles can be formed from block copolymers with hydrophilic and hydrophobic domains[19, 20]. In addition to providing functional groups, surface-bound ligands also contribute to the stability of nanoparticles. The stability of the nano-conjugates is an important consideration for their potential use as therapeutic agents because they must maintain their stability under harsh conditions present in the cell or in the bloodstream[21].

2) Targeted Delivery of Nanoparticles:

Nanocarriers encounter numerous barriers *en route* to their target, such as mucosal barriers and non-specific uptake[22, 23]. To address the challenges of targeting tumours, it is necessary to combine the rationale design of nanocarriers with the fundamental understanding of tumour biology.

A) Passive Targeting by Nanoparticles:

i) <u>Enhanced permeability and retention effect:</u>

General features of tumours include leaky blood vessels and poor lymphatic drainage. Whereas free drugs may diffuse nonspecifically, a nanocarrier can extravasate

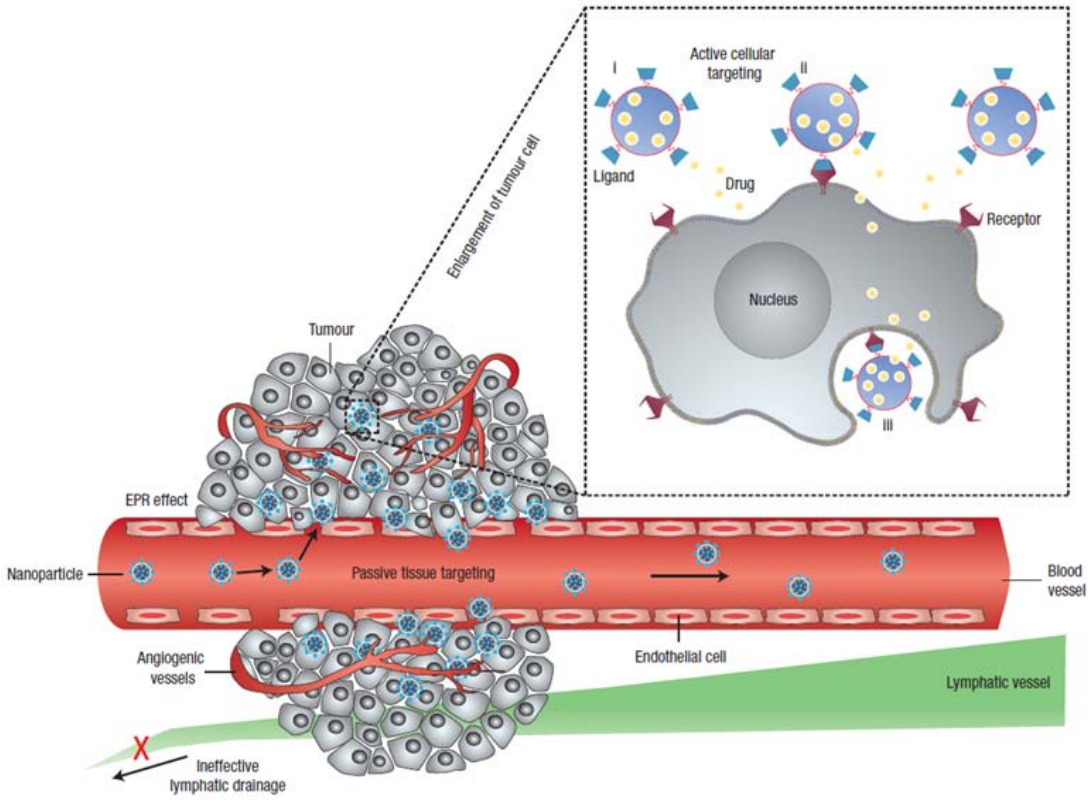

Figure 1: *Schematic representation of different mechanisms by which nanocarriers can deliver drugs to tumours. Polymeric nanoparticles are shown as representative nanocarriers (circles). Passive tissue targeting is achieved by extravasation of nanoparticles through increased permeability of the tumour vasculature and ineffective lymphatic drainage (Enhanced Permeation and Retention effect). Active cellular targeting (inset) can be achieved by functionalizing the surface of nanoparticles with ligands that promote cell-specific recognition and binding. The nanoparticles can (i) release their contents in close proximity to the target cells; (ii) attach to the membrane of the cell and act as an extracellular sustained-release drug depot; or (iii) internalize into the cell (Image courtesy Ref No: 5).*

(escape) into the tumour tissues via the leaky vessels by the enhanced permeation and retention effect (EPR effect)[24] (Figure 1). The increased permeability of the blood vessels in tumours is characteristic of rapid and defective angiogenesis (formation of new blood vessels from existing ones). Furthermore, the dysfunctional lymphatic drainage in tumours retains the accumulated nanocarriers and allows them to release drugs into the vicinity of the tumour cells. Nanoparticles that satisfy the size and surface characteristics requirements described above for escaping reticuloendothelial

capture system have the ability to circulate for longer times in the bloodstream and a greater chance of reaching the targeted tumor tissues. The unique pathophysiologic characteristics of tumor vessels enable macromolecules, including nanoparticles, to selectively accumulate in tumor tissues[25]. Fast-growing cancer cells demand the recruitment of new vessels (neovascularization) or re-routing of existing vessels near the tumor mass to supply them with oxygen and nutrients[26]. The resulting imbalance of angiogenic regulators such as growth factors and matrix metalloproteinases makes tumor vessels highly disorganized and dilated with numerous pores showing enlarged gap junctions between endothelial cells and compromised lymphatic drainage[26]. These features are called the enhanced permeability and retention effect, which constitutes an important mechanism by which macromolecules, including nanoparticles, with a molecular weight above 50 kDa but below 300 kDa (for avoiding macrophage capture), can selectively accumulate in the tumor interstitium[25].

ii) Tumor microenvironment:

Another contributor to passive targeting is the unique microenvironment surrounding tumor cells, which is different from that of normal cells. Fast-growing, hyper proliferative cancer cells show a high metabolic rate, and the supply of oxygen and nutrients is usually not sufficient for them to maintain this. Therefore, tumor cells use glycolysis to obtain extra energy, resulting in an acidic environment[27]. Such an effect was used to design pH-sensitive liposomes that are stable at a physiologic pH of 7.4, but degrade to release active drug in target tissues in which the pH is less than physiologic values, such as in the acidic environment of tumor cells[28]. Additionally, cancer cells express and release unique enzymes such as matrix metalloproteinases (MMP), which are implicated in their movement and survival mechanisms[29]. Based on this, Mansour *et al* assessed a drug targeting strategy in which the protease activity of MMP-2 is exploited to release an anticancer agent from a macromolecular carrier, *i.e.*, circulating albumin. An albumin-bound form of doxorubicin incorporating a matrix metalloproteinase-2-specific octapeptide sequence between the drug and the carrier is especially cleaved efficiently by activated MMP-2 and MMP-9 liberating doxorubicin[30]. This lead to the release of the drug and effective killing of the cancer cells.

iii) Local Drug Application:

Direct local application allows the drug to be given directly to tumor tissue, avoiding systemic circulation. Various approaches have been developed to improve the tumor delivery of anticancer agents, such as intravesical injection and intraperitoneal administration of various agents. These approaches require exposure to higher concentrations of antitumor agents, which is not always feasible. Localized drug delivery through intratumoral administration is an attractive approach that has been tried and tested[31]. The administration of mitomycin directly into tumor tissue resulted in an increased concentration of the drug at the tumor site and decreased toxicity[32].

B) Active Targeting by Nanoparticles:

A drug delivery system comprising a binary conjugate (i.e., polymer-drug conjugate) that depends only on passive targeting mechanisms inevitably faces intrinsic limitations to its specificity. One approach suggested to overcome these limitations is the inclusion of a targeting ligand or antibody in polymer-drug conjugates[15]. Initially, direct conjugation of an antibody to a drug was attempted. However, in clinical trials conducted thus far, such early antibody-drug conjugates have been ineffective[33]. The limited number of drug molecules loaded on the antibody while preserving its immune recognition being cited as one of the reasons for such observation. The recent development and introduction of a wide variety of liposomes, polymers and inorganic nanoparticles as drug delivery carriers increases the potential number of drugs that can be conjugated to nanoparticles without compromising their targeting affinity relative to earlier antibody-drug conjugates. Taking advantage of this array of carriers, targeting moieties, and drugs, many recently developed carriers involve a ternary structure composed of a ligand or antibody as a targeting moiety, a polymer or lipid as a carrier that is loaded with an active chemotherapeutic drug.

i) <u>Receptor- and Antigen-Directed Targeting:</u>

For targeted delivery, cell surface antigens and receptors are particularly suitable as tumor-specific targets[15]. First, they should be expressed exclusively on tumor cells and not expressed on normal cells. Second, they should be expressed homogeneously on all targeted tumor cells. Last, cell-surface antigens and receptors should not be shed into the blood circulation. For example the folate receptor is a well-known tumor marker that binds vitamin folate and folate-drug conjugates with a high affinity and carries these bound molecules into the cells via receptor mediated endocytosis[34]. Folate receptor expression was found in 53 % of tumor samples whereas normal bone

marrow cells did not show any folate receptor expression[35]. Cho and coworkers have developed a folate receptor targeted nanoparticle formulation of paclitaxel using heparin as a carrier [heparin-folate-Taxol (paclitaxel), HFT] and tested it using nude mouse animal models. This novel ternary nanoparticle HFT showed more potent activity against the growth of tumor xenografts of human KB and paclitaxel-resistant KB derivatives than did binary heparin-Taxol or free drug[36].

Transferrin, a serum glycoprotein, works as a transporter to deliver iron through the blood and into cells by binding to the transferrin receptor and subsequently being internalized via receptor-mediated endocytosis [37]. Because the transferring receptor is overexpressed in tumor tissues compared with normal tissues, it has been investigated as a target for tumor specific drug delivery [38]. Transferrin-conjugated paclitaxel loaded [poly(lactic-co-glycolic acid) polymer] nanoparticles displayed greater inhibitory effects on cell growth than free paclitaxel in MCF-7 and MCF-7/Adr cells[39]. Transferrin was also conjugated to liposomes to increase the transfection efficacy of p53, resulting in the sensitization of the transfected cancer cells/xenografts to ionizing radiation[40]. Similarly, growth factor or vitamin interactions with cancer cells represent a commonly used targeting strategy, as cancer cells often overexpress the receptors for nutrition to maintain their fast-growing metabolism. Epidermal growth factor receptor (EGFR) has been found to be overexpressed in a variety of tumour cells and anti-EGFR antibodies have been successfully grafted onto gold nanoparticle surface and utilized in conjunction with hyperthermia to selectively kill cancer cells[41, 42].

ii) Carbohydrate-Directed Targeting:

Cancer cells often express different glycans compared with their normal counterparts. Lectins are proteins that recognize and bind to carbohydrate moieties attached to protein molecules (glycans) on the extracellular side of the plasma membrane. Therefore, lectins could be used as targeting molecules to direct drugs specifically to desired cells and tissues[43]. This protein (lectin)-carbohydrate interaction can be applied to develop two types of nanoparticles: one incorporates lectins into nanoparticles as targeting moieties that are directed to cell surface carbohydrates (direct lectin targeting), and the other is a reverse scenario in which carbohydrate moieties are coupled to nanoparticles to target lectins (reverse lectin targeting)[44]. Thus far, drug delivery systems that have been developed based on this novel interaction

between carbohydrates and lectins are directed to whole organs, and could thus be harmful to normal tissues[45]. Despite some of their problems, lectins are continuing to be studied for the development of ''smart carrier'' molecules for drug delivery and their unique affinity for sugar moieties on the surface of tumor tissue seems to be an attractive tool for further enhancement of nano-drug delivery[46].

3) Potential of Nanoparticles to Overcome Drug Resistance:

Drug resistance has emerged as a major obstacle limiting the therapeutic efficacy of chemotherapeutic agents. Among several mechanisms of drug resistance, P-glycoprotein is the best known and most extensively investigated[47]. It has been suggested that nanoparticles may be able to circumvent P-glycoprotein–mediated resistance. One possible mechanism is that nanoparticles may avoid recognition by the P-glycoprotein efflux pump by means of being enveloped in an endosome after entering the cell, leading to high intracellular drug concentrations[48]. Ligand-targeted strategies, especially those using receptor-targeting ligands, may have particular potential for overcoming drug resistance because these ligands are usually internalized via receptor-mediated endocytosis. Indeed, a folate receptor–targeted, pH-sensitive polymeric micelle containing doxorubicin[49] and transferrin-conjugated paclitaxel-loaded nanoparticles[39] exhibited greater inhibitory activity against drug-resistant MCF-7 cells and/or xenografts than their non targeted free drug counterparts.

4) Types of nanoparticles used as drug delivery systems:

A variety of materials including polymers (polymeric nanoparticles, micelles, or dendrimers), lipids (liposomes), and inorganic nanoparticles are being pursued as DDS with great vigor[50].

A) Liposomes:

Lipid-based carriers have attractive biological properties, including general biocompatibility, biodegradability, isolation of drugs from the surrounding environment, and the ability to entrap both hydrophilic and hydrophobic drugs[12]. Liposomes are self-assembling closed colloidal structures composed of lipid bilayer and have a spherical shape in which an outer lipid bilayer surrounds a central aqueous space (Figure 2). Liposomes have been investigated as carriers of various pharmacologically active agents such as antineoplastic and antimicrobial drugs, chelating agents, steroids, vaccines and genetic material[51]. Several kinds of cancer

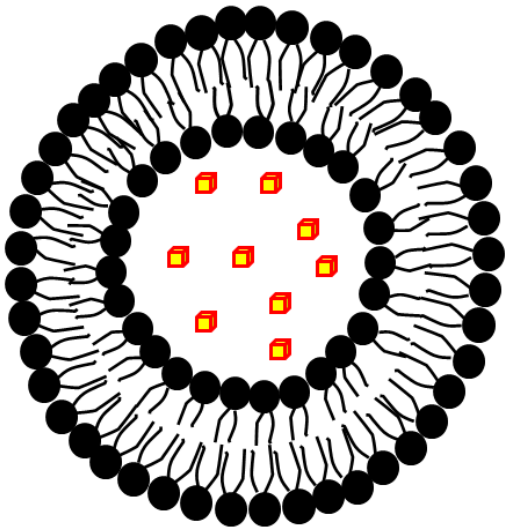

Figure 2: *Drug encapsulation in liposomes.*

drug-lipid conjugates using a variety of preparation methods have been developed so far. Among them, liposomal formulations of the anthracyclines doxorubicin (Doxil, Myocet) and daunorubicin (DaunoXome) are approved for the treatment of metastatic breast cancer and AIDS-related Kaposi's sarcoma[52-54]. Beside these approved agents, many liposomal chemotherapeutics are currently being evaluated in clinical trials[55]. The next generation of liposomal drugs may be immunoliposomes, which selectively deliver the drug to the desired sites of action[56].

Immunoliposomes are complex drug or gene delivery systems that are developed for specific cell targeting by attachment of functionalized antibodies or antibody fragments to the outer surface of the liposomes. The modern immunoliposomes are PEG-liposomes to which receptor specific molecules are attached, preferably at the distal tips of the PEG chains. Immunoliposomes target cell specific receptors and facilitate receptor-mediated endocytosis for cell uptake[57]. In earlier studies whole IgG antibodies were linked to the liposome surface by various coupling methods[58]. Today the most advanced immunoliposomes are the anti-p185/HER2 liposomes that target the herceptin receptor which is over-expressed in various cancers, especially breast cancer. The epidermal growth factor receptor (EGFR) is another target for immunoliposomes that bind to and internalize in tumor cells that over-express EGFR[59-61]. A large number of antibodies directed against other

target molecules expressed on colon[62], B-cell lymphoma[63], and neuroblastoma[64] tumors have been used for the preparation of immunoliposomes.

As described above, liposomes have a great potential in the area of drug delivery. However, liposome-based drug formulations have not entered the market in great numbers so far. Some of the problems limiting the manufacture and development of liposomes are the stability issues, batch to batch reproducibility, sterilization method, low drug entrapment, particle size control, production of large batch sizes and short circulation half-life[65]. The chemical instability of liposomes may be caused by hydrolysis of ester bond and/or oxidation of unsaturated acyl chains of lipids. Physical instability may be caused by drug leakage from the vesicles and/or aggregation or fusion of vesicles to form larger particles. Both of these processes (drug leakage and change in liposome size) influence the *in vivo* performance of the drug formulation, and therefore may affect the therapeutic index of the drug. Identification of a suitable method for sterilization of liposome formulations is a major challenge because phospholipids are thermolabile and sensitive to sterilization procedures involving the use of heat, radiation and/or chemical sterilizing agents[65]. Liposome can entrap tens of thousands of drug molecules[66] and hence drug potency is less of an issue for this type of carrier. However, even the relatively high carrying capacity of liposomes becomes problematic for very large therapeutic molecules such as proteins, particularly if small liposome diameters are desirable for reasons of biodistribution. Hydrophilic drugs can be readily entrapped with a high degree of latency within the liposome aqueous interior, but neutral hydrophobic drugs or those with intermediate solubilities tend to be rapidly released in the presence of plasma proteins or cell membranes[67]. Long circulating liposomes may lead to extravasation of the drug in unexpected sites. The most commonly experienced clinical toxic effect from the PEGylated liposomal doxorubicin is palmar-plantar erythrodysesthesia (PPE), also called the hand-foot syndrome. Here, a dermatologic toxicity reaction is seen with high doses of many types of chemotherapy[68]. On the other hand, lipid-based carriers upon intravenous injection, are rapidly cleared from the bloodstream by the reticuloendothelial defence mechanism, regardless of particle composition[69, 70]. Due to intrinsic structural constraints, most liposomal particles are over 90 nm in diameter, which may considerably limit their transport in tumor tissues. For example, Yuan and coworkers have shown limited liposomal penetration to only 30 μm (a few cell layers)

following particle extravasation[71]. Later studies have shown that fibril collagen is the main structural barrier for interstitial transport[72]. Moreover, drug release from conventional liposomal formulations is quite limited once these particles reach the tumor target. Hence, instability of the carrier, fast burst release of the chemotherapeutic drugs from the liposomes, as well as non-specific uptake by the mononuclear phagocytic system (MPS), provides additional challenges for translating these carriers to the clinic from research space.

B) Polymer-based drug carriers:

Polymers are the most commonly explored materials for constructing nanoparticle-based drug carriers. Depending on the method of preparation, the drug is either physically entrapped in or covalently bound to the polymer matrix[73]. The resulting compounds may have the structure of capsules (polymeric nanoparticles), amphiphilic core/shell (polymeric micelles), or hyperbranched macromolecules (dendrimers). The conjugated drug can be released in a controlled manner through surface or bulk erosion, diffusion through the polymer matrix, swelling followed by diffusion, or in response to the local environment[12].

i) Polymeric nanoparticles (Polymer-drug conjugates):

Polymers used as drug conjugates can be divided into two groups: natural and synthetic polymers. Polymers such as albumin, chitosan, and heparin occur naturally

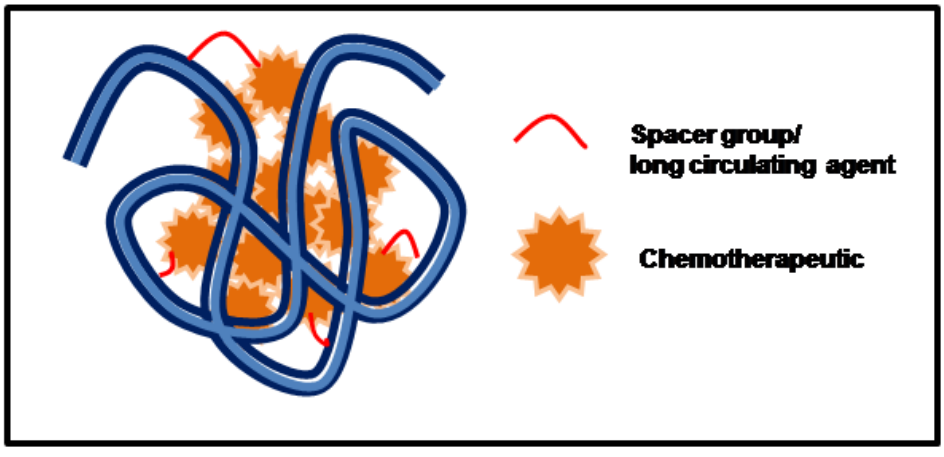

Figure 3: *Polymer-drug conjugate as a drug carrier (Image courtesy Ref No. 5).*

and have been a material of choice for the delivery of oligonucleotides, DNA, and protein, as well as drugs (Figure 3). One of the earliest reports of the use of polymers for cancer therapy dates back to 1979 when adsorption of anticancer drugs to

polyalkylcyanoacrylate nanoparticles was described[74]. Couvreur *et al.* revealed the release mechanism of the drugs from the polymer in calf serum, followed by tissue distribution and efficacy studies in a tumour model[75]. This work laid the foundation for the development of doxorubicin loaded polyalkylcyanoacrylate nanoparticles that were tested in clinical trials in the mid 1980[76]. Recently, a nanoparticle formulation of paclitaxel, [nanometer-sized albumin bound paclitaxel (Abraxane)], in which serum albumin is included as a carrier has been applied in the clinic for the treatment of metastatic breast cancer. Besides metastatic breast cancer, Abraxane has also been evaluated in clinical trials involving many other cancers including non–small-cell lung cancer (phase II trial) and advanced non hematologic malignancies (phase I and pharmacokinetics trials)[77, 78].

Among synthetic polymers such as N-(2-hydroxypropyl)- methacrylamide copolymer (HPMA), polystyrene-maleic anhydride copolymer, polyethylene glycol (PEG), and poly-L-glutamic acid (PGA), PGA was the first biodegradable polymer to be used for conjugate synthesis[79]. Several representative chemotherapeutics that are used widely in the clinic have been tested as conjugates with PGA *in vitro* and *in vivo* and showed encouraging abilities to circumvent the shortcomings of their free drug counterparts[79]. Among them, Xyotax (PGApaclitaxel)[80] and CT-2106 (PGA-camptothecin[81]) are now in clinical trials. HPMA and PEG are the most widely used nonbiodegradable synthetic polymers[82]. PK1, which is a conjugate of HPMA with doxorubicin, was the synthetic polymer-drug conjugate to be evaluated in clinical trials as an anticancer agent. A phase I clinical trial has been completed in patients with a variety of tumors that were refractory or resistant to prior therapy such as chemotherapy and/or radiation[83].

Even though polymer based carriers appear to be promising drug delivery systems, they suffer from problem that limit their applications in therapy. The major shortcoming of polymer-drug conjugates is the lack of specificity for cancer cells. Although one of the well known water-soluble paclitaxel conjugates, poly(L-glutamic acid)-paclitaxel has shown both tumor effect and improved index *in vivo,* these ‘‘binary nanoparticle,’’ also binds to the proteins and enzymes of normal cells[46]. Both polymer-drug conjugates and dendrimer systems necessitate the covalent conjugation of drug molecules to the carriers[84]. This in turn would require the presence of functionalizable chemical groups on the drug molecules, limiting the generality of this

approach. In light of the high chemical stability of covalent bonds, specific chemical strategies (e.g. enzymatic degradation, acid-catalyzed hydrolysis) are necessary to release the drug molecules at tumor sites[85]. Moreover, due to the small size of these systems (typically <10 nm), they can easily cross basement membranes in the glomeruli of kidneys and be quickly cleared, leading to much shortened blood half-lives[12,86]. They also have limitations in terms of cytotoxicity, because their nanometric size range is conducive to internalization by cells (macrophages), and degradation inside the cell can lead to cytotoxic effects as reported for polyester polymers[87].

ii) *Dendrimers:*

A dendrimer is a synthetic polymeric macromolecule of nanometer dimensions, composed of multiple highly branched monomers that emerge radially from the central core (Figure 4). Properties associated with the dendrimers such as their monodispersity, modifiable surface functionality, multivalency, water solubility, and

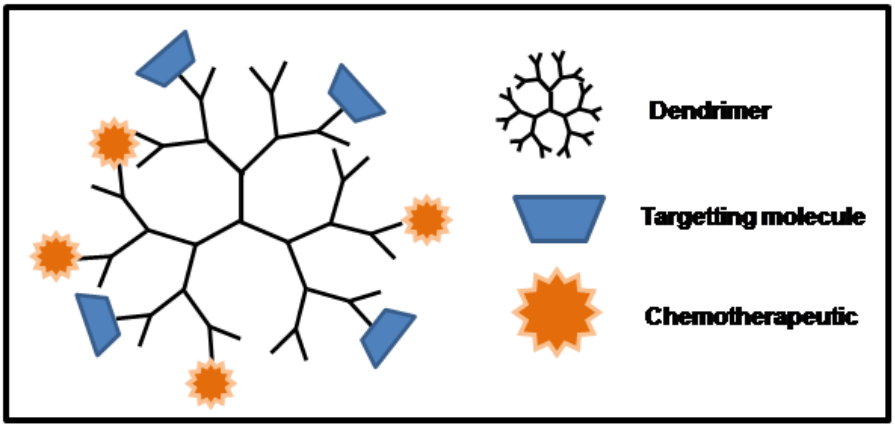

Figure 4: *Dendrimer as a drug carrier (Image courtesy Ref No. 5).*

available internal cavity make them attractive for drug delivery[88]. Drug molecules can be loaded either in the interior, or can be adsorbed or attached to the surface groups. Dendrimers are made up of different types of polymers such as polyamidoamine (PAMAM), poly(L-glutamic acid), polyethyleneimine, polypropyleneimine, and polyethylene glycol[89]. The easily modifiable surface characteristic of dendrimers enables them to be simultaneously conjugated with several molecules such as imaging contrast agents, targeting ligands, or therapeutic drugs, yielding a dendrimer-based multifunctional drug delivery system[88]. Polyamidoamine dendrimers, most widely used as a scaffold, have promises for biomedical applications because they (1) can be easily conjugated with targeting molecules, imaging agents, and drugs, (2) have high

water solubility and well-defined chemical structures, (3) are biocompatible, and (4) are rapidly cleared from the blood through the kidneys, made possible by their small size (<5 nm), which eliminates the need for biodegradability. They were successfully conjugated with cisplatin[90] and an *in vivo* delivery of dendrimer–methotrexate conjugates using multivalent targeting resulted in a tenfold reduction in tumour size compared with that achieved with the same molar concentration of free systemic methotrexate[91,92]. This work provided motivation for further pre-clinical development, and a variety of dendrimers are now under investigation for cancer treatment. Choi *et al.* have developed DNA assembled polyamidoamine dendrimer clusters for cancer cell specific targeting[93].

Although promising, dendrimers are more expensive than other nanoparticles and require many repetitive steps for synthesis, posing a challenge for large-scale production. Despite its very attractive design, the 'dendritic box' lacks practical value in drug delivery because of its very limited capacity and the harsh conditions that are required to remove the densely packed shell and release its contents.

iii) *Polymeric micelles (amphiphilic block copolymers):*

Polymeric micelles are supramolecular, core-shell nanoparticles that offer considerable advantages for cancer diagnosis and therapy[94]. Their relatively small size (5-100 nm), ability to solubilize hydrophobic drugs as well as imaging agents, and improved pharmacokinetics provide a useful bioengineering platform for cancer applications. The spherical particles are nanosized supramolecular constructs formed from the self-assembly of biocompatible amphiphilic block copolymers in aqueous environments (Figure 5). In water, the hydrophobic portion of the block copolymer self-associates into a semi-solid core, with the hydrophilic segment of the copolymer forming a coronal layer. The resulting core-shell architecture is important for drug delivery purposes, because the hydrophobic core can act as a reservoir for water insoluble drugs, while the outer shell protects the micelle from recognition by the reticuloendothelial system and therefore preliminary elimination of the micelles from the bloodstream[95]. It also stabilizes the hydrophobic core and renders the polymers water soluble, making the particle an appropriate candidate for i.v. administration[20]. The drug can be loaded into a polymeric micelle in two ways: physical encapsulation[96] or chemical covalent attachment[97]. Moreover, the hydrophilic blocks can form hydrogen bonds with the aqueous surroundings and form a tight shell around

the micellar core. As a result, the contents of the hydrophobic core are effectively protected against hydrolysis and enzymatic degradation. By encapsulation of the drug within the hydrophobic core of the micelle, the apparent solubility of the drug can be significantly increased. For example, micelle encapsulation of paclitaxel increased the solubility over three orders of magnitude from 0.0015 to 2 mg/mL[98]. Hence, polymer micelles allow for the *in vivo* use of previously existing drugs otherwise deemed too hydrophobic or toxic, without having to manipulate the chemical structure of the agent. Additionally, encapsulating the drug within the polymer core affords drug stability by hindering enzymatic degradation and inactivation. A final feature that makes amphiphilic block copolymers attractive for drug delivery applications is that

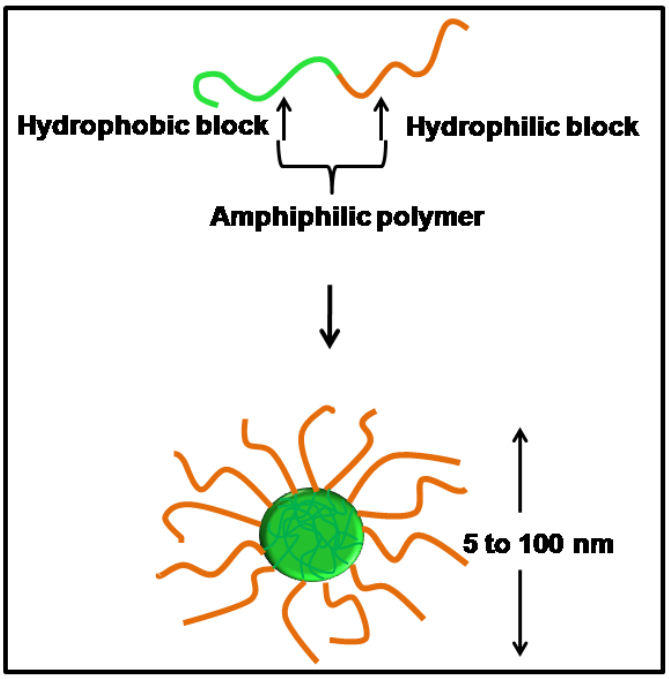

Figure 5: *Schematic of the core-shell architecture of a polymer micelle and its dimensions.*

their chemical composition, total molecular weight and block length ratios can be easily changed, which allows control of the size and morphology of the micelles.

Although several functional aspects of the constituent blocks have been explored (e.g. temperature or pH sensitive blocks), the most important criteria are biocompatibility and/or biodegradability[94]. Currently, the most commonly used corona-forming polymer is polyethylene glycol (PEG), with a molecular weight range

from 2 to 15 kD. Core-forming blocks typically consist of poly(propylene oxide) (PPO), poly(D,L-lactic acid) (PDLLA), poly(ε-caprolactone) (PCL), and poly(L-aspartic acid) to name a few[99]. The use of polymeric micelles for cancer treatment was first reported in the early 1980s by Ringsdorf and coworkers[100]. The first polymeric micelle formulation of paclitaxel, Genexol-PM (PEG-poly(D,L-lactide)-paclitaxel), is a cremophor-free polymeric micelle-formulated paclitaxel. A phase I and pharmacokinetic study has been conducted in patients with advanced refractory malignancies [101]. Multifunctional polymeric micelles containing targeting ligands and imaging and therapeutic agents are being actively developed[94, 102-104].

Despite many advantages of polymer micelles for *in vivo* applications, several challenges exist in this case too. For example, the small micellar size of 10-100 nm limits the amount of drug that can be incorporated within the core, with higher drug loading coming at the cost of increased micelle size and aggregation[105, 106]. This small size and limited drug loading in turn results in faster release from the micelles[107], which may cause premature release prior to the micelle reaching its intended site of action. Even below a critical micelle concentration, the polymeric aggregates dissociate into free chains, leading to the sudden release of the drug. Therefore, chemical conjugation strategies, as mentioned above, as well as increasing the compatibility of the micelle core with the intended drug[108], are being investigated to address these concerns. Additionally, several questions have been raised regarding the long-term stability of polymer micelles[109].

C) Inorganic nanoparticles based drug delivery systems:

Over the past few decades, inorganic nanoparticles, which exhibit significantly distinct physical, chemical and biological properties from their bulk counterpart's, have elicited much interest. Discoveries in the past decade have demonstrated that the electromagnetic, optical and catalytic properties of noble-metal nanoparticles such as gold, silver and platinum, are strongly influenced by shape and size. The advantages of inorganic nanoparticles over traditional nanoparticles system that have been described above include the possibility of multiple loading and multiple therapies. Since nanoparticle surface chemistry can be easily manipulated they can be used to load ligands depending upon the applications viz. targeting, diagnostics and therapeutics[110]. Gold nanoparticles can be used to generate heat (hyperthermia) by absorption of light. Due to the heat translated by the gold nanoparticles to the

surrounding tissue, cancerous tissues can be destroyed locally without exposing the entire organism to elevated temperatures[111, 112]. Another attractive system for hyperthermia treatment is magnetic particles. Upon irradiating magnetic particles with radiofrequency (RF) fields, heat is generated by repetitive cycling of the magnetic hysteresis loop[113, 114]. Compared with the optical excitation of gold nanoparticles at wavelengths of between 500–1000 nm, the excitation of magnetic nanoparticles works at lower frequencies (RF). As those are absorbed much less by normal tissue and thus penetrate deeper, particles inside the body can also be heated. On the other hand it is much more complicated to focus microwaves or radiofrequency waves than visible light and therefore photo-induced heating of gold particles is favourable for local heating of only small parts of tissue. In any case the ability to load the drug and deliver it, the ease with which targeting molecules also can be attached along with the drug combined with the possible therapeutic characteristic as described above, make inorganic nanoparticles a very attractive choice for the development of DDS. This has motivated an upsurge in research on the synthesis routes that allow better control of shape and size of inorganic nanoparticles for various nano-biotechnological applications. Biomedical applications of metal nanoparticles have been dominated by the use of nanobioconjugates that started in 1971 after the discovery of immunogold labeling by Faulk and Taylor[115]. However, the modern era of gold nanoparticle synthesis began over 150 years ago with the work of Michael Faraday, who was possibly the first to observe that colloidal gold solutions have properties that differ from bulk gold[116].

Various metals, such as gold (Au), copper (Cu), and silver (Ag), and inorganic carriers, such as silica or alumina, have been used for the preparation of nanoparticles. Among these gold nanoparticles are most widely used due to their excellent optical and photoelectric properties. According to the Mie theory[117], an electromagnetic frequency induces a resonant coherent oscillation of the free electrons, called the surface plasmon resonance (SPR), at the surface of a spherical nanoparticles if it is much smaller than the light wavelength. This absorption lies in the visible region for Au, Ag and Cu. For spherical gold nanoparticles of 5 nm diameter, the surface plasmon band is located at 520 nm in ethanol, but it is very sensitive to the composition, size, shape, inter-particle distance and environment (dielectric properties) of the gold nanoparticles. It is the high sensitivity to these factors that

makes the basis of their use for biological labeling, detection, diagnostic and sensing. For instance, 5-nm gold nanoparticles are orange-red, but they turn blue-purple upon aggregation (network formation) to larger gold nanoparticles. Likewise, a change of refractive index of the solvent shifts the plasmon band. The dramatic influence of the inter-gold nanoparticle distance on the plasmon resonance, when this distance is reduced to less than the gold nanoparticles diameter, is indeed the crucial factor in the sensor applications of gold nanoparticles. In 1996, the research groups of Mirkin and Alivisatos pioneered the preparation of gold nanoparticles functionalized with thiol-terminated DNA oligonucleotides[118, 119]. The as prepared conjugates (or probes) allow for the ultrasensitive detection of complementary DNA targets, with the gold nanoparticles serving as the signal reporter[118].

From the Mie theory, it follows that the frequency of the plasmon band varies from spherical to non-spherical nanoparticles of various shapes (rods, prisms, triangles, tetrapods, dogbones, cubes, shells). For instance, with gold nanorods, two plasmon bands are observed, one corresponding to oscillations along the length of the gold nanorod (longitudinal plasmon band) and the other along the width of the gold nanorod (transverse plasmon band). The positions of these two bands vary with the gold nanorod aspect ratio. Thus gold nanorods exhibit plasmon bands with maxima around 500 and 1600 nm. Since the ratio influences the position of the plasmon band absorption, the syntheses of gold nanorods can be adjusted with suitable ratio so that they correspond to commercial lasers (e.g. 360 nm, 785 nm and 1064 nm). Moreover, the shift of the plasmon band to the near-IR region for gold nanorods allows obtaining a penetration into living tissues that is much deeper than that of visible light. In addition the multi-component plasmon absorption provides richer information than the single visible band of spherical gold nanoparticles. Similarly, the plasmon band of gold nanoshells on silica nanoparticles is shifted to the near-IR region and can be tuned by adjusting the ratio of the thickness of the gold nanoshell to the diameter of the silica core. Halas group has shown that the smaller this ratio, the more red shifted is the plasmon absorption of the gold nanoshell[120]. This property of gold shells could be exploited for the local heating when they are irradiated with light in the "water window" (800 nm–1200 nm)[121-123]. El-Sayed *et al.* have reported about potential use of gold nanoparticles in photothermal destruction of tumors[121]. In this study, citrate-stabilized gold nanoparticles (approx. 30 nm in diameter) were coated with anti-

EGFR (epidermal growth factor receptor) to target HSC3 cancer cells (human oral squamous cell carcinoma). The use of gold nanoparticles enhanced the efficacy of photothermal therapy by 20 times. In another approach, optically responsive delivery systems have been designed by incorporation of gold nanospheres into the shells of capsules. Caruso *et al.* prepared microcapsules via layer-by-layer (LBL) technique to encapsulate macromolecules like fluorescein-labeled dextrans[124]. The capsule–shells were doped with gold nanoparticles, which response against near infra red (NIR) light. FITC-dextran was released upon laser (1064 nm) treatment due to rupture of the shell. Skirtach, Parak and coworkers have extended this strategy to deliver encapsulated materials from polyelectrolyte-multilayer capsules inside living cancer cells[125].

Reliable and high-yielding methods for the synthesis of gold nanoparticle, including those with spherical and non-spherical shapes, have been developed over the last half century[126]. The resulting gold nanoparticles have high surface area to volume ratio and, as a result, a high density of ligands can be appended for targeting or drug-loading purposes. For example, a 2 nm diameter core gold nanoparticle can load ~ 100 ligands per particle[127]. The surface of gold nanoparticles can be readily modified with ligands containing functional groups such as thiols, phosphines, and amines, which exhibit affinity for gold surfaces[110, 126, 128]. By using these functional groups, apart from anchoring the surface passivating ligands, additional moieties such as oligonucleotides[129], thiol-conjugated small interfering RNA (siRNA)[130], insulin[131], and genes can be conjugated to the gold nanoparticle surface[110] (Figure 6). The realization of such gold nanoconjugates has enabled a broad range of investigations, including programmed assembly and crystallization of materials[118, 132], arrangement of nanoparticles into dimers and trimers onto DNA templates[119], bioelectronics[133, 134], and detection methods[135, 136].

Moreover, gold exhibits specific advantages. Gold core is essentially inert, non-toxic, and biocompatible, making it an ideal starting point for carrier construction[137, 138]. Gold nanoparticles are highly effective contrast agents in cancer diagnosis and photodermal cancer therapy[128]. Their photophysical properties could trigger drug release at remote place[125]. More significantly, the unique biodistribution of gold nanoparticles within tumors have led to the discovery of gold-based nanosystems as delivery vehicles for chemotherapeutic agents[139].

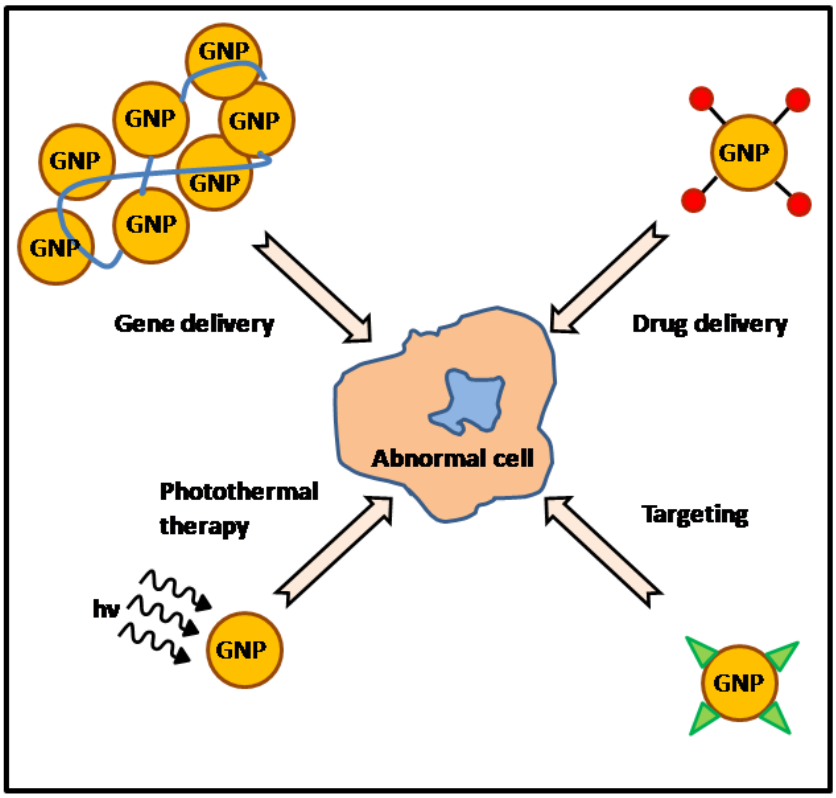

Figure 6: *Various applications of gold nanoparticles in therapy (Image courtesy Ref No. 103).*

The choice of an appropriate nanocarrier among the inorganic particles is not obvious, and the few existing comparative studies are difficult to interpret because several factors may simultaneously affect biodistribution and targeting. However, based on numerous studies carried out thus far, it can be concluded that gold nanoparticles have emerged as promising candidate for drug and gene delivery that provide a useful alternative to more traditional delivery vehicles. Their combination of low inherent toxicity, high surface area and tunable stability provides them with unique attributes that should enable new delivery strategies.

A review of the literature identifies the following as main requirements for gold nanoparticle based targeted delivery systems: (i) the biocompatibility of the gold nanoparticles; (ii) stability of the nanoparticles system after drug loading, (iii) a highly selective interaction with biological targets; (iv) the capability to retain activity/efficacy of the drug after loading; (v) the required amount of delivered drug and its high effectiveness at the target; (vi) the maximum effect on a given number of

target cells; (vii) flexibility for various chemical classes of drugs and targets. Figure 7 shows a hypothetical nanoparticle-carrier of drugs.

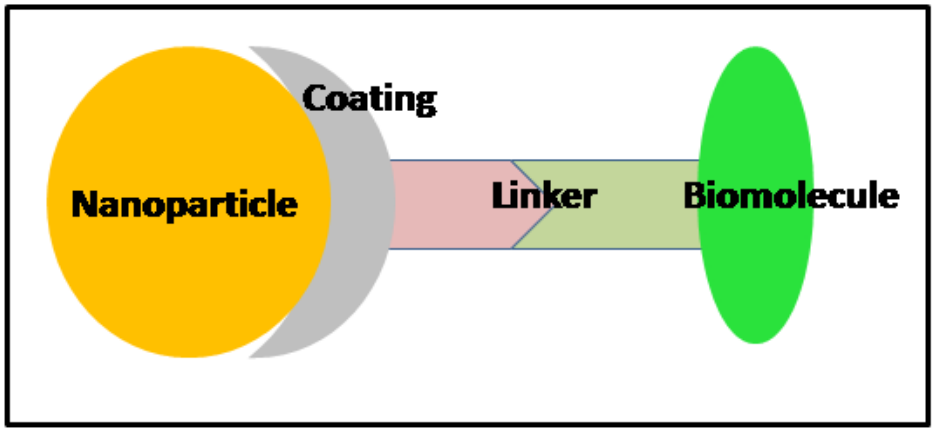

Figure 7: *A hypothetical nanoparticle-carrier of drugs.*

To meet all these selection criteria for the synthesis of drug delivery agent, we envisaged BSA-capped gold nanoparticles as ideal drug delivery systems. The results of our investigations starting with the synthesis of BSA-capped gold nanoparticles where BSA also acts as a reducing agent, their biocompatibility assessment, drug loading and delivery studies using these BSA-gold nanoparticle conjugates form the content of this thesis.

1.2 Outline of the thesis:

In this thesis we cover various issues of BSA-gold nanoparticle based drug delivery systems and evaluate their possible important biological applications. The thesis consists of seven chapters.

The ***First Chapter*** is an introduction to the thesis and gives a brief review about the drug delivery systems and their applications.

The ***Second Chapter*** describes in detail about the synthesis of stable, water soluble Bovine Serum Albumin capped silver and gold nanoparticles. The synthetic mechanism is probed by using UV-vis and fluorescence studies. The particle characterization is done via established techniques like UV-vis, X-ray diffraction (XRD) and TEM measurements. A detailed description of CV studies is presented to elucidate the mechanism of synthesis of nanoparticles.

The ***Third Chapter*** describes the role of BSA capping on the stability of gold and silver nanoparticles against varying pH and salt concentrations. FTIR and CD spectroscopies were performed to investigate the secondary structure of the protein present on the nanoparticles surface. Later the cytocompatibility of these nanoparticles against mouse fibroblast (NIH3T3) cells is demonstrated.

The ***Fourth Chapter*** discusses the uptake behavior of BSA protected gold nanoparticles into cancerous (human glioma LN229) and normal (mouse embryonic fibroblast NIH3T3) cell lines. These results are compared with another BSA-capped gold nanocarrier system, namely BSA-Au nanoclusters. The results suggested an enhanced uptake of both these nanocarrier systems into the cancerous cells in comparison to the normal cells. Although the nanoparticles and clusters are significantly different in their sizes and electronic properties, the extent of their uptake by human glioma cells is almost similar.

The ***Fifth Chapter*** discusses the conjugation of BSA capped gold nanoparticles to methotrexate and their evaluation of cytotoxicity against human breast cancer cell line MCF-7. The drug conjugated to BSA gold nanoparticles was found to evoke more toxicity to the cell lines than the equivalent concentration of drug alone. Drug loading was characterized by UV-vis spectroscopy, FTIR, ICP and TGA analysis. Cell death with Au-BSA-MTX was confirmed by MTT assay, Trypan blue viability counting, immunostaining, western analysis, DNA laddering assay, cell cycle analysis by FACS and TUNEL assay.

The ***Sixth Chapter*** deals with the biodistribution and toxicity studies of Au-BSA nanoparticles to demonstrate their applicability for drug delivery application *in vivo*. For this, Au-BSA sol of three doses 300 ppm, 150 ppm and 75 ppm (high, medium and low doses) were given orally to Wistar rats respectively for a period of 28 days. The results suggested no adverse behavioral, hematological, biochemical and histopathological changes being associated with the BSA capped gold nanoparticles at the investigated concentrations. These studies establish that BSA reduced gold nanoparticles produced no treatment related toxicity in rats following oral administration and the results can be exploited for potential therapeutic applications.

The ***Seventh chapter*** summarizes the work presented in the thesis and projects out the possible avenues for further research in this area.

References:

1. Kayser, O.; Lemke, A.; Hernandez-Trejo, N., The impact of nanobiotechnology on the development of new drug delivery systems. *Current Pharmaceutical Biotechnology* **2005,** 6, (1), 3-5.

2. Hilder, T. A.; Hill, J. M., Modeling the encapsulation of the anticancer drug cisplatin into carbon nanotubes. *Nanotechnology* **2007,** 18, 275704.

3. Kreuter, J.; Shamenkov, D.; Petrov, V.; Ramge, P.; Cychutek, K.; Koch-Brandt, C.; Alyautdin, R., Apolipoprotein-mediated transport of nanoparticle-bound drugs across the blood-brain barrier. *Journal of drug targeting* **2002,** 10, (4), 317-325.

4. Kaparissides, C.; Alexandridou, S.; Kotti, K.; Chaitidou, S., Recent advances in novel drug delivery systems. *Journal of Nanotechnology, Online* **2006,** 2, 1-11.

5. Costantino, L.; Gandolfi, F.; Tosi, G.; Rivasi, F.; Vandelli, M. A.; Forni, F., Peptide-derivatized biodegradable nanoparticles able to cross the blood-brain barrier. *Journal of Controlled Release* **2005,** 108, (1), 84-96.

6. Gao, K.; Jiang, X., Influence of particle size on transport of methotrexate across blood brain barrier by polysorbate 80-coated polybutylcyanoacrylate nanoparticles. *International journal of pharmaceutics* **2006,** 310, (1-2), 213-219.

7. Kreuter, J., Nanoparticulate systems for brain delivery of drugs. *Advanced drug delivery reviews* **2001,** 47, (1), 65-81.

8. Chang, J.; Jallouli, Y.; Kroubi, M.; Yuan, X.; Feng, W.; Kang, C.; Pu, P.; Betbeder, D., Characterization of endocytosis of transferrin-coated PLGA nanoparticles by the blood-brain barrier. *International journal of pharmaceutics* **2009,** 379, (2), 285-292.

9. Rao, K. S.; Reddy, M. K.; Horning, J. L.; Labhasetwar, V., TAT-conjugated nanoparticles for the CNS delivery of anti-HIV drugs. *Biomaterials* **2008,** 29, (33), 4429-4438.

10. Stewart, B. W.; Kleihues, P., *World cancer report*. Iarc: 2003.

11. Jemal, A.; Siegel, R.; Xu, J.; Ward, E., Cancer statistics, 2010. *CA: a cancer journal for clinicians*, caac. 20073v1.

12. Peer, D.; Karp, J. M.; Hong, S.; Farokhzad, O. C.; Margalit, R.; Langer, R., Nanocarriers as an emerging platform for cancer therapy. *Nature nanotechnology* **2007,** 2, (12), 751-760.

13. Mainardes, R. M.; Silva, L. P., Drug delivery systems: past, present, and future. *Current Drug Targets* **2004,** 5, (5), 449-455.

14. Nazarov, G.; Galan, S.; Nazarova, E.; Karkishchenko, N.; Muradov, M.; Stepanov, V., Nanosized forms of drugs (A Review). *Pharmaceutical Chemistry Journal* **2009,** 43, (3), 163-170.

15. Allen, T. M., Ligand-targeted therapeutics in anticancer therapy. *Nature Reviews Cancer* **2002,** 2, (10), 750-763.

16. Wisse, E.; Braet, F., Structure and function of sinusoidal lining cells in the liver. *Toxicologic pathology* **1996,** 24, (1), 100.

17. Yuan, F.; Dellian, M.; Fukumura, D.; Leunig, M.; Berk, D. A.; Torchilin, V. P.; Jain, R. K., Vascular permeability in a human tumor xenograft: molecular size dependence and cutoff size. *Cancer research* **1995,** 55, (17), 3752.

18. Moghimi, S. M.; Szebeni, J., Stealth liposomes and long circulating nanoparticles: critical issues in pharmacokinetics, opsonization and protein-binding properties. *Progress in lipid research* **2003,** 42, (6), 463-478.

19. Harris, J. M.; Martin, N. E.; Modi, M., Pegylation: a novel process for modifying pharmacokinetics. *Clinical pharmacokinetics* **2001,** 40, (7), 539-551.

20. Adams, M. L.; Lavasanifar, A.; Kwon, G. S., Amphiphilic block copolymers for drug delivery. *Journal of pharmaceutical sciences* **2003,** 92, (7), 1343-1355.

21. Giljohann, D. A.; Seferos, D. S.; Daniel, W. L.; Massich, M. D.; Patel, P. C.; Mirkin, C. A., Gold Nanoparticles for Biology and Medicine. *Angewandte Chemie International Edition* 49, (19), 3280-3294.

22. Couvreur, P.; Vauthier, C., Nanotechnology: Intelligent design to treat complex disease. *Pharmaceutical research* **2006,** 23, (7), 1417-1450.

23. Alonso, J., Nanomedicines for overcoming biological barriers. *Biomedecine & Pharmacotherapy* **2004,** 58, (3), 168-172.

24. Matsumura, Y.; Maeda, H., A new concept for macromolecular therapeutics in cancer chemotherapy: mechanism of tumoritropic accumulation of proteins and the antitumor agent smancs. *Cancer research* **1986,** 46, (12 Part 1), 6387.

25. Maeda, H., The enhanced permeability and retention (EPR) effect in tumor vasculature: the key role of tumor-selective macromolecular drug targeting. *Advances in enzyme regulation* **2001,** 41, 189.

26. Carmeliet, P.; Jain, R. K., Angiogenesis in cancer and other diseases. *Nature* **2000,** 407, (6801), 249-257.

27. Pelicano, H.; Martin, D. S.; Xu, R. H.; Huang, P., Glycolysis inhibition for anticancer treatment. *Oncogene* **2006,** 25, (34), 4633-4646.

28. Yatvin, M. B.; Kreutz, W.; Horwitz, B. A.; Shinitzky, M., pH-sensitive liposomes: possible clinical implications. *Science* **1980,** 210, (4475), 1253.

29. Ei, D., Quigley JP, Matrix metalloproteinases and tumor metastasis. *Cancer Metastasis Rev* **2006,** 25, 9-34.

30. Mansour, A. M.; Drevs, J.; Esser, N.; Hamada, F. M.; Badary, O. A.; Unger, C.; Fichtner, I.; Kratz, F., A new approach for the treatment of malignant melanoma: enhanced antitumor efficacy of an albumin-binding doxorubicin prodrug that is cleaved by matrix metalloproteinase 2. *Cancer research* **2003,** 63, (14), 4062.

31. Yockman, J. W.; Maheshwari, A.; Han, S.; Kim, S. W., Tumor regression by repeated intratumoral delivery of water soluble lipopolymers/p2CMVmIL-12 complexes. *Journal of Controlled Release* **2003,** 87, (1-3), 177-186.

32. Nomura, T.; Saikawa, A.; Morita, S.; Sakaeda ne Kakutani, T.; Yamashita, F.; Honda, K., Pharmacokinetic characteristics and therapeutic effects of mitomycin C-

dextran conjugates after intratumoural injection. *Journal of Controlled Release* **1998,** 52, (3), 239-252.

33. Tolcher, A. W.; Sugarman, S.; Gelmon, K. A.; Cohen, R.; Saleh, M.; Isaacs, C.; Young, L.; Healey, D.; Onetto, N.; Slichenmyer, W., Randomized phase II study of BR96-doxorubicin conjugate in patients with metastatic breast cancer. *Journal of Clinical Oncology* **1999,** 17, (2), 478.

34. Leamon, C. P.; Reddy, J. A., Folate-targeted chemotherapy. *Advanced drug delivery reviews* **2004,** 56, (8), 1127-1141.

35. Saba, N. F.; Wang, X.; Müller, S.; Tighiouart, M.; Cho, K.; Nie, S.; Chen, Z. G.; Shin, D. M., Examining expression of folate receptor in squamous cell carcinoma of the head and neck as a target for a novel nanotherapeutic drug. *Head & neck* **2009,** 31, (4), 475-481.

36. Cho, K.; Wang, X.; Kim, G. J.; Gjyrezi, A.; Giannakakou, P.; Nie, S. In *Investigation of Taxol-resistance using folate-targeted ternary therapeutic nanoparticle*, 2007; 2007.

37. Qian, Z. M.; Tang, P. L., Mechanisms of iron uptake by mammalian cells. *Biochimica et Biophysica Acta (BBA)-Molecular Cell Research* **1995,** 1269, (3), 205-214.

38. Qian, Z. M.; Li, H.; Sun, H.; Ho, K., Targeted drug delivery via the transferrin receptor-mediated endocytosis pathway. *Pharmacological reviews* **2002,** 54, (4), 561.

39. Sahoo, S. K.; Labhasetwar, V., Enhanced antiproliferative activity of transferrin-conjugated paclitaxel-loaded nanoparticles is mediated via sustained intracellular drug retention. *Mol. Pharm* **2005,** 2, (5), 373-383.

40. Xu, L.; Pirollo, K. F.; Tang, W. H.; Rait, A.; Chang, E. H., Transferrin-liposome-mediated systemic p53 gene therapy in combination with radiation results in regression of human head and neck cancer xenografts. *Human gene therapy* **1999,** 10, (18), 2941-2952.

41. El-Sayed, I. H.; Huang, X.; El-Sayed, M. A., Selective laser photo-thermal therapy of epithelial carcinoma using anti-EGFR antibody conjugated gold nanoparticles. *Cancer letters* **2006,** 239, (1), 129-135.

42. Chen, P. C.; Mwakwari, S. C.; Oyelere, A. K., Gold nanoparticles: From nanomedicine to nanosensing. *Nanotechnology, Science and Applications* **2008,** 1, 45-66.

43. Bies, C.; Lehr, C. M.; Woodley, J. F., Lectin-mediated drug targeting: history and applications. *Advanced drug delivery reviews* **2004,** 56, (4), 425-435.

44. Minko, T., Drug targeting to the colon with lectins and neoglycoconjugates. *Advanced drug delivery reviews* **2004,** 56, (4), 491-509.

45. Yamazaki, N.; Kojima, S.; Bovin, N. V.; Andre, S.; Gabius, S.; Gabius, H. J., Endogenous lectins as targets for drug delivery. *Advanced drug delivery reviews* **2000,** 43, (2-3), 225-244.

46. Sinha, R.; Kim, G. J.; Nie, S.; Shin, D. M., Nanotechnology in cancer therapeutics: bioconjugated nanoparticles for drug delivery. *Molecular cancer therapeutics* **2006,** 5, (8), 1909.

47. Gottesman, M. M.; Fojo, T.; Bates, S. E., Multidrug resistance in cancer: role of ATP–dependent transporters. *Nature Reviews Cancer* **2002,** 2, (1), 48-58.

48. Wong, H. L.; Bendayan, R.; Rauth, A. M.; Xue, H. Y.; Babakhanian, K.; Wu, X. Y., A mechanistic study of enhanced doxorubicin uptake and retention in multidrug resistant breast cancer cells using a polymer-lipid hybrid nanoparticle system. *Journal of Pharmacology and Experimental Therapeutics* **2006,** 317, (3), 1372.

49. Lee, E. S.; Na, K.; Bae, Y. H., Doxorubicin loaded pH-sensitive polymeric micelles for reversal of resistant MCF-7 tumor. *Journal of Controlled Release* **2005,** 103, (2), 405-418.

50. Cho, K.; Wang, X.; Nie, S.; Chen, Z. G.; Shin, D. M., Therapeutic nanoparticles for drug delivery in cancer. *Clinical Cancer Research* **2008,** 14, (5), 1310.

51. Gregoriadis, G.; Florence, A. T., Liposomes in drug delivery: clinical, diagnostic and ophthalmic potential. *Drugs* **1993,** 45, (1), 15-28.

52. Markman, M., Pegylated liposomal doxorubicin in the treatment of cancers of the breast and ovary. *Expert Opin. Pharmacother.* **2006,** 7, (11), 1469-1474.

53. Rivera, E., Current status of liposomal anthracycline therapy in metastatic breast cancer. *Clinical Breast Cancer* **2003,** 4, 76-83.

54. Rosenthal, E.; Poizot-Martin, I.; Saint-Marc, T.; Spano, J. P.; Cacoub, P., Phase IV study of liposomal daunorubicin (DaunoXome) in AIDS-related Kaposi sarcoma. *American journal of clinical oncology* **2002,** 25, (1), 57.

55. Hofheinz, R. D.; Gnad-Vogt, S. U.; Beyer, U.; Hochhaus, A., Liposomal encapsulated anti-cancer drugs. *Anti-cancer drugs* **2005,** 16, (7), 691.

56. Wu, J.; Liu, Q.; Lee, R. J., A folate receptor-targeted liposomal formulation for paclitaxel. *International journal of pharmaceutics* **2006,** 316, (1-2), 148-153.

57. Harasym, T. O.; Bally, M. B.; Tardi, P., Clearance properties of liposomes involving conjugated proteins for targeting. *Advanced drug delivery reviews* **1998,** 32, (1-2), 99-118.

58. Schwendener, R. A.; Trüb, T.; Schott, H.; Langhals, H.; Barth, R. F.; Groscurth, P.; Hengartner, H., Comparative studies of the preparation of immunoliposomes with the use of two bifunctional coupling agents and investigation of in vitro immunoliposome-target cell binding by cytofluorometry and electron microscopy. *Biochimica et Biophysica Acta (BBA)-Biomembranes* **1990,** 1026, (1), 69-79.

59. Mamot, C.; Drummond, D. C.; Greiser, U.; Hong, K.; Kirpotin, D. B.; Marks, J. D.; Park, J. W., Epidermal growth factor receptor (EGFR)-targeted immunoliposomes mediate specific and efficient drug delivery to EGFR-and EGFRvIII-overexpressing tumor cells. *Cancer research* **2003,** 63, (12), 3154.

60. Mamot, C.; Drummond, D. C.; Noble, C. O.; Kallab, V.; Guo, Z.; Hong, K.; Kirpotin, D. B.; Park, J. W., Epidermal Growth Factor Receptor–Targeted

Immunoliposomes Significantly Enhance the Efficacy of Multiple Anticancer Drugs In vivo. *Cancer research* **2005,** 65, (24), 11631.

61. Mamot, C.; Ritschard, R.; Küng, W.; Park, J. W.; Herrmann, R.; Rochlitz, C. F., EGFR-targeted immunoliposomes derived from the monoclonal antibody EMD72000 mediate specific and efficient drug delivery to a variety of colorectal cancer cells. *Journal of drug targeting* **2006,** 14, (4), 215-223.

62. Hosokawa, S.; Tagawa, T.; Niki, H.; Hirakawa, Y.; Nohga, K.; Nagaike, K., Efficacy of immunoliposomes on cancer models in a cell-surface-antigen-density-dependent manner. *British journal of cancer* **2003,** 89, (8), 1545-1551.

63. Sapra, P.; Moase, E. H.; Ma, J.; Allen, T. M., Improved therapeutic responses in a xenograft model of human B lymphoma (Namalwa) for liposomal vincristine versus liposomal doxorubicin targeted via anti-CD19 IgG2a or Fab fragments. *Clinical Cancer Research* **2004,** 10, (3), 1100.

64. Pastorino, F.; Brignole, C.; Marimpietri, D.; Sapra, P.; Moase, E. H.; Allen, T. M.; Ponzoni, M., Doxorubicin-loaded Fab fragments of anti-disialoganglioside immunoliposomes selectively inhibit the growth and dissemination of human neuroblastoma in nude mice. *Cancer research* **2003,** 63, (1), 86.

65. Sharma, A.; Sharma, U. S., Liposomes in drug delivery: progress and limitations. *International journal of pharmaceutics* **1997,** 154, (2), 123-140.

66. Huwyler, J.; Wu, D.; Pardridge, W. M., Brain drug delivery of small molecules using immunoliposomes. *Proceedings of the National Academy of Sciences of the United States of America* **1996,** 93, (24), 14164.

67. Chowdhary, R. K.; Shariff, I.; Dolphin, D., Drug release characteristics of lipid based benzoporphyrin derivative. *Journal of Pharmacy and Pharmaceutical Sciences* **2003,** 6, (1), 13–19.

68. Lorusso, D.; Di Stefano, A.; Carone, V.; Fagotti, A.; Pisconti, S.; Scambia, G., Pegylated liposomal doxorubicin-related palmar-plantar erythrodysesthesia ('hand-foot'syndrome). *Annals of Oncology* **2007,** 18, (7), 1159.

69. Brigger, I.; Dubernet, C.; Couvreur, P., Nanoparticles in cancer therapy and diagnosis. *Advanced drug delivery reviews* **2002,** 54, (5), 631-651.

70. Kreuter, J.; Higuchi, T., Improved delivery of methoxsalen. *Journal of pharmaceutical sciences* **1979,** 68, (4), 451-454.

71. Yuan, F.; Leunig, M.; Huang, S. K.; Berk, D. A.; Papahadjopoulos, D.; Jain, R. K., Mirovascular permeability and interstitial penetration of sterically stabilized (Stealth) liposomes in a human tumor xenograft. *Cancer research* **1994,** 54, (13), 3352.

72. McKee, T. D.; Grandi, P.; Mok, W.; Alexandrakis, G.; Insin, N.; Zimmer, J. P.; Bawendi, M. G.; Boucher, Y.; Breakefield, X. O.; Jain, R. K., Degradation of fibrillar collagen in a human melanoma xenograft improves the efficacy of an oncolytic herpes simplex virus vector. *Cancer research* **2006,** 66, (5), 2509.

73. Rawat, M.; Singh, D.; Saraf, S., Nanocarriers: promising vehicle for bioactive drugs. *Biological & pharmaceutical bulletin* **2006,** 29, (9), 1790-1798.

74. Couvreur, P.; Kante, B.; Roland, M.; Speiser, P., Adsorption of antineoplastic drugs to polyalkylcyanoacrylate nanoparticles and their release in calf serum. *Journal of pharmaceutical sciences* **1979,** 68, (12), 1521-1524.

75. Couvreur, P.; Kante, B.; Lenaerts, V.; Scailteur, V.; Roland, M.; Speiser, P., Tissue distribution of antitumor drugs associated with polyalkylcyanoacrylate nanoparticles. *Journal of pharmaceutical sciences* **1980,** 69, (2), 199-202.

76. Couvreur, P.; Kante, B.; Grislain, L.; Roland, M.; Speiser, P., Toxicity of polyalkylcyanoacrylate nanoparticles II: Doxorubicin loaded nanoparticles. *Journal of pharmaceutical sciences* **1982,** 71, (7), 790-792.

77. Green, M. R.; Manikhas, G. M.; Orlov, S.; Afanasyev, B.; Makhson, A. M.; Bhar, P.; Hawkins, M. J., Abraxane®, a novel Cremophor®-free, albumin-bound particle form of paclitaxel for the treatment of advanced non-small-cell lung cancer. *Annals of Oncology* **2006,** 17, (8), 1263.

78. Nyman, D. W.; Campbell, K. J.; Hersh, E.; Long, K.; Richardson, K.; Trieu, V.; Desai, N.; Hawkins, M. J.; Von Hoff, D. D., Phase I and pharmacokinetics trial of ABI-007, a novel nanoparticle formulation of paclitaxel in patients with advanced nonhematologic malignancies. *Journal of Clinical Oncology* **2005,** 23, (31), 7785.

79. Li, C., Poly (-glutamic acid)-anticancer drug conjugates. *Advanced drug delivery reviews* **2002,** 54, (5), 695-713.

80. Sabbatini, P.; Aghajanian, C.; Dizon, D.; Anderson, S.; Dupont, J.; Brown, J. V.; Peters, W. A.; Jacobs, A.; Mehdi, A.; Rivkin, S., Phase II study of CT-2103 in patients with recurrent epithelial ovarian, fallopian tube, or primary peritoneal carcinoma. *Journal of Clinical Oncology* **2004,** 22, (22), 4523.

81. Bhatt, R.; de Vries, P.; Tulinsky, J.; Bellamy, G.; Baker, B.; Singer, J. W.; Klein, P., Synthesis and in vivo antitumor activity of poly (L-glutamic acid) conjugates of 20 (S)-camptothecin. *J. Med. Chem* **2003,** 46, (1), 190-193.

82. Duncan, R., The dawning era of polymer therapeutics. *Nature Reviews Drug Discovery* **2003,** 2, (5), 347-360.

83. Vasey, P. A.; Kaye, S. B.; Morrison, R.; Twelves, C.; Wilson, P.; Duncan, R.; Thomson, A. H.; Murray, L. S.; Hilditch, T. E.; Murray, T., Phase I clinical and pharmacokinetic study of PK1 [N-(2-hydroxypropyl) methacrylamide copolymer doxorubicin]: first member of a new class of chemotherapeutic agents—drug-polymer conjugates. *Clinical Cancer Research* **1999,** 5, (1), 83.

84. Gillies, E. R.; Frechet, J. M. J., Dendrimers and dendritic polymers in drug delivery. *Drug Discovery Today* **2005,** 10, (1), 35-43.

85. Gopin, A.; Ebner, S.; Attali, B.; Shabat, D., Enzymatic activation of second-generation dendritic prodrugs: conjugation of self-immolative dendrimers with poly (ethylene glycol) via click chemistry. *Bioconjugate Chem* **2006,** 17, (6), 1432-1440.

86. Greenwald, R. B.; Choe, Y. H.; McGuire, J.; Conover, C. D., Effective drug delivery by PEGylated drug conjugates. *Advanced drug delivery reviews* **2003,** 55, (2), 217-250.

87. Smith, A.; Hunneyball, M., Evaluation of poly (lactic acid) as a biodegradable drug delivery system for parenteral administration. *International journal of pharmaceutics* **1986,** 30, (2-3), 215-220.

88. Svenson, S.; Tomalia, D. A., Dendrimers in biomedical applications--reflections on the field. *Advanced drug delivery reviews* **2005,** 57, (15), 2106-2129.

89. Aulenta, F.; Hayes, W.; Rannard, S., Dendrimers: a new class of nanoscopic containers and delivery devices. *European Polymer Journal* **2003,** 39, (9), 1741-1771.

90. Malik, N.; Evagorou, E. G.; Duncan, R., Dendrimer-platinate: a novel approach to cancer chemotherapy. *Anti-cancer drugs* **1999,** 10, (8), 767.

91. Kukowska-Latallo, J. F.; Candido, K. A.; Cao, Z.; Nigavekar, S. S.; Majoros, I. J.; Thomas, T. P.; Balogh, L. P.; Khan, M. K.; Baker, J. R., Nanoparticle targeting of anticancer drug improves therapeutic response in animal model of human epithelial cancer. *Cancer research* **2005,** 65, (12), 5317.

92. Hong, S.; Leroueil, P. R.; Majoros, I. J.; Orr, B. G.; Baker Jr, J. R.; Banaszak Holl, M. M., The binding avidity of a nanoparticle-based multivalent targeted drug delivery platform. *Chemistry & biology* **2007,** 14, (1), 107-115.

93. Choi, Y.; Thomas, T.; Kotlyar, A.; Islam, M. T.; Baker Jr, J. R., Synthesis and functional evaluation of DNA-assembled polyamidoamine dendrimer clusters for cancer cell-specific targeting. *Chemistry & biology* **2005,** 12, (1), 35-43.

94. Blanco, E.; Kessinger, C. W.; Sumer, B. D.; Gao, J., Multifunctional micellar nanomedicine for cancer therapy. *Experimental biology and medicine (Maywood, NJ)* **2009,** 234, (2), 123.

95. Torchilin, V. P., Structure and design of polymeric surfactant-based drug delivery systems. *Journal of Controlled Release* **2001,** 73, (2-3), 137-172.

96. Batrakova, E. V.; Dorodnych, T. Y.; Klinskii, E. Y.; Kliushnenkova, E. N.; Shemchukova, O. B.; Goncharova, O. N.; Arjakov, S. A.; Alakhov, V. Y.; Kabanov, A. V., Anthracycline antibiotics non-covalently incorporated into the block copolymer

micelles: in vivo evaluation of anti-cancer activity. *British journal of cancer* **1996,** 74, (10), 1545.

97. Nakanishi, T.; Fukushima, S.; Okamoto, K.; Suzuki, M.; Matsumura, Y.; Yokoyama, M.; Okano, T.; Sakurai, Y.; Kataoka, K., Development of the polymer micelle carrier system for doxorubicin. *Journal of Controlled Release* **2001,** 74, (1-3), 295-302.

98. Soga, O.; van Nostrum, C. F.; Fens, M.; Rijcken, C. J. F.; Schiffelers, R. M.; Storm, G.; Hennink, W. E., Thermosensitive and biodegradable polymeric micelles for paclitaxel delivery. *Journal of Controlled Release* **2005,** 103, (2), 341-353.

99. Sutton, D.; Nasongkla, N.; Blanco, E.; Gao, J., Functionalized micellar systems for cancer targeted drug delivery. *Pharmaceutical research* **2007,** 24, (6), 1029-1046.

100. Gros, L.; Ringsdorf, H.; Schupp, H., Polymeric antitumor agents on a molecular and on a cellular level? *Angewandte Chemie International Edition in English* **1981,** 20, (4), 305-325.

101. Kim, T. Y.; Kim, D. W.; Chung, J. Y.; Shin, S. G.; Kim, S. C.; Heo, D. S.; Kim, N. K.; Bang, Y. J., Phase I and pharmacokinetic study of Genexol-PM, a cremophor-free, polymeric micelle-formulated paclitaxel, in patients with advanced malignancies. *Clinical Cancer Research* **2004,** 10, (11), 3708.

102. Nasongkla, N.; Bey, E.; Ren, J.; Ai, H.; Khemtong, C.; Guthi, J. S.; Chin, S. F.; Sherry, A. D.; Boothman, D. A.; Gao, J., Multifunctional polymeric micelles as cancer-targeted, MRI-ultrasensitive drug delivery systems. *Nano Lett* **2006,** 6, (11), 2427-2430.

103. Bae, Y.; Jang, W. D.; Nishiyama, N.; Fukushima, S.; Kataoka, K., Multifunctional polymeric micelles with folate-mediated cancer cell targeting and pH-triggered drug releasing properties for active intracellular drug delivery. *Molecular BioSystems* **2005,** 1, (3), 242-250.

104. Lee, E. S.; Na, K.; Bae, Y. H., Super pH-sensitive multifunctional polymeric micelle. *Nano Lett* **2005,** 5, (2), 325-329.

105. Allen, C.; Maysinger, D.; Eisenberg, A., Nano-engineering block copolymer aggregates for drug delivery. *Colloids and Surfaces B: Biointerfaces* **1999,** 16, (1-4), 3-27.

106. Gaucher, G.; Dufresne, M. H.; Sant, V. P.; Kang, N.; Maysinger, D.; Leroux, J. C., Block copolymer micelles: preparation, characterization and application in drug delivery. *Journal of Controlled Release* **2005,** 109, (1-3), 169-188.

107. Kim, S. Y.; Shin, I. L. G.; Lee, Y. M.; Cho, C. S.; Sung, Y. K., Methoxy poly (ethylene glycol) and -caprolactone amphiphilic block copolymeric micelle containing indomethacin. II. Micelle formation and drug release behaviours. *Journal of Controlled Release* **1998,** 51, (1), 13-22.

108. Liu, J.; Xiao, Y.; Allen, C., Polymer–drug compatibility: a guide to the development of delivery systems for the anticancer agent, ellipticine. *Journal of pharmaceutical sciences* **2004,** 93, (1), 132-143.

109. Jones, M. C.; Leroux, J. C., Polymeric micelles-a new generation of colloidal drug carriers. *European journal of pharmaceutics and biopharmaceutics* **1999,** 48, (2), 101-111.

110. Ghosh, P.; Han, G.; De, M.; Kim, C. K.; Rotello, V. M., Gold nanoparticles in delivery applications. *Advanced drug delivery reviews* **2008,** 60, (11), 1307-1315.

111. Huff, T. B.; Tong, L.; Zhao, Y.; Hansen, M. N.; Cheng, J. X.; Wei, A., Hyperthermic effects of gold nanorods on tumor cells. *Nanomedicine* **2007,** 2, (1), 125-132.

112. Lowery, A. R.; Gobin, A. M.; Day, E. S.; Halas, N. J.; West, J. L., Immunonanoshells for targeted photothermal ablation of tumor cells. *International journal of nanomedicine* **2006,** 1, (2), 149.

113. Pankhurst, Q. A.; Connolly, J.; Jones, S.; Dobson, J., Applications of magnetic nanoparticles in biomedicine. *Journal of Physics D: Applied Physics* **2003,** 36, R167.

114. Hiergeist, R.; Andrä, W.; Buske, N.; Hergt, R.; Hilger, I.; Richter, U.; Kaiser, W., Application of magnetite ferrofluids for hyperthermia. *Journal of Magnetism and Magnetic Materials* **1999,** 201, (1-3), 420-422.

115. Faulk, W. P.; Taylor, G. M., An immunocolloid method for the electron microscope. *Immunochemistry* **1971,** 8, (11), 1081.

116. Hayat, M. A., Colloidal gold. Principles, methods, and applications. *San Diego, etc* **1989,** 2.

117. Mie, G., Articles on the optical characteristics of turbid tubes, especially colloidal metal solutions. *Ann. Phys* **1908,** 25, (3), 377–445.

118. Mirkin, C. A.; Letsinger, R. L.; Mucic, R. C.; Storhoff, J. J., A DNA-based method for rationally assembling nanoparticles into macroscopic materials. **1996**.

119. Alivisatos, A. P.; Johnsson, K. P.; Peng, X.; Wilson, T. E.; Loweth, C. J.; Bruchez, M. P.; Schultz, P. G., Organization of'nanocrystal molecules' using DNA. **1996**.

120. Lal, S.; Clare, S. E.; Halas, N. J., Nanoshell-enabled photothermal cancer therapy: impending clinical impact. *Accounts of chemical research* **2008,** 41, (12), 1842-1851.

121. Huang, X.; Qian, W.; El-Sayed, I. H.; El-Sayed, M. A., The potential use of the enhanced nonlinear properties of gold nanospheres in photothermal cancer therapy. *Lasers in Surgery and Medicine* **2007,** 39, (9), 747-753.

122. Jain, P. K.; Huang, X.; El-Sayed, I. H.; El-Sayed, M. A., Noble metals on the nanoscale: optical and photothermal properties and some applications in imaging, sensing, biology, and medicine. *Accounts of chemical research* **2008,** 41, (12), 1578-1586.

123. Huang, X.; Jain, P. K.; El-Sayed, I. H.; El-Sayed, M. A., Gold nanoparticles: interesting optical properties and recent applications in cancer diagnostics and therapy. *Nanomedicine* **2007,** 2, (5), 681-693.

124. Angelatos, A. S.; Radt, B.; Caruso, F., Light-responsive polyelectrolyte/gold nanoparticle microcapsules. *J. Phys. Chem. B* **2005,** 109, (7), 3071-3076.

125. Skirtach, A. G.; Muñoz Javier, A.; Kreft, O.; Köhler, K.; Piera Alberola, A.; Möhwald, H.; Parak, W. J.; Sukhorukov, G. B., Laser Induced Release of Encapsulated Materials inside Living Cells. *Angewandte Chemie* **2006,** 118, (28), 4728-4733.

126. Daniel, M. C.; Astruc, D., Gold Nanoparticles: Assembly. *Supramolecular Chemistry, Quantum-Size-Related Properties, and Applications toward Biology, Catalysis, and Nanotechnology. Chem. Rev* **2004,** 104, (1), 293-346.

127. Hostetler, M. J.; Wingate, J. E.; Zhong, C. J.; Harris, J. E.; Vachet, R. W.; Clark, M. R.; Londono, J. D.; Green, S. J.; Stokes, J. J.; Wignall, G. D., Alkanethiolate gold cluster molecules with core diameters from 1.5 to 5.2 nm: core and monolayer properties as a function of core size. *Langmuir* **1998,** 14, (1), 17-30.

128. Jain, P. K.; El-Sayed, I. H.; El-Sayed, M. A., Au nanoparticles target cancer. *Nano Today* **2007,** 2, (1), 18-29.

129. Blasi, P.; Giovagnoli, S.; Schoubben, A.; Ricci, M.; Rossi, C., Solid lipid nanoparticles for targeted brain drug delivery. *Advanced drug delivery reviews* **2007,** 59, (6), 454-477.

130. Oishi, M.; Nakaogami, J.; Ishii, T.; Nagasaki, Y., Smart PEGylated gold nanoparticles for the cytoplasmic delivery of siRNA to induce enhanced gene silencing. *Chemistry Letters* **2006,** 35, (9), 1046-1047.

131. Bhumkar, D. R.; Joshi, H. M.; Sastry, M.; Pokharkar, V. B., Chitosan reduced gold nanoparticles as novel carriers for transmucosal delivery of insulin. *Pharmaceutical research* **2007,** 24, (8), 1415-1426.

132. Park, S. Y.; Lytton-Jean, A. K. R.; Lee, B.; Weigand, S.; Schatz, G. C.; Mirkin, C. A., DNA-programmable nanoparticle crystallization. *Nature* **2008,** 451, (7178), 553-556.

133. Park, S. J.; Taton, T. A.; Mirkin, C. A., Array-based electrical detection of DNA with nanoparticle probes. *Science* **2002,** 295, (5559), 1503.

134. Xiao, Y.; Patolsky, F.; Katz, E.; Hainfeld, J. F.; Willner, I., " Plugging into Enzymes": Nanowiring of Redox Enzymes by a Gold Nanoparticle. *Science* **2003,** 299, (5614), 1877.

135. He, L.; Musick, M. D.; Nicewarner, S. R.; Salinas, F. G.; Benkovic, S. J.; Natan, M. J.; Keating, C. D., Colloidal Au-enhanced surface plasmon resonance for ultrasensitive detection of DNA hybridization. *J. Am. Chem. Soc* **2000,** 122, (38), 9071-9077.

136. Liu, J.; Lu, Y., A colorimetric lead biosensor using DNAzyme-directed assembly of gold nanoparticles. *J. Am. Chem. Soc* **2003,** 125, (22), 6642-6643.

137. Murawala, P.; Phadnis, S. M.; Bhonde, R. R.; Prasad, B. L. V., In situ synthesis of water dispersible bovine serum albumin capped gold and silver nanoparticles and their cytocompatibility studies. *Colloids and Surfaces B-Biointerfaces* **2009,** 73, (2), 224-228.

138. Connor, E. E.; Mwamuka, J.; Gole, A.; Murphy, C. J.; Wyatt, M. D., Gold nanoparticles are taken up by human cells but do not cause acute cytotoxicity. *Small* **2005,** 1, (3), 325-327.

139. Paciotti, G. F.; Kingston, D. G. I.; Tamarkin, L., Colloidal gold nanoparticles: a novel nanoparticle platform for developing multifunctional tumor targeted drug delivery vectors. *Drug Development Research* **2006,** 67, (1), 47-54.

Chapter 2

Bovine Serum Albumin reduced/capped silver and gold nanoparticles: synthesis, characterization and efforts to understand the mechanism of nanoparticle formation

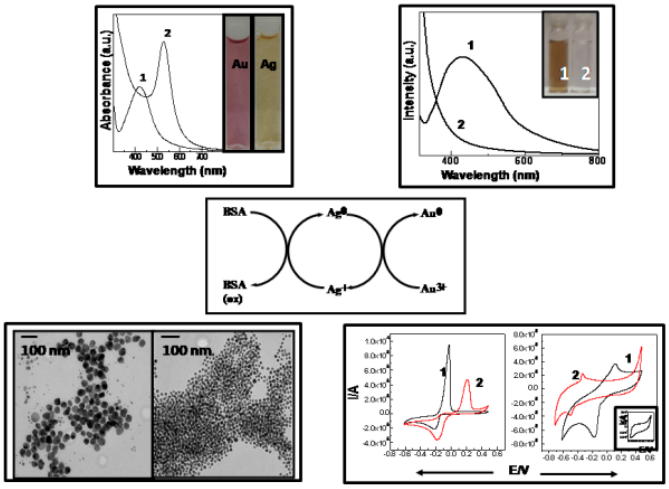

This chapter describes in detail about the synthesis of stable, water soluble Bovine Serum Albumin reduced/capped silver and gold nanoparticles. The particles are characterized using UV-vis, X-ray diffraction (XRD) and TEM measurements. The mechanism of nanoparticle formation is probed with the help of fluorescence and cyclic voltammetric studies.

Part of work has been published in:

Priyanka Murawala, S. M. Phadnis, R. R. Bhonde, B. L. V. Prasad, *Colloids and Surfaces B: Biointerfaces*, **2009**, 73, 224-228.

2.1 Introduction:

The unique electronic, optical, and catalytic properties of metal nanoparticles upon integration with biomolecules lead to the generation of new functional materials. The fact that biomolecules such as proteins, enzymes, antigens or DNA exhibit dimensions comparable to those of nanoparticles suggest that biomolecule-nanoparticles hybrid systems may represent new materials revealing combined and synergistic properties originating from the hybrid composite. A substantial progress has been accomplished in the last few decades in the synthesis and applications of biomolecule–nanoparticle hybrid systems. Having decided that BSA conjugated gold nanoparticles as a good choice for drug delivery and cell imaging studies; we carefully looked at the prior art to check for the options available to prepare such BSA-gold nanoparticle conjugates. Thorough literature survey presented us two options:

1) To prepare the nanoparticles first by established routes and then conjugate BSA to these preformed particles.
2) To prepare the nanoparticles using the BSA itself.

We will briefly review both these strategies in the following section.

1) Conjugation of biomolecules with pre-formed particles:

To apply nanoparticles for biomedical applications it is crucial to develop strategies towards their biofunctionalization. These include the proper linkage of biomolecules to nanoparticles (bioconjugation) and the design of appropriate biocompatible coatings. This section outlines the several possible strategies to bioconjugate nanoparticles.

A) Bioconjugation through electrostatic interactions:

Simple adsorption of biomolecules to the nanoparticle surface via non covalent forces represents the least demanding and easiest approach[1] (Figure 2.1 A). In such case, nanoparticles that are stabilized by anionic ligands such as citrate, tartrate, lipoic acid etc, the adsorption of positively charged proteins occurs due to electrostatic interactions[2-8]. Such an electrostatic coupling approach has been applied to link negatively charged gold and silver nanoparticles, which are produced by the citrate

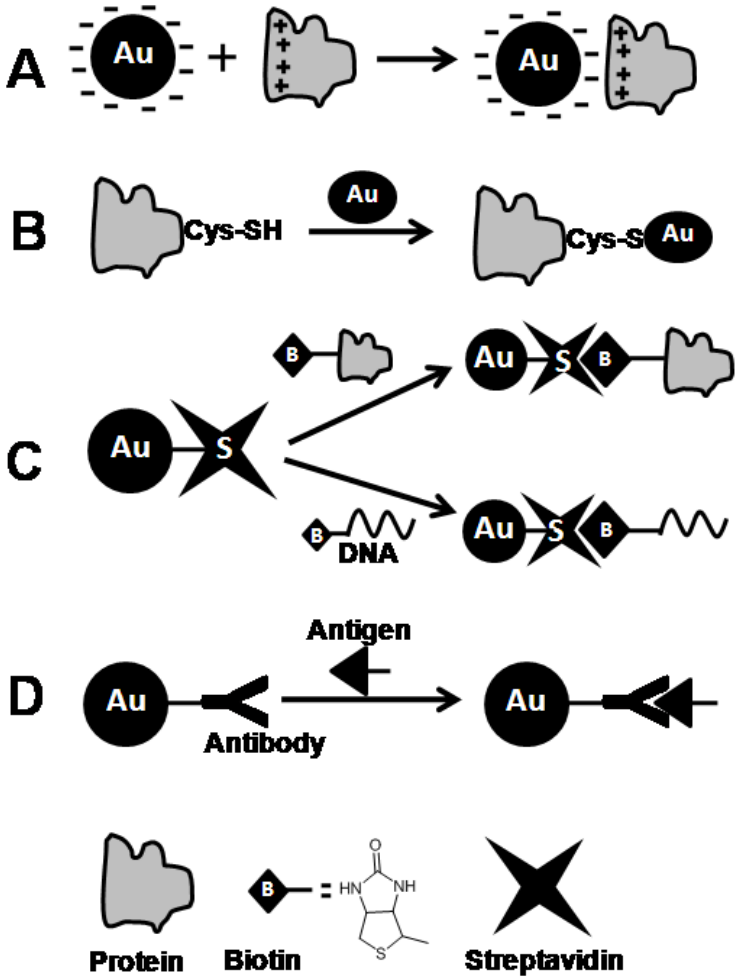

Figure 2.1: *A schematic representing formation of nanoparticle-biomolecule conjugates:* **(A)** *The assembly of nanoparticle–protein conjugates by electrostatic interactions.* **(B)** *The formation of nanoparticle–protein conjugates by adsorption of nanoparticles on thiol groups of the protein.* **(C), (D)** *The assembly of biomolecule–nanoparticle conjugates by the use of bio-affinity interactions upon streptavidin–biotin binding* **(C)** *and antibody–antigen associations* **(D) (**Adopted from Katz *et al*[1]**).**

method, with IgG molecules at pH values that are slightly above the isoelectric point of the citrate ligand[5]. This allows an effective binding between the positively charged amino acid side chains of the protein and the negatively charged citrate groups of the colloids. However, in this case, some proteins and enzymes that were directly adsorbed on nanoparticles showed conformational changes and loss of biological activity. In these procedures, the amount of bound biomolecules per nanoparticle and the proper orientation of the biomolecules on the nanoparticle surface are difficult to

control[9, 10]. Unfortunately, such simple adsorption approaches are also of limited use when applied in serum. This is because serum proteins compete with antibodies for adsorption site and may replace them[11, 12].

B) Bioconjugation through covalent interactions:

It is obvious that the activity of ligands bound to nanoparticles strongly depends on the stability of the ligand–nanoparticle linkage and the proper orientation of the ligand. To address these needs, ligands have been bound covalently to the nanoparticles using several different conjugation approaches. One of it is ligand exchange approach in which a labile capping layer such as citrate can be exchanged directly with the chemisorption of thiol-containing biomolecules (e.g. cysteine residues in IgG and serum proteins[10, 13]) having stronger binding affinity towards the metal nanoparticles (Figure 2.1 B). If no thiolated residues are available in the native proteins, thiol groups can be incorporated by chemical means, for example, with 2-iminothiolane[14] or by genetic engineering. Similarly, n-alkylthiolated DNA and DNA containing several adenosyl phosphothioate residues at their ends have been used to interact directly with the metal surface of nanoparticles[15, 16].

Another popular approach is to use low molecular bifunctional linkers, which on one end have thiols, disulfides and phosphine anchor groups for their attachment to nanoparticles surfaces and functional groups on the other end for their further covalent coupling to the target biomolecules[10, 17-19]. These anchor groups substitute weakly adsorbed molecules to stabilize the pre-synthesized nanoparticles or may be incorporated during the synthesis of the nanoparticle to yield a functionalized nanoparticle surface. Scheme 2.1 shows fabricated delivery systems based on gold nanoparticles bearing functional moieties, which are anchored with thiol linkers, in their monolayers. A wide variety of monolayer protected clusters (MPCs) can be formed rapidly and in scalable fashion using the one-pot protocol developed by Schiffrin *et al*. in 1994 (Scheme 2.1)[20]. In this preparation, $AuCl_4^-$ salts are reduced with $NaBH_4$ in the presence of the desired thiol capping ligand or ligands. The core size of the particles can be varied from 1.5 nm to ~6 nm by varying the thiol–gold stoichiometry. The functional diversity of MPCs can be extended through the formation of mixed monolayer protected clusters (MMPCs) that can be synthesized directly or through post-functionalization of MPCs. A versatile method for the

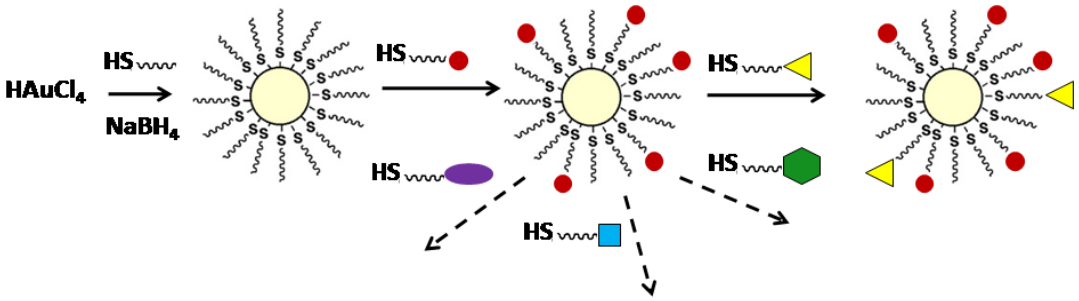

Scheme 2.1: *Formation of MPCs using the Schiffrin reaction and MMPCs using the Murray's place-exchange reaction.*

creation of MMPCs is the place-exchange reaction developed by Murray (Scheme 2.1)[21]. In this protocol, foreign thiols displace the native ligands of MPCs in an equilibrium process. A wide variety of terminal functional groups are available in different bifunctional linkers. Most commonly amine, active ester, and maleimide groups are used to couple biological compounds covalently by means of carbodiimide-mediated esterification and amidation reactions or through reactions with thiol groups[1, 10]. Another approach is to link biotinylated ligands or target biomolecules to streptavidin (or avidin)-functionalized nanoparticles with high specificity (Figure 2.1 C). In this case, the biotin-binding proteins, avidin or streptavidin, act as linker molecules[22, 23]. Also, nanoparticle–antibody conjugates were used for affinity binding of their respective antigens (Figure 2.1 D)

However, the ligand replacement reaction certainly has several disadvantages. First, unlike direct synthesis, it is a multi-step process. Secondly, harsh reaction conditions often lead to the degradation and inactivation of sensitive biological compounds. Thirdly, ligand exchange reactions occur at the colloid surface and often hinder the formation of stable bioconjugates. Lastly, the synthesis of stoichiometrically defined nanoparticle-biomolecule complexes is a great challenge, and is particularly important from a molecular engineering point of view to generate well defined nanostructures.

2) Direct synthesis of nanoparticles by the biomolecules itself:

In situ synthetic methods for the generation of nanoparticles by the biomolecules itself are gaining much interest, as they avoid the use of any external reducing agent or stabilizer and are a one-step process. This method has advantages of:

- Minimizing the number of steps involved in synthesizing nanoparticles and then tagging them with ligands as it is a one step process,
- Avoiding the formation of any toxic byproducts which can limit biological applications of the conjugate,
- Minimizing the possibility of aggregation of nanoparticles which can occur while attaching biomolecules on the surface of nanoparticles by various methods (e.g. adsorption, ligand exchange, covalent cross linking etc.).

In one interesting report, Mandal and coworkers have demonstrated the formation of gold and silver nanoparticles by using the redox-active tyrosine/tryptophan-based peptides[24-27]. Further, Rangnekar *et al* have shown that pure enzyme α-Amylase can be used for the reductive synthesis of gold nanoparticles without any loss of enzymatic activity and without the need of any chemical reducing agent[28]. These results gave us inspiration and we started looking for a procedure for synthesizing gold nanoparticles using BSA as a reducing and capping agent. Serum albumins are the most abundant proteins in the blood plasma and major soluble protein constituents of the circulatory system[29]. However, it has been reported that BSA cannot reduce Au^{3+} ions to Au^{0} under normal circumstances.

Taking the inability of BSA to reduce Au^{3+} to Au^{0} as a challenge, in the past few years, attempts were made to synthesize gold nanoparticles by using BSA. In 2007, Xie *et al* have demonstrated the synthesis of gold triangular and hexagonal nanoplates by the reduction of chloroaurate ions by BSA at 37° C for 48 h[30]. In the same year another report for the synthesis of gold nanoparticles by BSA at elevated temperature was published by Basu *et al*[31]. Similarly, in 2008, Housini *et al* have synthesized gold nanoparticles photochemically by using BSA in the presence of a photoinitiator, Irgacure (I-2959)[32]. However, in all the above instances elevated temperatures [31] and/or long periods[30] or photo-irradiation in the presence of additional initiators had to be resorted to unveil the reducing nature of BSA[32].

We have been looking for a simple and green method for the synthesis of silver and gold nanoparticles using Bovine serum albumin as a capping and reducing agent under ambient condition and in aqueous medium. The work incorporated in this

chapter reports our successful accomplishments of the synthesis of silver and gold nanoparticles using BSA as a capping and reducing agent albeit simultaneous to many of the reports described above.

2.2 Experimental details:

This section describes the synthetic procedure used to make silver and gold nanoparticles using BSA as reducing and capping agent at room temperature (Figure 2.2). The experimental conditions maintained were as following:

2.2.1Synthesis of silver and gold nanoparticles by BSA:

2.2.1.A *Synthesis of silver nanoparticles*

For the synthesis of silver nanoparticles, in the 25 mL of reaction mixture only $AgNO_3$ was added to the BSA solution and the pH was adjusted to 3.7. The final concentration of $AgNO_3$ into the solution was $1x10^{-3}$ M.

2.2.1.B *Synthesis of gold nanoparticles*

While exploring the synthesis of gold nanoparticles, two reaction conditions were maintained which were as follows:

i) In the first experiment, a predetermined amount of $HAuCl_4$ that leads to a concentration of $5x10^{-4}$ M in the final solution, was added to the BSA solution (3 mg/mL) whose pH was adjusted to 3.7 by adding HCl (3 N)). The final volume of reaction mixture was 25 mL.

ii) In the second synthetic condition, both $HAuCl_4$ (final concentration in solution $5x10^{-4}$ M) and $AgNO_3$ ($1x10^{-3}$ M final concentration) were added to the BSA solution (3 mg/mL). The pH was adjusted to 3.7 and the final volume of the reaction mixture was 25 mL.

Reactions were kept at room temperature and at regular time intervals formation of silver and gold nanoparticles by BSA were monitored spectroscopically. The as prepared gold and silver nanoparticle solutions were then taken further for TEM and XRD analysis. We found evidence of silver nanoparticles formation (when $AgNO_3$ alone was added to BSA) and gold nanoparticle formation (where $AgNO_3$ and $HAuCl_4$ were both added to BSA). However, upon XRD analysis we found that AgCl impurity was present in these nanoparticle suspensions. To remove the impurity, 2 mL

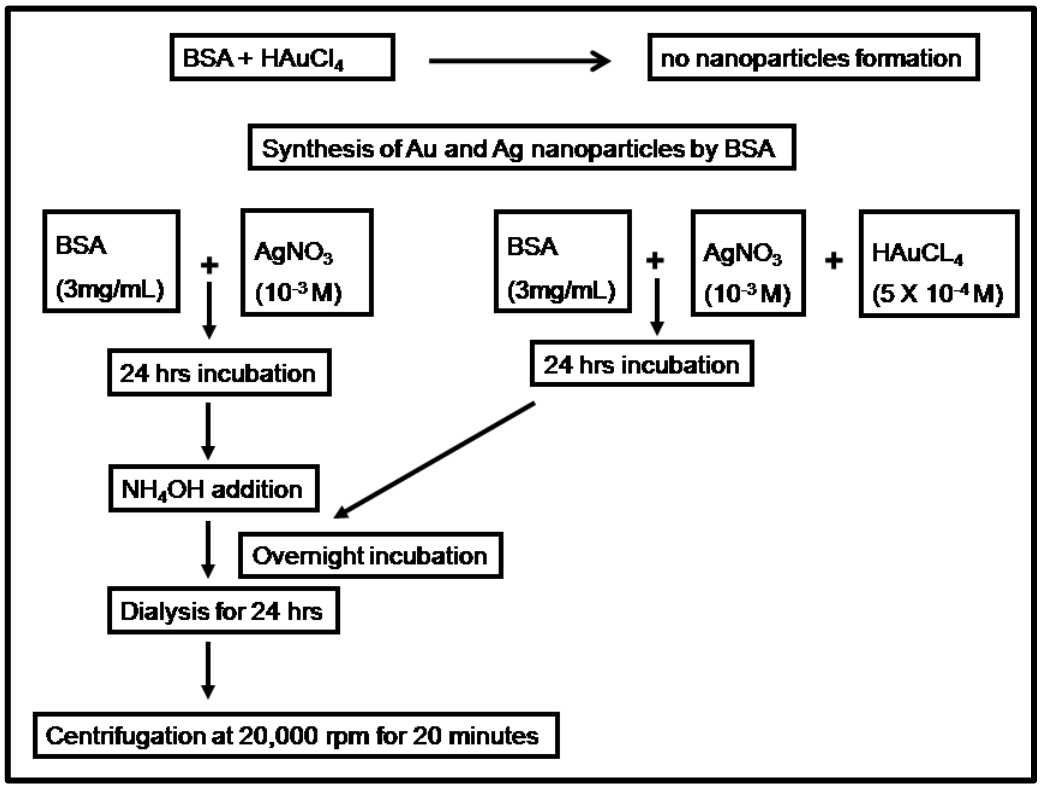

Figure 2.2: *A schematic representation for the synthesis of silver and gold nanoparticles using BSA as a reducing and capping agent.*

of NH_4OH was added to the final reaction products. These solutions were then furtherpurified by dialyzing them against Millipore water for 24 h using a dialysis bag with a cut off value of 12.5 kDa. Further purification was done by subjecting the solutions to centrifugation at 20,000 rpm for 20 minutes. These purification methods completely removed any AgCl formed as the reaction side product. The resulting pellets were redispersed in deionised water and were used for further characterization.

2.3 Results and Discussion:

This section is divided into two parts dealing with the results obtained with as prepared and purified gold and silver nanoparticles separately.

A) As prepared gold and silver nanoparticles:

2.3.1UV-vis absorption spectroscopy:

Stable colloidal solutions of nanoparticles were subjected to UV-vis spectral analysis to study the optical properties. Figure 2.3 A shows the UV-vis absorption spectra of as prepared gold and silver nanoparticles suspensions. Curve 1 show the absorption

spectrum recorded when only $HAuCl_4$ was added to the BSA solution. No characteristic SPR signature of gold nanoparticles was obtained suggesting that nanoparticle synthesis has not occurred[33]. This is in accordance with the reported literatures where BSA has reportedly failed to synthesize gold nanoparticles under

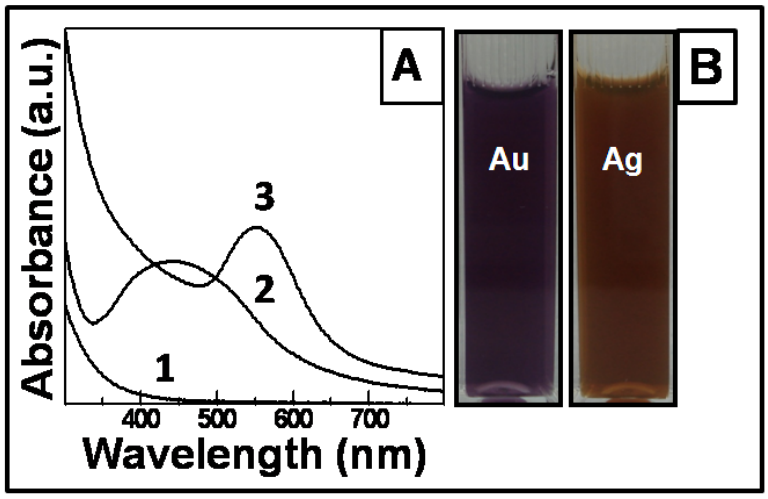

Figure 2.3 (A) *UV-vis absorption spectra corresponding to the addition of only $HAuCl_4$ (Curve 1), only $AgNO_3$ (Curve 2) and $AgNO_3$ + $HAuCl_4$ (Curve 3) respectively to BSA.* **(B)** *Photograph depicting the as prepared Au-BSA and Ag-BSA.*

normal conditions[28, 30]. It was hypothesized that the synthesis of Au nanoparticles by proteins would involve the free thiol groups present in cysteine residues. Support from this hypothesis was drawn from the fact that α-amylase and *Eco*RI having 2 and1 cysteine moieties could reduce Au^{3+} to Au^0 nanoparticles[28]. It was argued that while BSA also had a cysteine group, this residue is buried deep down in the three dimensional structure and hence is not accessible to reduce Au^{3+} to gold nanoparticles[28]. Similarly, Xie *et al* observed that incubating Au^{3+} did not yield any gold nanoparticle formation with BSA at room temperature[30]. However, when the temperature was increased to 37° C plate like gold nanoparticles were seen to form.

We observed that while incubating $HAuCl_4$ with BSA did not lead to any nanoparticle formation, addition of Ag^+ only to BSA at a pH 3.7 did result in the formation of silver nanoparticles. It is well known that silver metal can reduce Au^{3+} to Au^0. The redox reaction between silver and gold ions can be represented in the following way:

$$3\ Ag^0 + Au^{3+} \longrightarrow Au^0 + 3\ Ag^+$$

Accordingly when we added Ag^+ and Au^{3+} ions together to BSA (at pH-3.7) the reaction mixture started developing a violet color indicating the gold nanoparticle formation. Curve 3 shows the absorption spectrum recorded from this solution having SPR maxima at 552 nm. Similarly, when silver ions alone were added to BSA, a brown color (Figure 2.3 B) characteristic to silver nanoparticles formation started developing. Absorption spectra recorded for the same showed a broad nature of SPR band with peak maxima at 441 nm (Curve 2). The broad nature of SPR peaks for both gold and silver colloidal solutions indicated aggregated nanostructures. This was also ascertained by the TEM images (Figure 2.4 A and B).

2.3.2 Transmission Electron Microscopy:

The TEM images obtained from the as prepared gold and silver nanoparticle solutions are shown in the Figure 2.4 A and B respectively. TEM images clearly show aggregated and polydisperse nanoparticles explaining the broad nature of SPR bands of both gold and silver colloidal suspensions.

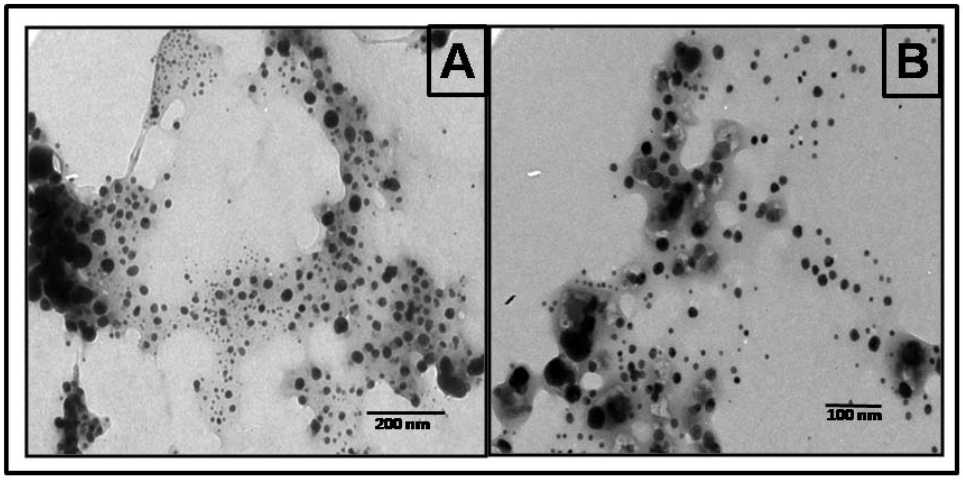

Figure 2.4 (A) *Representative TEM images of as prepared gold* **(A)** *and silver* **(B)** *nanoparticles.*

2.3.3 X-Ray Diffraction analysis:

X-Ray diffraction analysis of as prepared gold and silver nanoparticles was carried out to determine the crystallinity and structure of nanoparticles. Figure 2.5 A and B shows the X-Ray curve obtained from the gold and silver nanoparticle suspensions. Diffractograms obtained clearly show the presence of AgCl impurities formed as the

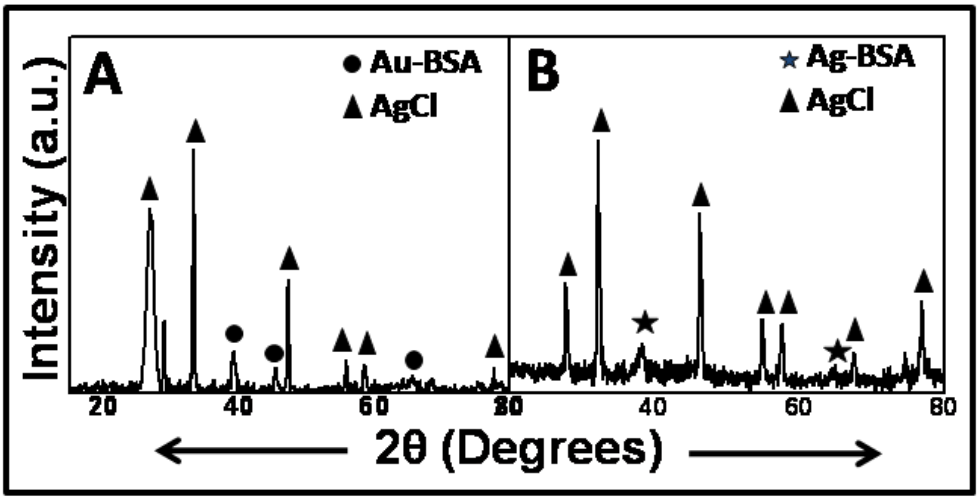

Figure 2.5 (A) *X-ray diffractograms of as prepared* **(A)** *gold and* **(B)** *silver nanoparticles. Intense AgCl peaks show the presence of impurity in nanoparticle suspensions.*

side product. To remove this, NH_4OH was added followed by the dialysis for 24 h and then centrifuged at 20,000 rpm for 20 minutes.

B) Purified gold and silver nanoparticles:

2.3.4UV-vis absorption spectroscopy:

Curve 1 of Figure 2.6 A show the absorption spectrum recorded from the purified silver nanoparticle (hereafter called as Ag-BSA) solution having SPR maxima at 420 nm. Compared to the UV-vis of as prepared product a 21 nm blue shift in the SPR peak positions and narrowing of the peak along with the change in the color from brown to yellow was obtained. Similarly, after purification, for the gold nanoparticle (hereafter called as Au-BSA) solution (Curve 2), a 25 nm blue shift and narrowing of the peak (peak maxima at 526 nm) compared to the UV-vis of as prepared product along with the change in the color from violet to ruby red was seen. These changes in the peak characteristics can be attributed to the narrowing of size distribution, evasion of aggregation after the removal of AgCl impurities from the nanoparticles suspensions followed by purification step[33].

2.3.5 Transmission Electron Microscopy:

The TEM images obtained from the purified Ag-BSA and Au-BSA nanoparticle solutions are shown in the Figure 2.7 A and B respectively. TEM images show well separated nanoparticles. The gold nanoparticles are also characterized with very

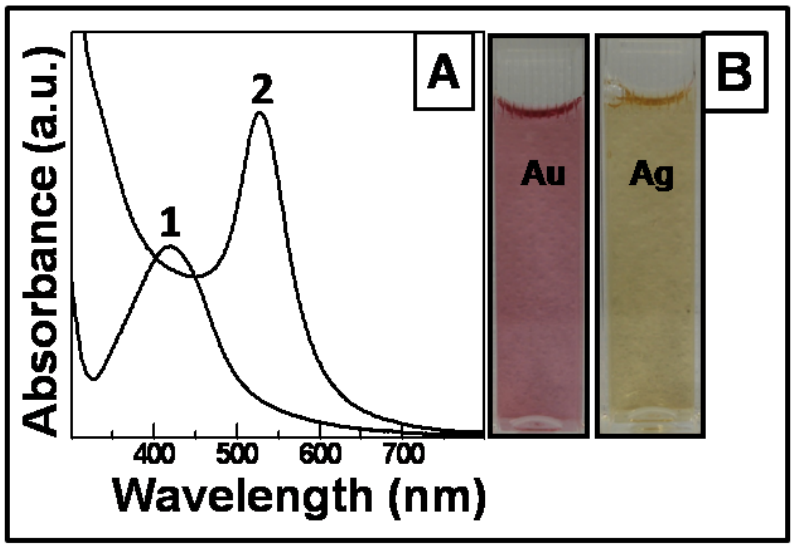

Figure 2.6 (A) *UV-vis absorption spectra of purified Ag-BSA (Curve 1) and Au-BSA (Curve 2) nanoparticles respectively.* **(B)** *Photographs depicting the purified Au-BSA and Ag-BSA nanoparticles.*

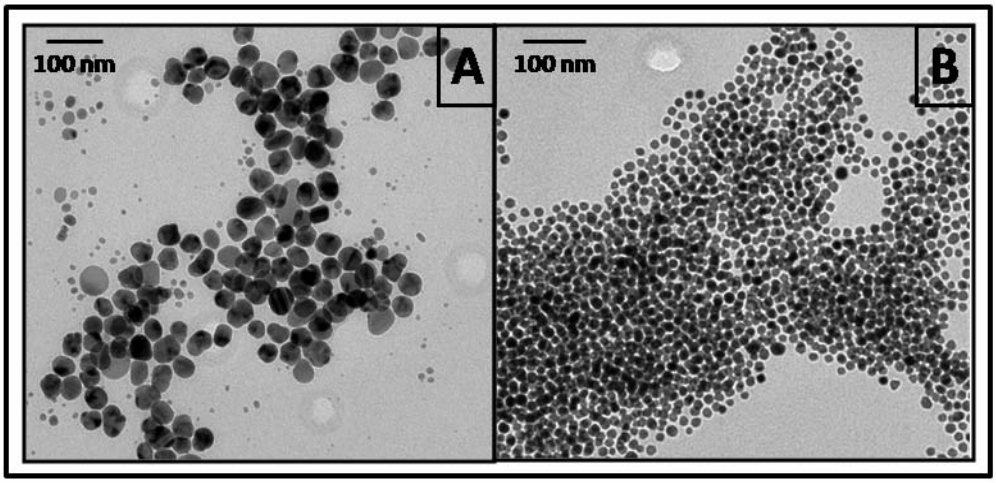

Figure 2.7 (A) *Representative TEM images of purified Ag-BSA* **(A)** *and Au-BSA* **(B)** *nanoparticles*

narrow size distribution. This is in accordance with presence of sharper SPR signatures in the purified samples.

2.3.6 X-Ray Diffraction analysis:

Figure 2.8 shows the X-Ray analysis of purified Au-BSA and Ag-BSA nanoparticles. Both the curves clearly show that AgCl impurity has been removed completely

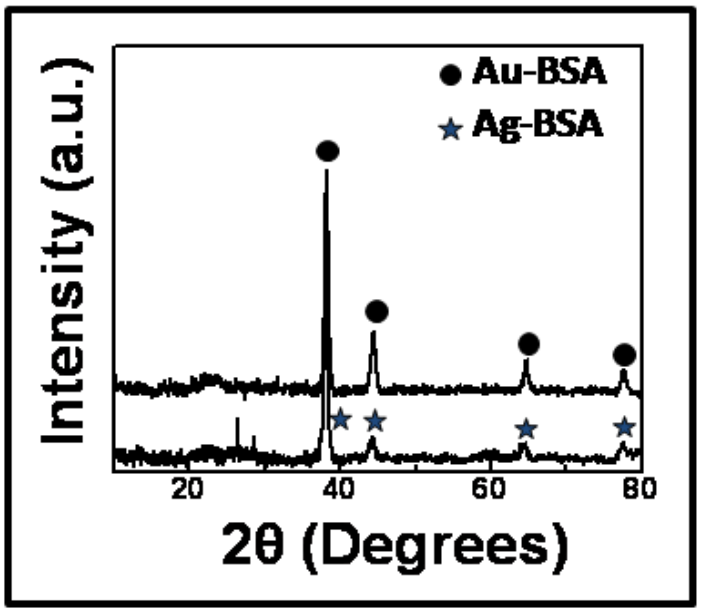

Figure 2.8 *X-ray diffractograms of purified Au-BSA and Ag-BSA nanoparticles.*

following the NH_4OH addition and dialysis and peaks corresponding only to metallic Au and Ag are present. The XRD pattern in both the cases corresponds well to the fcc crystalline phase of these metals.

2.3.7 Particle size distribution analysis of Au-BSA and Ag-BSA:

Particle size distribution analysis of 150 nanoparticles was done from the TEM images captured from different areas. The size of Au-BSA as inferred from the graph (Figure 2.9) is ~15 nm. Ag-BSA showed a bimodal distribution with particle sizes of 25 nm and 45 nm dominating the population.

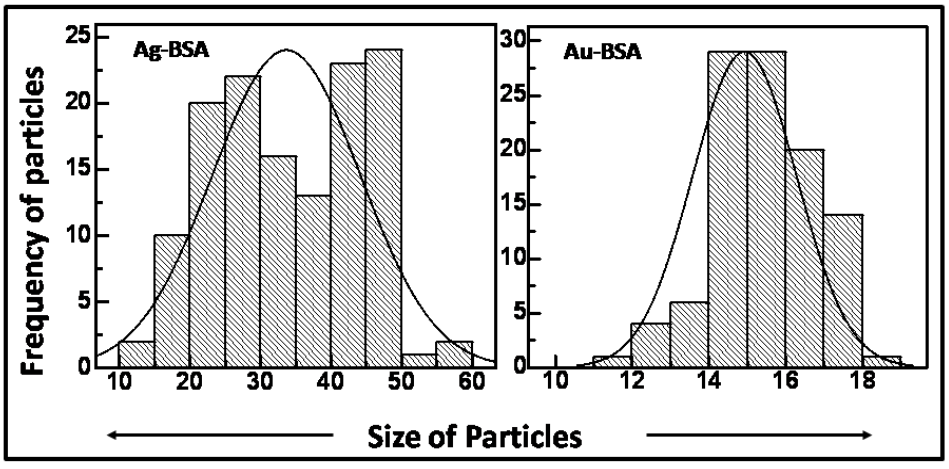

Figure 2.9 *Particle size distributions of Ag-BSA and Au-BSA nanoparticles respectively.*

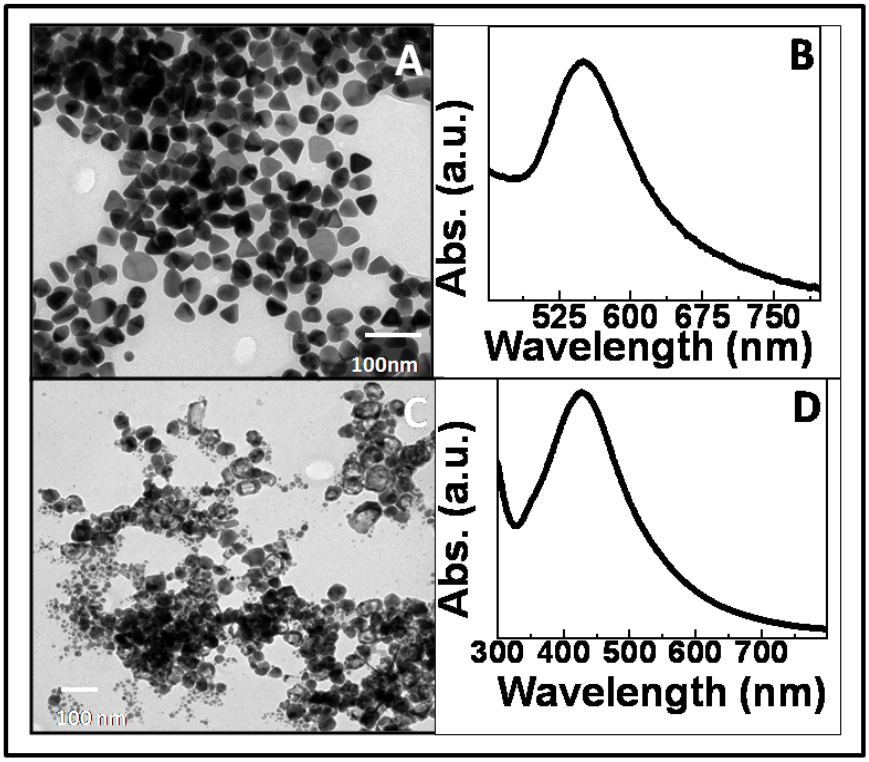

Figure 2.10 (A) *TEM image of sample obtained when Ag^{+} ($1x10^{-5}$ M) and Au^{3+} ($5 x10^{-4}$ M) and* **(B)** *shows the respective absorption spectra.* **(C)** *TEM image of sample obtained when $1x10^{-2}$ M Ag^{+} and $5 x10^{-4}$ M Au^{3+} were added simultaneously to BSA and Figure* **(D)** *shows the respective absorption spectra.*

2.3.8 Determination of the mechanism of nanoparticles synthesis by BSA:

2.2.8.1 Effect of the concentration of silver ions on the gold nanoparticles synthesis:

From the results obtained so far we could clearly deduce that presence of silver ions is a pre-requisite for the synthesis of Au-BSA nanoparticles. To determine the effect of varying concentrations of Ag^{+} on the gold nanoparticles synthesis, experiments were performed with different concentrations of Ag^{+} and a constant concentration of Au^{3+} (5×10^{-4} M). Figure 2.10 A shows the TEM images of particles obtained when a low concentration of Ag^{+} ($1x10^{-5}$ M) was used. Here, Au-BSA nanoparticles formed were polyhedral in nature and larger in size. Figure 2.10 B shows the respective UV-vis absorption curve with maxima at 550 nm. On the other hand, when the concentration of Ag^{+} was high ($1x10^{-2}$ M), few hollow structures were obtained (Figure 2.10 C). Figure 2.10 D shows the respective UV-vis absorption curve with maxima at 425 nm. In order to establish the mechanism of synthesis of nanoparticles, a systematic attempt

was made to determine the role of Ag^+ in gold nanoparticle synthesis. It was observed very evidently that gold nanoparticles were not formed when chloroauric acid was added to BSA while BSA reduced silver ions to silver nanoparticles on the other hand. Interestingly when both silver ions and gold ions are present in the BSA solution, gold nanoparticles were formed and not silver nanoparticles. These results when taken together shows that when both the ions are present in the solution, Ag^+ is first reduced to Ag^0 by BSA and these Ag^0 in turn get consumed in a galvanic exchange reaction while reducing the Au^{3+} to Au^0 [34, 35]. Hence experiments were done in which concentration of Au^{3+} was kept constant while concentration of Ag^+ was varied. When the concentration of Ag^+ is low in comparison to the Au^{3+}, the reaction occurs slowly as the metallic silver (that acts as a reducing agent for Au^{3+} ions) formed needs to be recycled for the complete conversion of Au^{3+} ions into Au^0 state. Hence in this case gold nanoparticles formed will be bigger in size as a distinct nucleation and growth steps occur (Figure 2.10 A). When the concentration of Ag^+ is more than that of Au^{3+}, all Au^{3+}gets consumed at once and more uniform and narrow size distribution of particles are obtained. At the same time, when silver concentration is very high, only partial galvanic exchange reaction occur leading to the formation of hollow and irregular structures (Figure 2.10 B). Such a trend is typical of galvanic exchange reactions wherein nanoparticles of silver act as sacrificial templates for formation of gold nanostructures[34, 35]. A schematic of the above description is shown in Figure 2.11.

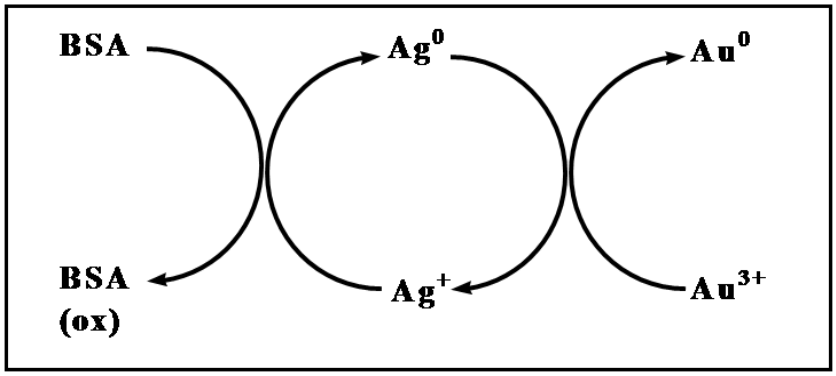

Figure 2.11 *Schematic representation of in-situ reduction of gold nanoparticles by BSA.*

2.2.8.2 N-bromosuccinimide (NBS) modification studies of tryptophan residues of BSA:

BSA is a small protein with a single polypeptide chain of molecular weight 66 kDa, which is cross-linked by 17 disulfide bonds [36]. It comprises of 583 amino acid residues out of which several amino acids have sulfur-, oxygen- and nitrogen- bearing groups which can potentially reduce Au^{3+} and Ag^{+} to produce nanoparticles and adsorb on the surface[37]. More specifically, it consists of 21 tyrosine residues and two tryptophan (Trp) residues. Amino acids especially tryptophan and tyrosine have been known to reduce metal ions to their metallic form and cap resultant nanoparticles [38-40]. In the present study it appears that the Trps are responsible for the reduction of Ag^{+} to Ag^{0} by BSA and that is ascertained the following way. NBS is well known to cause the oxidation of the indole ring of Tryptophan (Trp) to oxindole [41, 42]. It is also reported that in the case of serum albumins addition of 10-20 moles of N-bromosuccinimide (NBS) per mole of Trp causes the oxidation of Trp. So we have added 20 moles of NBS per mole of Trp to completely oxidize all the Trp present in

.

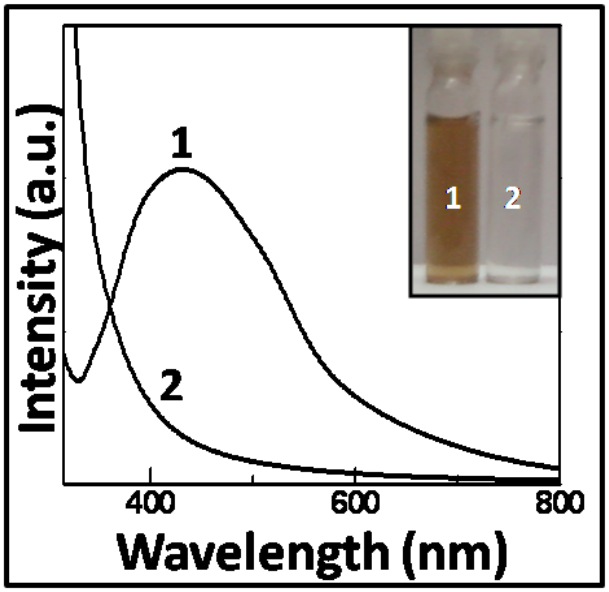

Figure 2.12 *UV-vis spectra of BSA treated with $AgNO_3$ (curve 1) and BSA with $AgNO_3$ after 1 h incubation with N-bromosuccinimide (curve 2). Inset shows the sample vials containing solutions corresponding to curve 1 and curve 2 respectively.*

BSA. Curve 1 of Figure 2.12 shows the absorption spectrum obtained when silver was added to the BSA solution. On the other hand when BSA was incubated with NBS for 1 h followed by the addition of Ag^{+} no SPR band of Ag-BSA was obtained as can be

seen from the curve 2. Inset shows the sample vials containing solutions corresponding to curve 1 and curve 2 respectively. This result proves our hypothesis that Trp residues of BSA are responsible for Ag^{+} reduction (Figure 2.12). If tyrosine residues were also involved in the reduction, the reduction should have still occurred as they reportedly need more NBS to get completely oxidized[40].

2.2.8.3 Cyclic Voltametry studies:

Cyclic voltammetry (CV) is a powerful technique for the investigation of redox reactions in aqueous solution, surface deposition and adsorption [43-45]. There have been a number of reports on the CV studies of protein using mercury electrodes [46] but the strong absorption of BSA molecule on the metal electrode surface may induce the

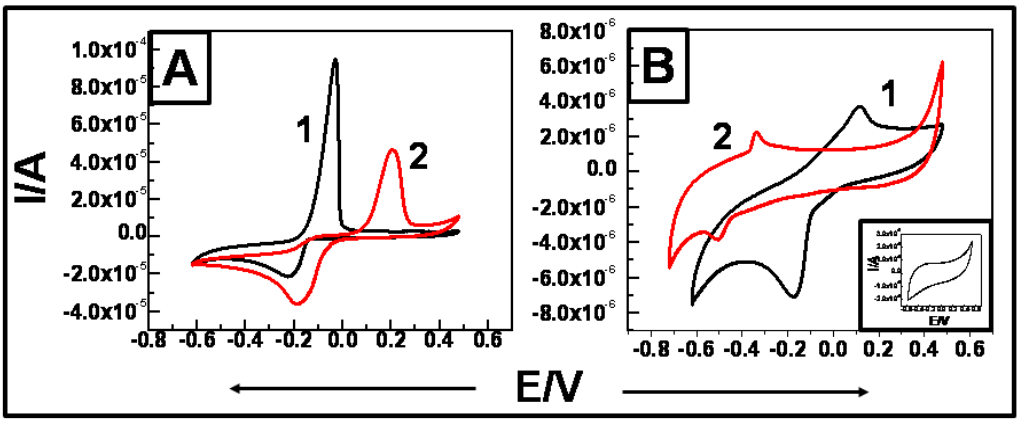

Figure 2.13 (A) *Cyclic voltammograms of* **(A)** *Ag^{+} (Curve 1) and Au^{3+} (Curve 2) in water with Na_2SO_4 as supporting electrolyte and* **(B)** *Ag^{+} (Curve 1) and Au^{3+} (Curve 2) in BSA solution at pH 3, using RHE as the reference electrode, at a scan rate of 50 mV/s.*

conformational changes and hence can lead to variation in the CV studies [36]. Thus in order to reduce the influence of BSA adsorption, a glassy carbon electrode is a recommended choice and hence was used in our study. To perform the electrochemical studies, gold and silver salts were dissolved in deionised water and sodium sulphate was used as supporting electrolyte. These were subjected to CV scans at 50 mVs^{-1} scan rate. Figure 2.13, curve 1 shows a typical cyclic voltammograms of silver on glassy carbon electrode conducted in an aqueous solution, where the cathodic peak was observed at a potential – 0.22 mV and the

anodic peak potential is -0.03 mV. Curve 2 shows the cyclic voltammograms of Au^{3+} in water where the cathodic peak is observed at – 0.19 mV and the anodic peak at +0.21 mV. Figure 2.13 B shows the cyclic voltammograms of both silver and gold ions in BSA solution. For this experiment, $HAuCl_4$ and $AgNO_3$ were added to the BSA solution and were subsequently subjected to the CV studies. From the curves 1 and 2, it is clearly visible that the cathodic and anodic peak potentials of Ag^+ and Au^{3+} in presence of BSA have drastically changed as compared to the same in case of pure aqueous solutions. Curve 1 represents the CV of Ag^+ in BSA solution having its cathodic and anodic peaks at -0.17 mV and +0.12 mV respectively. The cathodic and anodic peaks of Au^{3+} in BSA (curve 2) are -0.51 mV and -0.33 mV respectively. Inset in Figure B shows the cyclic voltammograms of pure BSA in water showing no redox peaks.

On comparing the redox peak positions of both the metal ions in Figure 2.13 A, it can be clearly seen that the reduction of gold ions is energetically more favorable than the silver ions in simple water. However, when the same metal ions are added to BSA solutions and scanned for CV analysis, dramatic changes in the redox peak positions were obtained (Figure 2.13 B). The curve 1 shows the condition when Ag^+ were added to the BSA solution. The reduction peak position has shifted from – 0.22 mV to -0.17 mV depicting that reduction of silver ions by BSA molecules is more feasible. In contrast to it, when Au^{3+} was added to BSA solution, reduction peak position has drastically shifted to more negative value i.e. from - 0.19 mV to - 0.51 mV. This predicts that reduction of gold ions by BSA molecules is energetically less favorable in comparison to the reduction of sliver ions by BSA. These results are in tune with our results where when only $HAuCl_4$ was added to the BSA solution no gold nanoparticle formation occurred whereas upon addition of silver to BSA, silver nanoparticles formed. Inset in the Figure 2.13 B shows the cyclic voltammogram of BSA. There are no redox peaks for the BSA and this is in accordance with the reported literature[36, 46]. CV results show that even though under normal conditions, reduction of gold ions is electrochemically more favorable than silver ions; in the presence of BSA the opposite happens. The mechanism or the reason behind this is yet far from clear and for the better understanding and insight, a detailed mechanistic study in the future is needed.

2.4 Conclusion:

A very simple and eco-friendly protocol for the green synthesis of gold and silver nanoparticles has been developed. In this the metal nanoparticles produced are reduced and capped by Bovine serum albumin. An attempt was made to determine the mechanism of nanoparticle synthesis by BSA. It was observed that when silver and gold ions are taken together the Ag^{+} are reduced to metallic silver first and a galvanic exchange reaction between them and Au^{3+} ions results in the formation of gold nanoparticles. From our NBS oxidation studies it is observed that tryptophan residues of BSA are proposed to be responsible for the reduction of silver ions to the nanoparticles. CV studies shows that when silver ions are present in the BSA solution, reaction is electrochemically favored which is accordance with our findings that BSA reduces silver ions and not gold ions.

References:

1. Katz, E.; Willner, I., Integrated nanoparticle-biomolecule hybrid systems: synthesis, properties, and applications. *Angewandte Chemie International Edition* **2004,** 43, (45), 6042-6108.

2. Larsericsdotter, H.; Oscarsson, S.; Buijs, J., Thermodynamic analysis of proteins adsorbed on silica particles: electrostatic effects. *Journal of colloid and interface science* **2001,** 237, (1), 98-103.

3. Meziani, M. J.; Rollins, H. W.; Allard, L. F.; Sun, Y. P., Protein-protected nanoparticles from rapid expansion of supercritical solution into aqueous solution. *J. Phys. Chem. B* **2002,** 106, (43), 11178-11182.

4. Meziani, M. J.; Sun, Y. P., Protein-conjugated nanoparticles from rapid expansion of supercritical fluid solution into aqueous solution. *J. Am. Chem. Soc* **2003,** 125, (26), 8015-8018.

5. Shenton, W.; Davis, S. A.; Mann, S., Directed self-assembly of nanoparticles into macroscopic materials using antibody-antigen recognition. *Advanced Materials* **1999,** 11, (6), 449-452.

6. Macdonald, I. D. G.; Smith, W. E., Orientation of cytochrome c adsorbed on a citrate-reduced silver colloid surface. *Langmuir* **1996,** 12, (3), 706-713.

7. Ibano, D.; Yokota, Y.; Tominaga, T., Preparation of gold nanoplates protected by an anionic phospholipid. *Chemistry Letters* **2003,** 32, (7), 574-575.

8. Mattoussi, H.; Mauro, J. M.; Goldman, E. R.; Anderson, G. P.; Sundar, V. C.; Mikulec, F. V.; Bawendi, M. G., Self-Assembly of CdSe- ZnS Quantum Dot Bioconjugates Using an Engineered Recombinant Protein. *J. Am. Chem. Soc* **2000,** 122, (49), 12142-12150.

9. Kumar, C., *Biofunctionalization of Nanomaterials*. Wiley-VCH: 2005.

10. Niemeyer, C. M., Nanoparticles, proteins, and nucleic acids: biotechnology meets materials science. *Angewandte Chemie International Edition* **2001,** 40, (22), 4128-4158.

11. Illum, L.; Jones, P. D. E.; Kreuter, J.; Baldwin, R. W.; Davis, S. S., Adsorption of monoclonal antibodies to polyhexylcyanoacrylate nanoparticles and subsequent immunospecific binding to tumour cells in vitro. *International Journal of Pharmaceutics* **1983,** 17, (1), 65-76.

12. Kubiak, C.; Manil, L.; Couvreur, P., Sorptive properties of antibodies onto cyanoacrylic nanoparticles. *International Journal of Pharmaceutics* **1988,** 41, (3), 181-187.

13. Hayat, M. A., Colloidal gold. Principles, methods, and applications. *San Diego, etc* **1989,** 2.

14. Ghosh, S. S.; Kao, P. M.; McCue, A. W.; Chappelle, H. L., Use of maleimide-thiol coupling chemistry for efficient syntheses of oligonucleotide-enzyme conjugate hybridization probes. *Bioconjugate Chemistry* **1990,** 1, (1), 71-76.

15. Bardea, A.; Dagan, A.; Ben-Dov, I.; Willner, I.; Amit, B., Amplified microgravimetric quartz-crystal-microbalance analyses of oligonucleotide complexes: a route to a Tay–Sachs biosensor device. *Chemical Communications* **1998,** 1998, (7), 839-840.

16. Patolsky, F.; Ranjit, K. T.; Lichtenstein, A.; Willner, I., Dendritic amplification of DNA analysis by oligonucleotide-functionalized Au-nanoparticles. *Chemical Communications* **2000,** 2000, (12), 1025-1026.

17. Safer, D.; Bolinger, L.; Leigh Jr, J. S., Undecagold clusters for site-specific labeling of biological macromolecules: simplified preparation and model applications. *Journal of inorganic biochemistry* **1986,** 26, (2), 77-91.

18. Dubertret, B.; Calame, M.; Libchaber, A. J., Single-mismatch detection using gold-quenched fluorescent oligonucleotides. *Nature biotechnology* **2001,** 19, (4), 365-370.

19. Alivisatos, A. P.; Johnsson, K. P.; Peng, X.; Wilson, T. E.; Loweth, C. J.; Bruchez, M. P.; Schultz, P. G., Organization of'nanocrystal molecules' using DNA. *Nature* **1996,** 382, (6592), 609-611.

20. Brust, M.; Walker, M.; Bethell, D.; Schiffrin, D. J.; Whyman, R. J., Synthesis of thiol-derivatized gold nanoparticles in a 2-phase liquid system, Chem. Soc. *Chem. Commun* **1994,** 7, 801-802.

21. Templeton, A. C.; Wuelfing, W. P.; Murray, R. W., Monolayer-protected cluster molecules. *Accounts of chemical research* **2000,** 33, (1), 27-36.

22. Goldman, E. R.; Balighian, E. D.; Mattoussi, H.; Kuno, M. K.; Mauro, J. M.; Tran, P. T.; Anderson, G. P., Avidin: a natural bridge for quantum dot-antibody conjugates. *J. Am. Chem. Soc* **2002,** 124, (22), 6378-6382.

23. Connolly, S.; Fitzmaurice, D., Programmed assembly of gold nanocrystals in aqueous solution. *Advanced Materials* **1999,** 11, (14), 1202-1205.

24. Si, S.; Mandal, T. K., Tryptophan Based Peptides to Synthesize Gold and Silver Nanoparticles: A Mechanistic and Kinetic Study. *Chemistry–A European Journal* **2007,** 13, (11), 3160-3168.

25. Si, S.; Bhattacharjee, R. R.; Banerjee, A.; Mandal, T. K., A Mechanistic and Kinetic Study of the Formation of Metal Nanoparticles by Using Synthetic Tyrosine Based Oligopeptides. *Chemistry–A European Journal* **2006,** 12, (4), 1256-1265.

26. Si, S.; Dinda, E.; Mandal, T. K., In Situ Synthesis of Gold and Silver Nanoparticles by Using Redox Active Amphiphiles and Their Phase Transfer to Organic Solvents. *Chemistry–A European Journal* **2007,** 13, (35), 9850-9861.

27. Bhattacharjee, R. R.; Das, A. K.; Haldar, D.; Si, S.; Banerjee, A.; Mandal, T. K., Peptide-Assisted Synthesis of Gold Nanoparticles and Their Self-Assembly. *Journal of nanoscience and nanotechnology* **2005,** 5, (7), 1141-1147.

28. Rangnekar, A.; Sarma, T. K.; Singh, A. K.; Deka, J.; Ramesh, A.; Chattopadhyay, A., Retention of Enzymatic Activity of -Amylase in the Reductive Synthesis of Gold Nanoparticles. *Langmuir* **2007,** 23, (10), 5700-5706.

29. Ravindran, A.; Singh, A.; Raichur, A. M.; Chandrasekaran, N.; Mukherjee, A., Studies on interaction of colloidal Ag nanoparticles with Bovine Serum Albumin (BSA). *Colloids and Surfaces B: Biointerfaces* 76, (1), 32-37.

30. Xie, J.; Lee, J. Y.; Wang, D. I. C., Synthesis of single-crystalline gold nanoplates in aqueous solutions through biomineralization by serum albumin protein. **2007**.

31. Basu, N.; Bhattacharya, R.; Mukherjee, P., Protein-mediated autoreduction of gold salts to gold nanoparticles. *Biomedical Materials* **2008,** 3, 034105.

32. Housni, A.; Ahmed, M.; Liu, S.; Narain, R., Monodisperse protein stabilized gold nanoparticles via a simple photochemical process. *The Journal of Physical Chemistry C* **2008,** 112, (32), 12282-12290.

33. Mulvaney, P., Surface plasmon spectroscopy of nanosized metal particles. *Langmuir* **1996,** 12, (3), 788-800.

34. Sun, Y.; Xia, Y., Increased sensitivity of surface plasmon resonance of gold nanoshells compared to that of gold solid colloids in response to environmental changes. *Anal. Chem* **2002,** 74, (20), 5297-5305.

35. Sun, Y.; Xia, Y., Mechanistic study on the replacement reaction between silver nanostructures and chloroauric acid in aqueous medium. *J. Am. Chem. Soc* **2004,** 126, (12), 3892-3901.

36. Zhu, Y.; Cheng, G.; Dong, S., The electrochemically induced conformational transition of disulfides in bovine serum albumin studied by thin layer circular dichroism spectroelectrochemistry. *Biophysical Chemistry* **2001,** 90, (1), 1-8.

37. Burt, J. L.; Gutiérrez-Wing, C.; Miki-Yoshida, M.; José-Yacamán, M., Noble-metal nanoparticles directly conjugated to globular proteins. *Langmuir* **2004,** 20, (26), 11778-11783.

38. Selvakannan, P. R.; Swami, A.; Srisathiyanarayanan, D.; Shirude, P. S.; Pasricha, R.; Mandale, A. B.; Sastry, M., Synthesis of Aqueous Au Core- Ag Shell Nanoparticles Using Tyrosine as a pH-Dependent Reducing Agent and Assembling Phase-Transferred Silver Nanoparticles at the Air- Water Interface. *Langmuir* **2004,** 20, (18), 7825-7836.

39. Selvakannan, P. R.; Mandal, S.; Phadtare, S.; Gole, A.; Pasricha, R.; Adyanthaya, S. D.; Sastry, M., Water-dispersible tryptophan-protected gold nanoparticles prepared by the spontaneous reduction of aqueous chloroaurate ions by the amino acid. *Journal of colloid and interface science* **2004,** 269, (1), 97-102.

40. Zhou, Y.; Chen, W.; Itoh, H.; Naka, K.; Ni, Q.; Yamane, H.; Chujo, Y., Preparation of a novel core–shell nanostructured gold colloid–silk fibroin bioconjugate by the protein in situ redox technique at room temperature. *Chemical Communications* **2001,** 2001, (23), 2518-2519.

41. Spande, T. F.; Witkop, B., In Methods in Enzymology (Hirs, CHW, ed.), Vol. 11. In Academic Press, New York: 1967.

42. Witkop, B., Nonenzymatic methods for the preferential and selective cleavage and modification of proteins. *Advances in protein chemistry* **1962,** 16, 221-321.

43. Wei, Z.; Somasundaran, P., Cyclic voltammetric study of arsenic reduction and oxidation in hydrochloric acid using a Pt RDE. *Journal of Applied Electrochemistry* **2004,** 34, (2), 241-244.

44. Polat, K.; Aksu, M. L.; Pekel, A. T., Electroreduction of nitrobenzene to p-aminophenol using voltammetric and semipilot scale preparative electrolysis techniques. *Journal of Applied Electrochemistry* **2002,** 32, (2), 217-223.

45. Wartena, R.; Winnick, J.; Pfromm, P. H., Recycling kraft pulping chemicals: cyclic voltammetry of molten salt mixtures containing Na2CO3, Na2SO4, Na2SNa2Sx and Na2ONa2O2. *Journal of Applied Electrochemistry* **2002,** 32, (7), 725-733.

46. Stankovich, M. T.; Bard, A. J., The electrochemistry of proteins and related substances part III. Bovine serum albumin. *Journal of Electroanalytical Chemistry* **1978,** 86, (1), 189-199.

Chapter 3

Evaluation of stability and cytocompatibility of BSA capped gold and silver nanoparticles

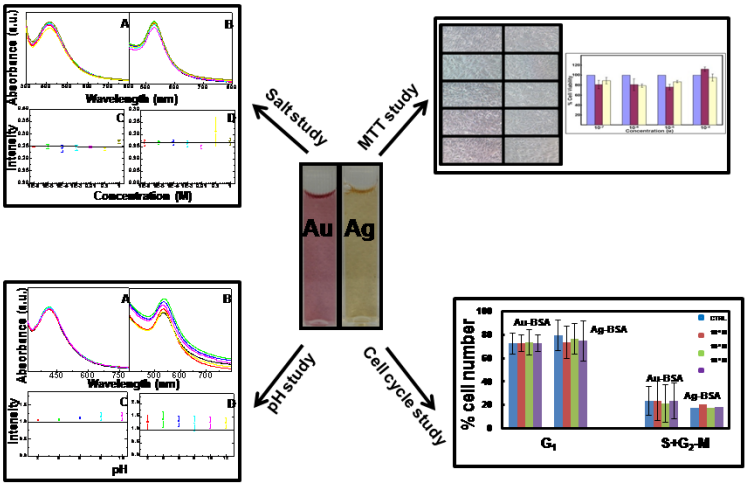

This chapter describes the role of BSA capping on the stability of gold and silver nanoparticles against varying pH and salt concentrations. FTIR and CD spectroscopic investigations were carried out to study the secondary structure of the protein present on the nanoparticles surface. Later the cytocompatibility of these nanoparticles against mouse fibroblast (NIH3T3) cells is discussed.

Part of work has been published in:

Priyanka Murawala, S. M. Phadnis, R. R. Bhonde, B. L. V. Prasad, *Colloids and Surfaces B: Biointerfaces*, **2009**, 73, 224-228.

3.1 Introduction:

In the previous chapters we have described the preparation of BSA capped gold nanoparticles. In this BSA acted as a reducing agent also. This avoids the use of exogenous reducing agents during the synthesis. As our ultimate aim is to establish the efficacy of these nanoparticles as drug delivery agents, we need to check their suitability for the same. For any potential drug delivery system the important criteria that should be met are the stability against electrolytic addition and pH changes. Agglomeration of nanoparticles has been demonstrated to have a profound impact on their toxicity in vitro[1]. Nanoparticles agglomerate and clump in solution, making it difficult to accurately deliver them for *in vivo* or *in vitro* experiments[2]. Although standard procedures for the synthesis of nanoparticles exist, we have to be critical about how precisely the properties of these nanoparticles are defined. Nanoparticles developed should be compatible with the physiological salt and pH values. For the use of nanoparticles in *in vitro* and *in vivo* assays, the dispersions must be isotonic, adapted to a pH of 7.4 and applicable in the presence of divalent ions and protein mixtures[3]. The interaction of the nanoparticles with the wealth of other components in the physiological media is one pitfall of nanotoxicology. Fernig and coworkers have synthesized a pentapeptide ligand CALNN which converts citrate stabilized gold nanoparticles into extremely stable, water-soluble gold nanoparticles[4]. CALNN-capped nanoparticles were stable at basic, neutral, and slightly acidic pH and to the addition of salt concentration of 1 M. In a similar study, Cooper and group have synthesized 5 nm gold nanoparticles protected with thio-ether and thiol-functionalized polymer ligands[5]. These nanoparticle preparations were highly stable and can withstand a salt concentration of 1.5 M and pH 13. These polymeric ligands were further exchanged with a mixture of peptide CALNN (95 %) and CALNNGK (biotin) G (5 %) demonstrating their use in biological applications. Schlenoff *et al* have synthesized highly stable water soluble gold nanoparticles by a new surface modification procedure involving ligand exchange of citrate-stabilized gold nanoparticles with a zwitterion disulfide. These colloidal suspensions were stable up to the addition of 3 M of NaCl. Similarly, the nanoparticles sol did not precipitate out of solution when charged polyelectrolytes or biopolymers were added, indicating the absence of nonspecific interactions[6]. Prasad and coworkers have used Gellan Gum

(used in food and confectionary industry as a thickening and gelling agent), for the reduction and stabilization of gold nanoparticles[7]. These Gellan gum reduced gold nanoparticles were highly stable and were used to load anticancer drug Doxorubicin and in turn have shown enhanced anticancer activity against human glioma cell lines.

Since the protein BSA, here, acts as a reducing and capping agent, retention of the secondary/tertiary structure of protein is also important as structural changes can induce unwanted immune responses. Too much loss of the original structure of the protein in the bioconjugates possibly means the loss of the biological activity of the protein that could hamper the biological applications of the conjugate[8].

Emerging biomedical application of nanoparticles as drug delivery agents, biosensors, or imaging agents involve deliberate, direct ingestion or injection of nanoparticles in body[9]. To attain these applications, nanoparticles are specially engineered to target specific cells for e.g. attachment of DNA, protein, antibody or a drug molecule. As these nanoparticles are intentionally engineered to interact with the cells, it is important to make sure that these do not cause adverse side effects. More important point to keep under consideration is whether either the naked nanoparticles or coated nanoparticles undergo biodegradation under physiological condition or if at all they do so what cellular responses are generated against them. Main factors playing role in their biocompatibility are size, shape, chemical compositions, surface properties and interaction of nanoparticle surface with the cells [9, 10]. Wyatt and co-workers in a detailed study have examined the uptake and toxicity of a series of gold nanoparticles in human leukemia cells[11]. The nanoparticle library consisted of gold nanoparticles that varied in both size (4, 12, and 18 nm diameter) and surface ligands. The surface ligands included a range of anionic, neutral, and cationic groups: citrate, cysteine, glucose, biotin, and cetyltrimethylammonium bromide (CTAB). The results indicated that although some precursors of nanoparticles were toxic but the nanoparticles themselves found to be non-toxic. In contrast to this study, another group Niidome *et al* have shown that CTAB-capped gold nanorods were cytotoxic when tested on a different cell line, HeLa cells[12]. However, cytotoxicity was reduced by over coating the nanorods with poly(ethylene glycol) (PEG), which is well-known to reduce nonspecific binding of biological molecules to surfaces[12]. Rotello *et al* have investigated the toxicity of 2 nm gold nanoparticles functionalized with both cationic

and anionic surface groups in three different cell types[13]. The results suggested that cationic particles are generally toxic at much lower concentrations than anionic particles, which can be attributed to the electrostatic interaction between the cationic nanoparticles and the negatively charged cell membranes[13]. Interestingly in a different study, 33 nm citrate-capped gold nanoparticles were found to be non toxic to baby hamster kidney and human hepatocellular liver carcinoma cells, but cytotoxic to a human carcinoma lung cell line at certain concentrations showing cell specific responses[14]. Here an important point to mention is to carefully differentiate between cytotoxicity and cellular damage. Nanoparticles that show little or no cytotoxicity via several standard assays may be still able to cause serious cellular damage. For example, 13 nm citrate-capped gold nanoparticles were not toxic according to an assay in skin cells, but the particles did apparently promote the formation of abnormal actin filaments, which led to decreases in cell proliferation, adhesion, and motility[15].

Thus we proceeded to evaluate the Au-BSA conjugate and see whether they are biocompatible and the results from the part of this chapter can meet the above mentioned criteria.

3.2 Results and Discussion:

This section is divided into two parts; first part deals with the stability of Au-BSA and Ag-BSA nanoparticles and in the later the cytocompatibility of the nanoparticles is discussed.

A) Assessment of the stability of Au-BSA and Ag-BSA:

3.2.1 Stability of nanoparticles in water with time:

Potential biological applications of nanoparticles greatly depend upon their stability and dispersibility in aqueous media[3, 5, 7, 16, 17]. In order to determine the stability of nanoparticles in water, UV-vis spectra were recorded after 30 days of synthesis of both Au-BSA and Ag-BSA nanoparticles. Figure 3.1 A shows the UV-vis absorption spectra of freshly prepared Au-BSA nanoparticles (curve 1) and after 30 days (curve 2) of the synthesis of the same sample. Freshly prepared Au-BSA has SPR peak position at 528 nm while spectra recorded for the same sample after 30 days of synthesis shows a red shift by 2 nm. Similarly absorption spectra of Ag-BSA were also monitored (Figure 3.1 B). Curve 1 shows the UV-vis absorption spectrum of

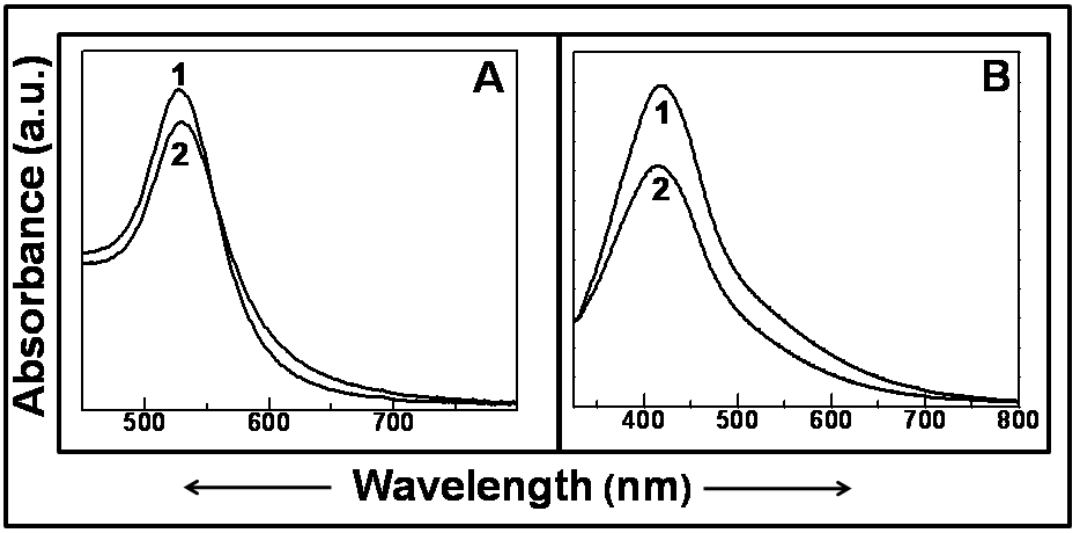

Figure 3.1 (A) *UV-vis spectra of Au-BSA nanoparticles recorded for the freshly prepared (Curve 1) and after 30 days (Curve 2) of synthesis of the same sample.* **(B)** *UV-vis spectra of Ag-BSA nanoparticles recorded for the freshly prepared (Curve 1) and after 30 days (Curve 2) of synthesis of the same sample.*

freshly prepared Ag-BSA nanoparticles having SPR peak at 418 nm while spectra of the same sample after 30 days has SPR peak at 415 nm (Curve 2). Thus, these results suggests that Au-BSA and Ag-BSA nanoparticles do not show any sign of aggregation after 30 days of standing and hence shows that these are very robust and stable systems.

3.2.2 Stability of nanoparticles under varying salt concentrations and pH conditions:

Figure 3.2 A and B shows the NaCl addition experiments performed with Ag-BSA and Au-BSA respectively. Spectra show that even after the addition of highest salt concentration (1 M), no aggregation has occurred. Figure C and D show the intensity of surface plasmon resonance peaks at various concentrations of NaCl. The solid lines in the figures indicate the intensity when no NaCl was added.

Figure 3.3 A and B summarize the effect of varying pH on Ag-BSA and Au-BSA respectively. Spectra show that within the tested pH range i.e. from pH 2 to pH 12, no aggregation has occurred in BSA capped gold nanoparticles while Ag-BSA at pH 12 got aggregated and hence SPR curve of it was not obtained. Figure C and D show the intensity of surface plasmon resonance peaks at varying pH conditions. The

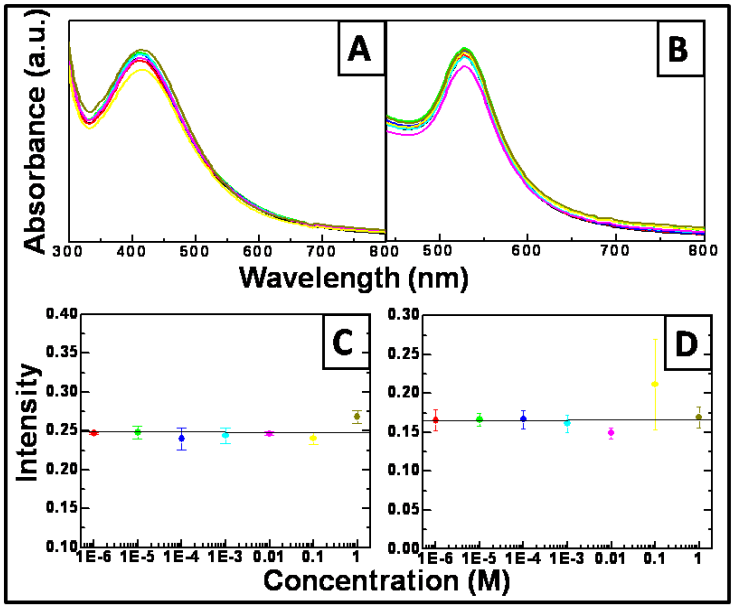

Figure 3.2 (A) *Effect of NaCl addition to BSA capped silver and* ***(B)*** *gold nanoparticles.* **(C)** *and* **(D)** *show the intensity of surface plasmon resonance peaks at various concentrations of NaCl added to Ag-BSA and Au-BSA, respectively . The solid lines in the figures indicate the intensity when no NaCl was added.*

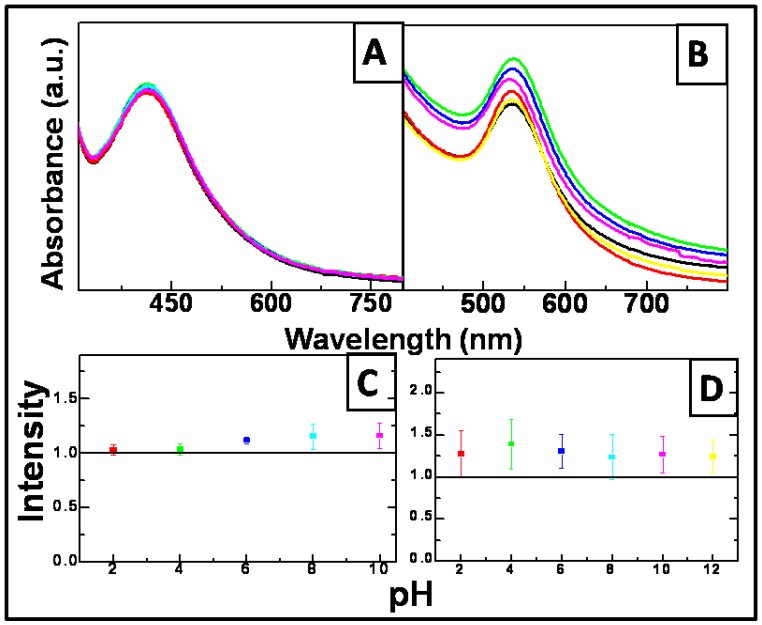

Figure 3.3 *Effect of varying pH on BSA capped silver* **(A)** *and* ***(B)*** *gold nanoparticles.* **(C)** *and* **(D)** *show the intensity of surface plasmon resonance peaks at varying pH conditions for Ag-BSA and Au-BSA, respectively. The solid lines in the figure indicate the intensity of nanoparticle solutions without adjusting the pH.*

solid lines in the figures indicate the intensity of nanoparticles without adjusting the pH.

Figure 3.2 summarizes the effect of varying concentration of NaCl on the Au-BSA and Ag-BSA solutions. Interestingly, both the nanoparticle solutions possessed high stability even to the addition of 1M NaCl. Similarly, Au-BSA solution was highly resistant to the various pH conditions while Ag-BSA at alkaline (pH 12) was unstable and got aggregated. However, all in all, results show that Au-BSA and Ag-BSA showed excellent colloidal stability in water, high salt concentration, and various pH conditions. This stability of nanoparticles can be attributed to the presence of protein BSA capping on the nanoparticle surface. It has been observed that citrate gold nanoparticle solutions are unstable with respect to precipitation and aggregate rapidly upon addition of electrolytes such as NaCl, KI, etc[18]. However, the same citrate reduced gold nanoparticles could be stabilized against aggregation by the addition of proteins such as BSA[18, 19]. Stability of colloidal nanoparticle solutions is well explained by DLVO theory. According to the DLVO theory, the stability of colloidal sols is determined by the balance of forces between the electrostatic repulsion of like- charged spheres and van der Waals attraction due to high polarizability of metal nanoparticles[20]. In general, addition of the electrolytes causes flocculation/aggregation due to the shielding of the double-layer charges[21, 22]. Proteins adsorbed onto the metal nanoparticles surface will provide stability to the sol due to large positive free energy input of protein desorption required prior to particle-particle fusion. Aggregation of nanoparticles occurs whenever colloidal particles approach closer enough so that the free protein is excluded from the interparticle region. This is an entropic effect as the protein leaves the interparticle space in response to the loss of configurational entropy upon compression by the particles. Loss of protein molecules leave behind the pure solvent molecules. A reduction in the free energy subsequently occurs when the solvent also leaves the interparticle region to mix with the protein. This “depletion flocculation” will only occur by demixing protein chains and solvent molecules in the interparticle region. Normally in good solvents, demixing is thermodynamically unfavorable, and the free protein in solution will actually stabilize the sols by preventing close approach of two particles (depletion stabilization)[18, 22]. The stability of nanoparticles in our study also can be attributed to the BSA capping present on them.

3.2.3 Fourier Transform Infrared Spectroscopy (FTIR):

Serum albumin is one of the most abundant and extensively studied proteins. In blood plasma its typical concentration is about 5g/100mL[23-25]. Its molecular weight is 66 kDa, is a single polypeptide chain containing 583 amino acids with no carbohydrate residues. Its secondary structure mostly comprises of α-helix[23, 24]. The tertiary structure of BSA is comprised of three homologous domains (domains I-III), with cysteine residues forming disulfide bonds to produce a double-loop bridging pattern[26]. FTIR is a powerful technique to study the secondary structure of protein. Figure 3.4 shows the FTIR spectra where curve 1 corresponds to pure BSA while curve 2 and 3

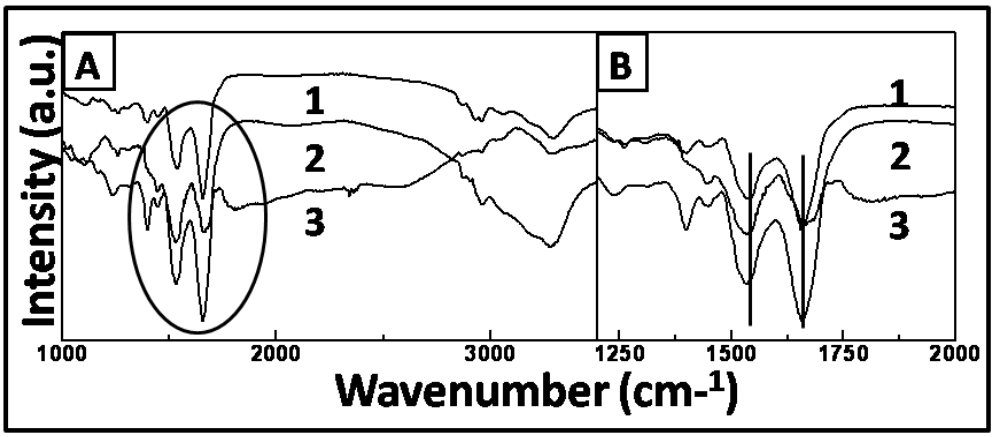

Figure 3.4 (A) *FTIR spectra corresponding to pure BSA (curve 1) and BSA capped Au (curve 2) and Ag nanoparticles (curve 3) respectively.* **(B)** *shows the enlarged region highlighted in* **(A)**.

correspond to Au-BSA and Ag-BSA respectively. In pure BSA, -C=O stretching termed as amide I and –N-H bending vibrations termed as amide II were found to occur at 1659 and 1535 cm^{-1} respectively. Their position in Au-BSA and Ag-BSA does not undergo any change (curves 2 and 3 respectively) and occur at the same positions as in the pure BSA molecule. This shows that the BSA molecules do not undergo any conformational changes upon attaching to the nanoparticle surfaces.

3.2.4 Circular Dichroism spectroscopy (CD):

CD is a powerful tool to study the conformational changes occurring in the secondary structure of a protein molecule. The CD spectra of BSA exhibited two negative minima in the ultraviolet region at 208 and 222 nm, which is characteristic of α-

helical structure of protein[27]. Since α-helix is one of the elements of secondary structure, any structural change of albumin can be easily evaluated by the content of α-helical structure. Figure 3.5 shows the CD studies performed on pure BSA, Au-BSA and Ag-BSA nanoparticles. Curve 1 corresponds to pure BSA where two negative minima at 208 nm and 222 nm present are characteristic of α-helical structure of protein [27,28]. In order to determine whether BSA has retained its secondary

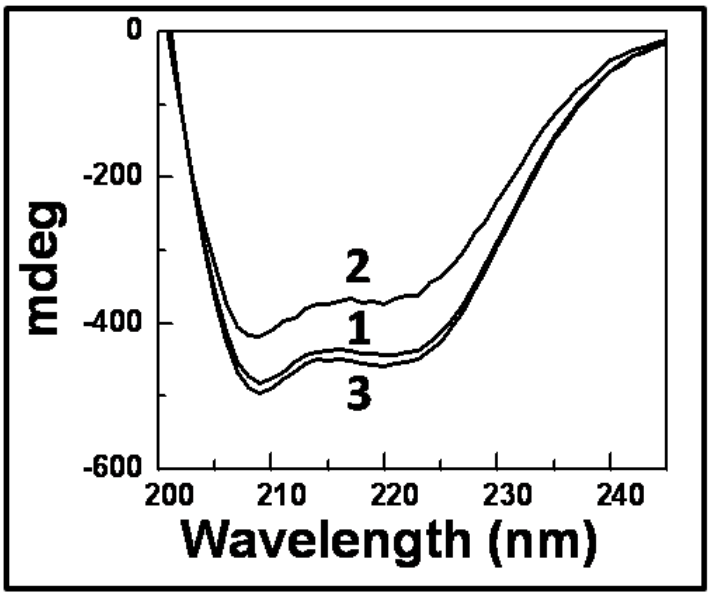

Figure 3.5 *CD spectra corresponding to pure BSA (curve 1) and BSA capped Ag (curve 2) and Au nanoparticles (curve 3) respectively.*

structure upon reduction and capping the nanoparticle surfaces, % MRE values at 208 nm and 222 nm were calculated. The CD spectra were taken in a wavelength range between 190 and 250 nm, and the results were expressed as MRE in deg cm^2 $dmol^{-1}$. The value of MRE was obtained using the equation MRE= [θ] /10*nlC* where [θ] is the CD in millidegrees, *n* is the number of amino acid residues in protein (total of 583 for BSA), *l* is the path length of the cell (1 cm), and *C* is the concentration of protein[27, 29].From the curves, % MRE values were 105 % and ~ 100 % at 208 nm and 222 nm for Au-BSA sample and 88.89 % and 87.5 % at 208 nm and 222 nm for Ag-BSA sample.

Thus, FTIR and CD studies show that the BSA does not suffer from any major structural changes. Indicating that its secondary and tertiary structures are conserved to a large extent after reducing and capping gold and silver nanoparticles (Figure 3.4

and 3.5 respectively). This can be a reason for highly stable BSA capped gold and silver nanoparticles.

B) Assessment of the cytocompatibility of Au-BSA and Ag-BSA against mouse embryonic fibroblast (NIH3T3) cell line:

3.2.5 In vitro cytocompatibility tests:

It is evident that for any clinical application, biocompatibility of nanoparticles is crucial. Size, shape, chemical compositions, surface properties and interaction of nanoparticle surface with the cells are the main factors that play a role in their biocompatibility[9, 10]. Since different nanoparticles can trigger distinctive biological responses, it is important that cytotoxicity studies are conducted for each nanoparticles type. One simple cytotoxicity test involves visual inspection of cells with bright field microscopy for changes in cellular or nuclear morphology[9]. NIH3T3 cells are mouse embryonic fibroblast cells. Fibroblast cells are large and flat, with elongated processes protruding from the body of each cell, create a spindle-like appearance of the cell. The nucleus in the body of the cell is flat and oval. Figure 3.6 summarizes the results of NIH3T3 viability studies after exposing to Au-BSA and Ag-BSA conjugate. A to J are the images of cells taken after the treatment with nanoparticles at different concentrations. A and F are the images of untreated or control cells. B and G correspond to the cells treated with 10^{-7} M Au-BSA and Ag-BSA respectively. C and H represent cells treated with 10^{-6} M Au-BSA and Ag-BSA respectively. D and I correspond to the cells treated with 10^{-5} M Au-BSA and Ag-BSA respectively while E and J depict the images of cells treated with 10^{-4} M Au-BSA and Ag-BSA respectively. It is clearly evident, from the images of control cells and cells treated with increasing concentration of Au-BSA and Ag-BSA, that the gross morphology of cells were not changed and no visible signs of toxicity were observed. Even though there were no visible signs of toxicity, we tested gold and silver nanoparticles for any effects on cellular proliferation of NIH3T3 cells.

We examined via MTT assay whether Au-BSA and Ag-BSA nanoparticles had any toxic biological properties. The MTT assay is a colorimetric assay that is based on measuring changes in absorbance at a specific wavelength and is widely used for measuring cytotoxicity and cell proliferation[30, 31]. Basically, the MTT assay measures the metabolic activity of viable cells. MTT is a water-soluble tetrazolium

salt (3-[4,5-dimethylthiazol-2-yl]-2,5-diphenyltetrazolium bromide) that yields a yellowish solution on dissolving. Dehydrogenase enzymes present in the cells catalyze the cleavage of the tetrazolium ring in MTT and convert dissolved MTT to formazan crystals. This cleavage is affected only by the mitochondria of living cells and not by the dead cells. The amount of MTT reduced to formazan can be measured spectrophotometrically after dissolving these water insoluble formazan crystals in

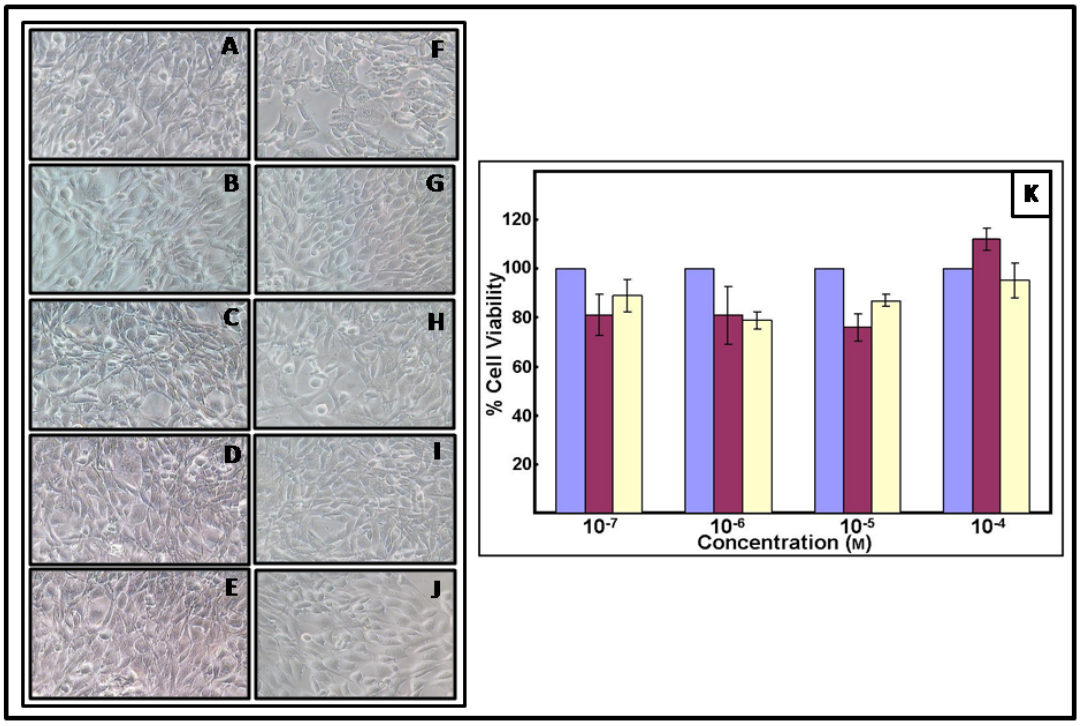

Figure 3.6 A-J *are the images of NIH3T3cells showing morphology of the cells after nanoparticles treatment.* **(K)** *Cytotoxicity assessment (MTT assay) of Au-BSA and Ag-BSA nanoparticles at various concentrations tested against NIH3T3 cell lines. Blue column: control (untreated cells), Purple column: Au-BSA treated cells and Yellow column: Ag-BSA treated cells.*

isopropanol or other solvents. The absorbance of dissolved formazan measured by a spectrophotometer at a wavelength of 570 nm is a function of the concentration of the converted dye, which is directly related to the number of viable cells since the MTT to formazan conversion takes place only when mitochondrial reductase enzymes are present.

In a typical experiment, cells in their exponential phase of growth were seeded at a density of 5000 cells/well of a 96-well tissue culture plate and incubated for 24 h. The cells were then treated with different concentrations of gold and silver nanoparticles for 3 h. NIH3T3 cells in medium and without nanoparticle treatment were taken as control. All experiments were performed 3 times in pentaplets, and average of all of the experiments has been shown as cell-viability percentage in comparison with the control experiment, while gold untreated controls were considered as 100% viable. The MTT viability results (Figure K) demonstrated that at various nanoparticles concentrations used, % mitochondrial activity of NIH3T3 cells is almost comparable to the control cell with the addition of increasing concentrations of Au-BSA and Ag-BSA nanoparticles in the cell growth media. At the highest dose used i.e. at 1 X 10^{-4} M of Au-BSA and Ag-BSA, more than 100% and≈ 95% cell viability was observed respectively. This revealed that both the Au-BSA and Ag-BSA nanoparticles were highly biocompatible and for the highest concentration of nanoparticles used (1X10^{-4} M) against NIH3T3 cells no harmful effect on the cellular proliferation was observed. Thus it can be conclusively inferred that BSA coated gold and silver nanoparticles to be biologically nontoxic and can be looked upon as a potential candidate for biomedical application.

3.2.6 Cell cycle analysis by Flow Cytometry (FACS):

Flow cytometry has been widely used as a means of investigating the cell cycle perturbations caused by a variety of chemotherapeutic agents[32]. The percentage number of cells in a particular stage of cell division is based on the amount of DNA present in the cell. *In vitro* effects of Au-BSA and Ag-BSA nanoparticles on cell cycle progression was studied by FACS analysis technique. For this analysis, NIH3T3 cells were seeded in 55 mm plates. After 24 h media was removed, and fresh media containing 10^{-4} M of Au-BSA and Ag-BSA was added to the NIH3T3 cells. After 24 h of incubation with nanoparticles, cells were trypsinized and collected in DMEM containing 10 % serum to neutralize the effect of trypsin. The cells were then collected by centrifugation at 1,500 rpm at room temperature for 5 min, washed with PBS and resuspended in PBS. To permeabilize the cells for PI, the cells were fixed by drop wise addition of 70 % ethanol while gently vortexing the cell suspension. This

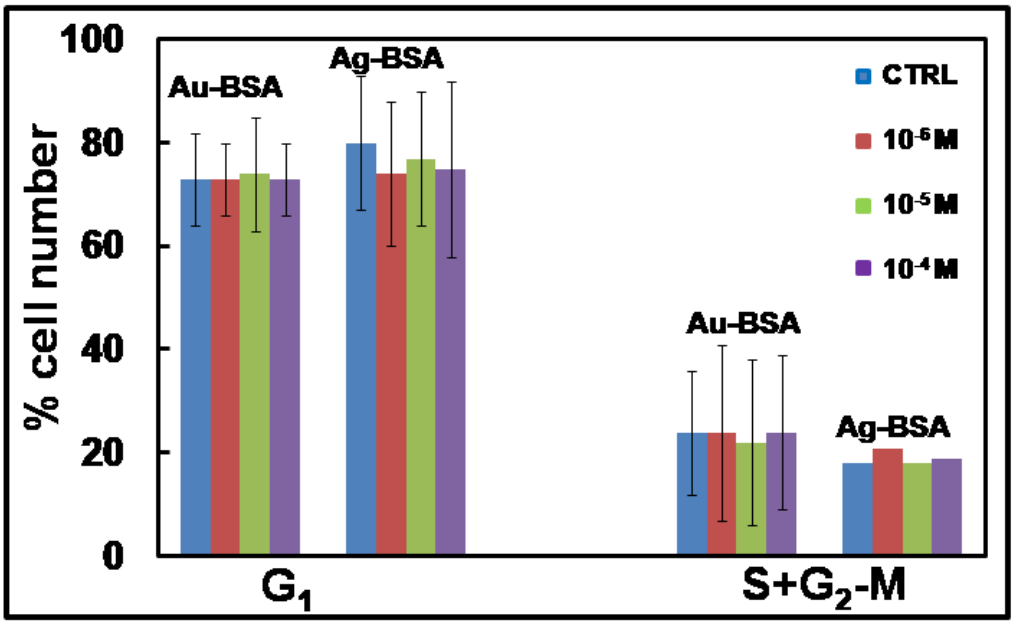

Figure 3.7 *Cell cycle analysis of NIH3T3 cells treated with Au-BSA and Ag-BSA nanoparticles over a period of 24 h.*

solution was left on ice for 1 h or at 4 °C overnight. After incubation period, cells were washed with PBS, followed by addition of 5 µL of RNase (10 µg/mL stock solution).This cell suspension was incubated at 37 °C for 1 h. After this, 5 µL of PI (2 mg/mL stock) was added 15 minutes prior to acquiring the sample. The graph in Figure 3.7 shows *in vitro* effects of Au-BSA and Ag-BSA on cell cycle progression. Untreated cells were taken as control. We observed that cells treated with increasing concentration of Au-BSA and Ag-BSA behave in the similar manner as control. The percentage numbers of cells present in G1 phase in control and at various concentrations of Au-BSA and Ag-BSA is almost near 75 % after 24 h and ~25 % in S+G2M. It is clearly evident from the graph that both the nanoparticle system does not have any harmful effect on the cell cycle of NIH3T3 cell line. After 24 h of treatment with Au-BSA and Ag-BSA, there was no difference obtained in the cell cycle progression between the control cells and Au-BSA and Ag-BSA treated cells. This shows that both the nanoparticles even at the highest concentrations used do not affect the cell cycle of NIH3T3 cells.

3.3 Conclusions:

Stability and biocompatibility of Au-BSA and Ag-BSA nanoparticles; which is a pre-requisite for biomedical applications, has been revealed in this chapter. It was

observed that BSA capping on the nanoparticles provided high stability against varying pH and salt concentrations. FTIR and CD studies show that the secondary structure of the protein BSA on the nanoparticles surface has been conserved. Additionally, the BSA capping on nanoparticles turn into an added advantage by making them highly biocompatible as shown by MTT assay and cell cycle analysis. Taken together, the current findings reveal that these stable and cytocompatible aqueous dispersions of gold and silver nanoparticles satisfy the essential requirements for biological applications and hence can be further studied as drug delivery systems.

References:

1. Liu, S.; Wei, L.; Hao, L.; Fang, N.; Chang, M. W.; Xu, R.; Yang, Y.; Chen, Y., Sharper and Faster "nano darts" kill more bacteria: A study of antibacterial activity of individually dispersed pristine single-walled carbon nanotube. *ACS nano* **2009,** 3, (12), 3891-3902.

2. Sager, T. M.; Porter, D. W.; Robinson, V. A.; Lindsley, W. G.; Schwegler-Berry, D. E.; Castranova, V., Improved method to disperse nanoparticles for in vitro and in vivo investigation of toxicity. *Nanotoxicology* **2007,** 1, (2), 118-129.

3. Schulze, C.; Kroll, A.; Lehr, C. M.; Schäfer, U. F.; Becker, K.; Schnekenburger, J.; Schulze Isfort, C., Not ready to use-overcoming pitfalls when dispersing nanoparticles in physiological media. *Nanotoxicology* **2008,** 2, (2), 51-61.

4. Levy, R.; Thanh, N. T.; Doty, R. C.; Hussain, I.; Nichols, R. J.; Schiffrin, D. J.; Brust, M.; Fernig, D. G., Rational and combinatorial design of peptide capping ligands for gold nanoparticles. *J Am Chem Soc* **2004,** 126, (32), 10076-84.

5. Wang, Z.; Tan, B.; Hussain, I.; Schaeffer, N.; Wyatt, M. F.; Brust, M.; Cooper, A. I., Design of polymeric stabilizers for size-controlled synthesis of monodisperse gold nanoparticles in water. *Langmuir* **2007,** 23, (2), 885-95.

6. Rouhana, L. L.; Jaber, J. A.; Schlenoff, J. B., Aggregation-resistant water-soluble gold nanoparticles. *Langmuir* **2007,** 23, (26), 12799-801.

7. Dhar, S.; Reddy, E. M.; Shiras, A.; Pokharkar, V.; Prasad, B. L. V., Natural gum reduced/stabilized gold nanoparticles for drug delivery formulations. *Chemistry–A European Journal* **2008,** 14, (33), 10244-10250.

8. Nakanishi, K.; Sakiyama, T.; Imamura, K., On the adsorption of proteins on solid surfaces, a common but very complicated phenomenon. *Journal of bioscience and bioengineering* **2001,** 91, (3), 233-244.

9. Lewinski, N.; Colvin, V.; Drezek, R., Cytotoxicity of nanoparticles. *Small* **2008,** 4, (1), 26-49.

10. Shukla, R.; Bansal, V.; Chaudhary, M.; Basu, A.; Bhonde, R. R.; Sastry, M., Biocompatibility of gold nanoparticles and their endocytotic fate inside the cellular compartment: a microscopic overview. *Langmuir* **2005,** 21, (23), 10644-10654.

11. Connor, E. E.; Mwamuka, J.; Gole, A.; Murphy, C. J.; Wyatt, M. D., Gold nanoparticles are taken up by human cells but do not cause acute cytotoxicity. *Small* **2005,** 1, (3), 325-7.

12. Niidome, T.; Yamagata, M.; Okamoto, Y.; Akiyama, Y.; Takahashi, H.; Kawano, T.; Katayama, Y.; Niidome, Y., PEG-modified gold nanorods with a stealth character for in vivo applications. *J Control Release* **2006,** 114, (3), 343-7.

13. Goodman, C. M.; McCusker, C. D.; Yilmaz, T.; Rotello, V. M., Toxicity of gold nanoparticles functionalized with cationic and anionic side chains. *Bioconjug Chem* **2004,** 15, (4), 897-900.

14. Patra, H. K.; Banerjee, S.; Chaudhuri, U.; Lahiri, P.; Dasgupta, A. K., Cell selective response to gold nanoparticles. *Nanomedicine* **2007,** 3, (2), 111-9.

15. Pernodet, N.; Fang, X.; Sun, Y.; Bakhtina, A.; Ramakrishnan, A.; Sokolov, J.; Ulman, A.; Rafailovich, M., Adverse effects of citrate/gold nanoparticles on human dermal fibroblasts. *Small* **2006,** 2, (6), 766-73.

16. Lévy, R.; Thanh, N. T. K.; Doty, R. C.; Hussain, I.; Nichols, R. J.; Schiffrin, D. J.; Brust, M.; Fernig, D. G., Rational and combinatorial design of peptide capping ligands for gold nanoparticles. *J. Am. Chem. Soc* **2004,** 126, (32), 10076-10084.

17. Choi, J.; Jun, Y.; Yeon, S. I.; Kim, H. C.; Shin, J. S.; Cheon, J., Biocompatible heterostructured nanoparticles for multimodal biological detection. *J. Am. Chem. Soc* **2006,** 128, (50), 15982-15983.

18. Xie, H.; Tkachenko, A. G.; Glomm, W. R.; Ryan, J. A.; Brennaman, M. K.; Papanikolas, J. M.; Franzen, S.; Feldheim, D. L., Critical Flocculation Concentrations, Binding Isotherms, and Ligand Exchange Properties of Peptide-Modified Gold

Nanoparticles Studied by UV- Visible, Fluorescence, and Time-Correlated Single Photon Counting Spectroscopies. *Anal. Chem* **2003,** 75, (21), 5797-5805.

19. Keating, C. D.; Musick, M. D.; Keefe, M. H.; Natan, M. J., Kinetics and Thermodynamics of Au Colloid Monolayer Self-Assembly: Undergraduate Experiments in Surface and Nanomaterials Chemistry. *Journal of chemical education* **1999,** 76, (7), 949.

20. Adamson, A. W., Physical Chemistry of Surfaces. *John Wiley & Sons:*

New York, **1990**

5th ed.

21. Niemeyer, C. M., Nanoparticles, proteins, and nucleic acids: biotechnology meets materials science. *Angewandte Chemie International Edition* **2001,** 40, (22), 4128-4158.

22. Hunter, R. J., Foundations of Colloid Science Oxford University Press. *New York* **1987**, 412.

23. Ho, J. X.; Carter, D. C., Structure of serum albumin. *Adv. Protein Chem* **1994,** 45, 153–203.

24. Friedli, G. L. Interaction of SWP with Bovine Serum Albumin (BSA). PhD Dissertation, University of Surrey, 1996.

25. Xie, J.; Lee, J. Y.; Wang, D. I. C., Synthesis of single-crystalline gold nanoplates in aqueous solutions through biomineralization by serum albumin protein. **2007**.

26. He, X. M.; Carter, D. C., Atomic structure and chemistry of human serum albumin. **1992**.

27. Shang, L.; Wang, Y.; Jiang, J.; Dong, S., pH-dependent protein conformational changes in albumin: gold nanoparticle bioconjugates: a spectroscopic study. *Langmuir* **2007,** 23, (5), 2714-2721.

28. Wangoo, N.; Bhasin, K. K.; Mehta, S. K.; Suri, C. R., Synthesis and capping of water-dispersed gold nanoparticles by an amino acid: Bioconjugation and binding studies. *Journal of colloid and interface science* **2008,** 323, (2), 247-254.

29. Ahmad, B.; Parveen, S.; Khan, R. H., Effect of albumin conformation on the binding of ciprofloxacin to human serum albumin: a novel approach directly assigning binding site. *Biomacromolecules* **2006,** 7, (4), 1350-1356.

30. Mossmann, T., Rapid colorimetric assay for cellular growth and survival: application to proliferation and cytotoxicity assays, Immunol. *Methods* **1983,** 65, 55-58.

31. Liu, H.; Yazici, H.; Ergun, C.; Webster, T. J.; Bermek, H., An in vitro evaluation of the Ca/P ratio for the cytocompatibility of nano-to-micron particulate calcium phosphates for bone regeneration. *Acta Biomaterialia* **2008,** 4, (5), 1472-1479.

32. Taylor, I. W.; Tattersall, M. H. N., Methotrexate cytotoxicity in cultured human leukemic cells studied by flow cytometry. *Cancer Research* **1981,** 41, (4), 1549.

Chapter 4

Enhanced Uptake of Gold Nanoparticles and self luminescent Gold Clusters into Cancerous Cells over Normal Cells

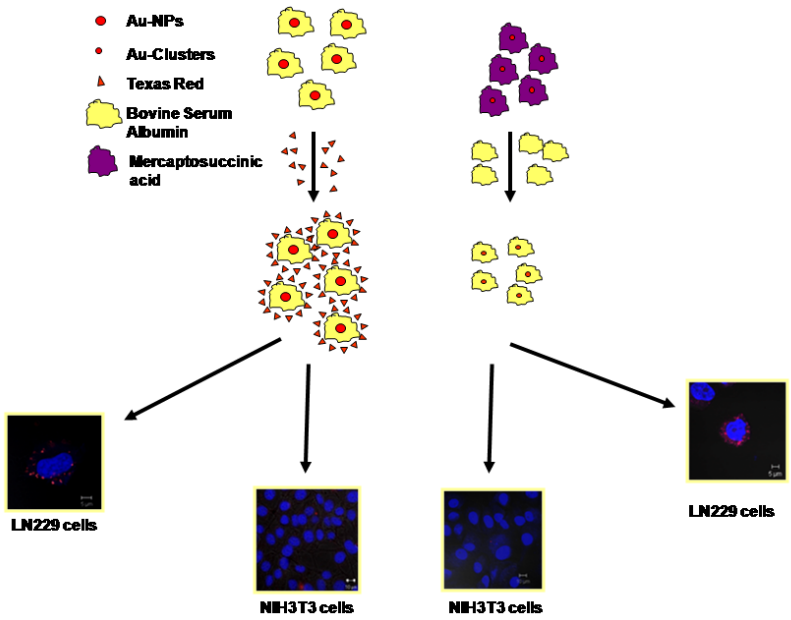

This chapter discusses the uptake of BSA protected gold nanoparticles and gold clusters into cancerous (human glioma LN229) and normal (mouse embryonic fibroblast NIH3T3) cell lines. The results suggest an enhanced uptake of both the nanoparticles systems into the cancerous cells in comparison to the normal cells. Although the nanoparticles and clusters are significantly different in their size, the extent of their uptake by human glioma cells is almost similar.

4.1 Introduction:

The main theme line of our entire studies is to develop a nanoparticle system that can act as a drug delivery vehicle and to this effect evaluating the efficacy of the BSA capped nanoparticles to enter into cancerous cells would be vital. If while doing so (entering into the cancerous cells) they also show some specificity to enter them it would be an extra added advantage. Cellular uptake and intracellular fate of nanoparticles has been shown to depend upon the size, shape, charge and surface chemistry[1-4]. The ionic interactions between the negative membrane potential of most cells with nanoparticles of a positive, negative or neutral charge density differ drastically. Other than the physicochemical properties of the nanoparticles, the characteristics of the target cell i.e. the cell type (i.e. cell origin) and the differentiation status ('normal' vs. cancer)[4] also play critical role in uptake behaviour[5]. The interactions of nanoparticles with their target cells could, in turn, determine the intracellular uptake and localization of the nanoparticles and their biological functions[5]. Understanding such interactions between cells and nanoparticles with different surface properties is important not only for engineering of nanoparticles that exhibit selective intracellular uptake (to subsequently alter cellular processes of interest) but also for determining the relative cytotoxicity of nanoparticles.

The focus of the investigation of our work incorporated in this chapter is to see whether the BSA capped nanoparticles prepared by us are being taken by the cells or not. Further, in order to test our system critically we also compared their cell uptake capabilities with another BSA capped systems, namely BSA capped fluorescent gold clusters which are about 1 mm in size. These were characterized to posses 26-28 gold atoms each and such clusters due to the quantum confinement of electronic structure display unique emission characterstics[6-8]. We wish to remind that the system developed as part of this thesis study is 15 nm gold particles. Further to test the uptake of these two different systems into different cells we considered normal fibroblast cells (NIH3T3) and cancerous cell line (LN229). To ensure that a better comparison of cellular uptake of these two different sized nanoparticles into different cell lines can be done properly, both the systems were capped by the same molecule, namely, Bovine serum albumin (BSA).

Our results indicate that in both, nanoparticles and clusters, intracellular localization were seen in cancerous cells (LN229) while negligible uptake was observed in normal cells (NIH3T3).

4.2 Experimental details:

The experimental conditions maintained were as following:

4.2.1Synthesis of gold nanoparticles by BSA:

The protocol of synthesis of gold nanoparticles by BSA is mentioned in section 2.2.1.ii.

4.2.2 Synthesis, characterization and quantification of texas red labeled Au-BSA:

For conjugation experiments, stock solution containing 1 mg of Texas red (TR) dissolved in 50 µL of DMSO was prepared and was stored at 4° C. 7 µL of the stock solution was added to 1 mL of $2X10^{-4}$ M Au-BSA and kept overnight for incubation at 4° C. Purification of TR labeled Au-BSA (hereafter Au-BSA-TR) from unbound TR was done by centrifuging the solution at 10,000 rpm for 10 min followed by washings (thrice) with 100 mM carbonate buffer (pH= 8.4). Finally, the pellet was redispersed in 500 µL of carbonate buffer such that the surface plasmon peak intensity of Au-BSA before and after the redispersion was same.

4.2.3Synthesis of gold clusters capped by BSA:

Gold clusters were prepared by following a published protocol[7] and were provided to us by Professor T. Pradeep's group from IITM, Chennai. In a typical experiment, mercaptosuccinic acid (MSA) capped nanoparticles were synthesized by sodium borohydride reduction of gold ions in the presence of MSA. Nanoparticles formed were of 2-3 nm in diameter and were used as precursor for synthesis of quantum clusters. For quantum cluster synthesis, nanoparticles were mixed with BSA (1:10 by weight) and kept under constant stirring. After 5 minutes, pH of solution was adjusted to 12 and again kept for stirring. Formation of quantum clusters was monitored by the development of luminescence in the solution. For convenience and brevity, the BSA reduced gold nanoparticles will be referred to as Au-BSA and luminescent clusters of gold as Au_{clust}-BSA further in the text.

4.2.4 Cellular uptake studies of Au-BSA and Au clusters on NIH3T3 and LN229 cells:

NIH3T3 and Human glioma cell line LN229 were procured from the Cell Repository of National Centre for Cell Science, Pune, India and were cultured in Dulbecco's modified eagle's medium (DMEM), supplemented with 1.5 gm/L sodium bicarbonate, 4 mM glutamine and 10 % fetal bovine serum. The cultures were maintained in a humidified atmosphere of 5 % CO_2 at 37 °C in an incubator. Uptake studies of Au-BSA and Au_{clust}-BSA were performed by seeding NIH3T3 and LN229 cells at low density on cover slips in a 24 well plate. After plating of the cells, in order to let them attach onto the cover slips they were incubated for 24 h prior to the administration of samples. After 24 h of incubation, cell medium was replaced with 500 µL of solution containing fresh medium, Au-BSA-TR and Au_{clust}-BSA. The cells were then further incubated for 3 h at 37 °C and 5 % CO_2 in a humidified environment.

Quantification of Au-BSA and Au_{clust}-BSA in NIH3T3 and LN229 was performed by ICP by seeding these cells in a 24 well plate. After plating of the cells, they were allowed to attach to 24 well plate and hence were incubated for 24 h prior to the administration of samples. After 24 h of incubation, cell medium was replaced with 500 µL of solution containing fresh medium, Au-BSA-TR and Au_{clust}-BSA. The cells were then further incubated for 3 h at 37 °C. After 3 h of incubation, cells were trypsinized and collected and washed thrice to remove nanoparticles on the surface of cells. These cells were then digested using 3N HCl and ICP analysis was performed on them. Standard graph for gold was made by using the known concentrations of gold. Finally, the concentration of Au-BSA and Au_{clust}-BSA were obtained from the standard graph.

For confocal imaging, after 3 h of incubation with nanoparticle solutions, media was removed and cover slips were washed extensively with 1X ice-cold phosphate buffered saline to remove the excess of Au-BSA-TR and Au_{clust}-BSA. After washing, cells were fixed in 4 % paraformaldehyde for 10 min at room temperature followed by washing with PBS. Cell's nuclei were then stained with DAPI (4',6-diamidino-2-phenylindole) for 10 min. To remove excess of DAPI, extensive washing of cover slips with PBS (RT) was done. After that the cells were

mounted onto glass slides with DABCO (1, 4-diazabicyclo[2.2.2]octane) as mounting medium. The cover slips were then observed under confocal microscope.

4.3 Results and Discussions:

Klaus *et al* proposed that the mechanism of cellular internalization of nanoparticles depends on[4]:

- The physico-chemical properties of the material, such as the chemical composition, size and shape, agglomeration status of the nanoparticles.
- The experimental conditions in the *in vitro* assays and the cellular (micro) environment where nanoparticles become located upon *in vivo* exposure (e.g., opsonization by serum components, modification by proteins or lipids such as albumin and surfactant).
- The characteristics of the target cell, i.e. the cell type (e.g., professional phagocytes versus non-professional phagocytic target cells) and their differentiation status (e.g., monocytes versus macrophages, 'normal' vs. cancer cells).

Since size and surface chemistry play crucial role in the behavior of nanoparticles, to probe the size effects more reliably we kept the surface capping molecule, BSA, the same. The composition of the nanoparticles was also kept the same, gold, except that the sizes were different. One class is a 15 nm sized and non-fluorescent gold nanoparticles synthesized by the ubiquitous bio-molecule BSA as a capping and reducing agent. The other is chemically synthesized extremely small in size (≤1 nm) gold clusters. These were *ex situ* capped by BSA. The most important aspect of these gold clusters is that they are inherently luminescent. In this report we have tried to elucidate the effect of size of gold nanoparticles and tried to investigate their cellular uptake in normal and cancerous cells. A schematic describing our experimental approach is presented in Figure 4.1

4.3.1UV-vis absorption spectroscopy of Au-BSA and Au_{clust}-BSA:

Figure 4.2 shows the UV-vis absorption curve recorded for gold nanoparticles and cluster solutions. Au-BSA, synthesized as described earlier 2.2.1.ii, showed SPR at

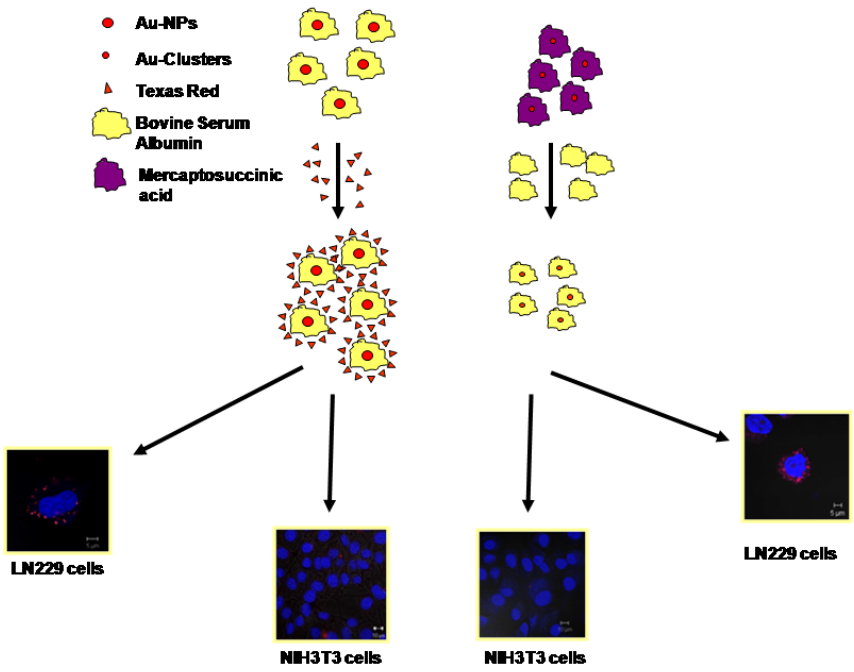

Figure 4.1: *A schematic representation for the determination of uptake of gold nanoparticles and clusters on NIH3T3 and human glioma LN229 cell lines.*

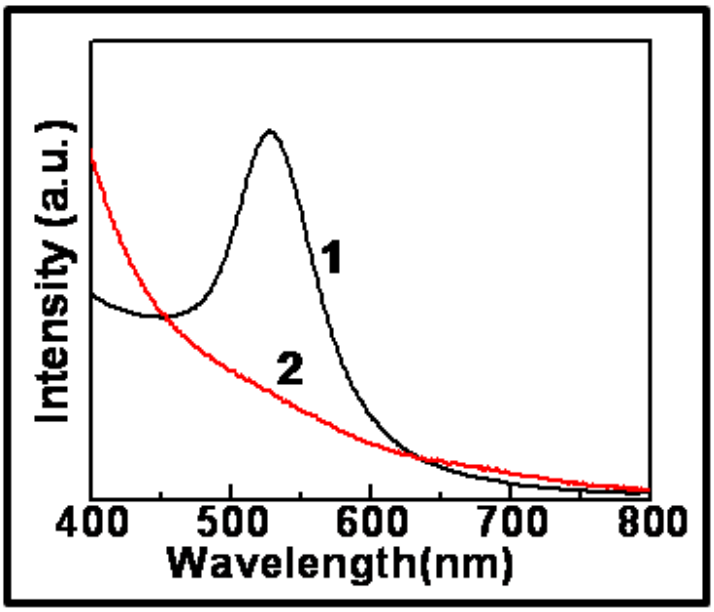

Figure 4.2: *UV-vis absorption spectra of Au-BSA (curve 1) and Au_{clust}-BSA(curve 2) respectively.*

531 nm (curve1) while UV absorption curve of Au_{clust}-BSA (curve 2) shows a monotonous increase in the intensity without any peak maximum. This is in

accordance with reported literature where nanoparticles having size less than 2 nm do not display any SPR signatures[9].

4.3.2Texas red (TR) loading on Au-BSA nanoparticles and its characterization.

Au-BSA nanoparticles are inherently non-fluorescent in nature hence TR was conjugated with Au-BSA so that the intracellular localization of these nanoparticles can be traced by fluorescence microscopy. Zeta potential value of as synthesized Au-BSA nanoparticles is –28.73 mV. The negative charge of nanoparticles is attributed to the surface bound BSA molecules. The electrostatic attachment of TR to the Au-BSA nanoparticles can be inferred from the increase in the zeta potential value to –13.99 mV upon conjugating Au-BSA with TR followed by thorough washing. Hereafter these samples will be referred as Au-BSA-TR. Figure 4.3 A shows the fluorescence emission spectra of Au-BSA-TR recorded after conjugation. It shows the characteristic emission maxima of TR at 612 nm. Gold nanoparticles surfaces have been known to quench the emission of many fluorophores[10, 11]. However, the retention of emission from TR clearly indicates that the BSA surface capping on these 15 nm gold particles is very uniform and that the fluorescent molecule is effectively shielded from interacting with the metal surface directly. Figure 4.3B shows the emission spectra recorded from the Au_{clust}-BSA sample having emission maxima at 640 nm. The emission from Au_{clust}-BSA is due to quantum size effects. Due to these inherent emission characteristics and low metallic content, Au_{clust}-BSA are biocompatible and can be used as such for biolabeling, bioimaging and detection applications without the necessity of additional fluorescent probe[7].

4.3.3 Cellular uptake studies on NIH3T3 and Human glioma LN229cell lines:

To probe the intracellular distribution of nanoparticles, NIH3T3 (mouse embryonic fibroblast cells) and LN229 (human glioma cells) were incubated with Au-BSA-TR and Au_{clust}-BSA. The untreated cells i.e. cells in medium alone were taken as control. For negative control experiments, cells were incubated with TR and Au-BSA nanoparticles alone. Figure 4.4 summarizes the results of NIH3T3 and LN229 cells treated with the two colloidal solutions. Control cells of NIH3T3 and LN229 cells do not show any fluorescence as can be seen in Figure 4.4 A (a) and Figure 4.4 B (a). Figure 4.4 A (b) and B (b), show the images of cells treated with TR. No fluorescence

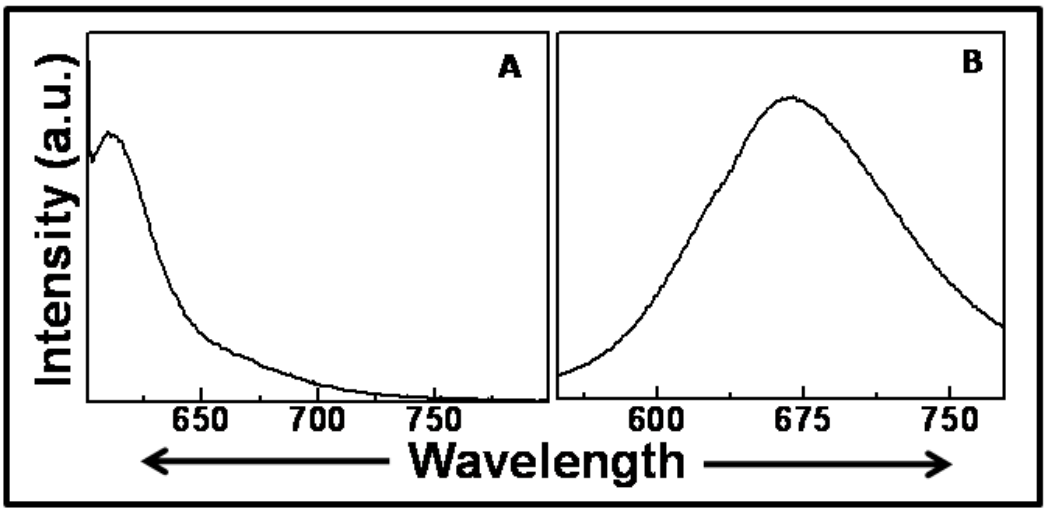

Figure 4.3: (A) *Florescence emission spectra of TR loaded on Au-BSA nanoparticles having emission maxima at 612 nm.* **(B)** *Emission spectra of Au_{clust}-BSA having emission maxima at 640 nm.*

is observed here again inside the cells as TR itself without any carrier cannot enter the cells. Au-BSA is inherently non-fluorescent and hence even if they would have been taken up by the cells no luminescence can be seen (Figure 4.4 A (c) and B (c). Figure 4.4A (d) and B (d) depict the images of cells treated with Au-BSA-TR nanoparticles. It can be seen here that no fluorescence is observed in NIH3T3 cells but from LN229 cells bright red fluorescence is observed. Same result was obtained with Au_{clust}-BSA where NIH3T3 cells were showing negligible luminescence while LN229 cells were brilliantly luminescent (Figure 4.4 A (e) and B (e) respectively). From the Z-stacking images it can be conclusively shown that the Au-BSA-TR nanoparticles (Figure 4.5) and Au_{clust}-BSA (Figure 4.6) have been internalized into the LN229 cells and the fluorescence is not just due to the non-specific/coincidental overlap of nanoparticles/cluster systems on the surface of the cells. In order to validate the fluorescent data, we tried to quantitate the amount of nanoparticles taken up by both the cell lines by Inductively Coupled Plasma (ICP) analysis. ICP results showed that concentration of Au-BSA-TR and Au_{clust}-BSA in LN229 cells were 4 ± 0.6 pg/cell and 0.22 ± 0.04 pg/cell respectively. At the same time, in NIH3T3 cell line no detectable amount of gold was seen when they were exposed to Au-BSA or Au_{clust}-BSA. From these results we can conclusively say that there is negligible uptake of either of the

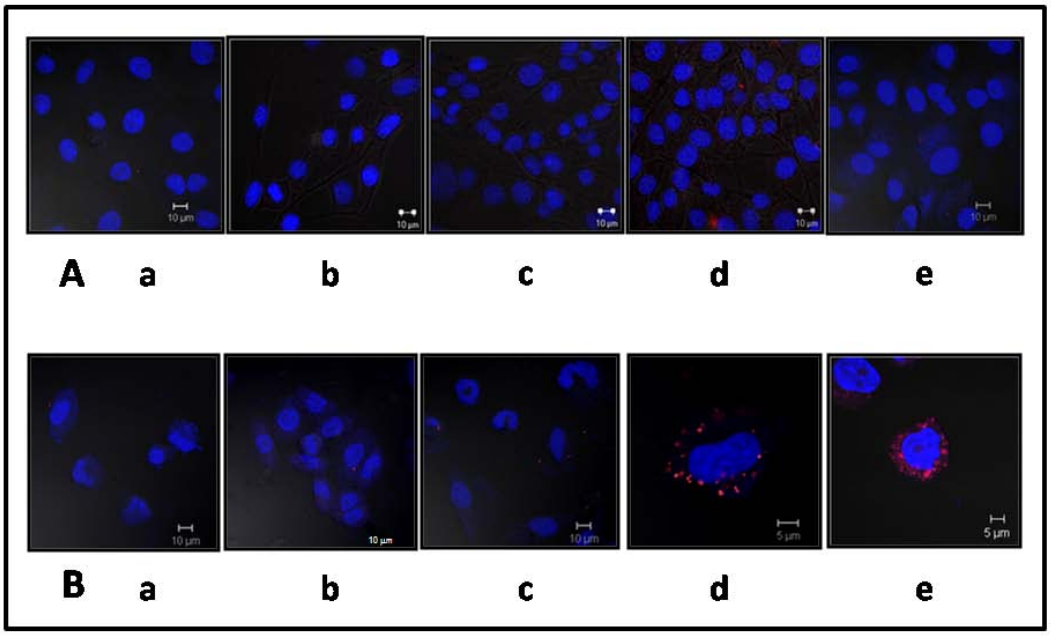

Figure 4.4: *(A) and (B) show the images of NIH3T3 and LN229 cells respectively treated with Au-BSA and Au_{clust}-BSA. A (a) and B (a) show the control cells of NIH3T3 and LN229 respectively. A (b) and B (b) show the cells treated with TR. A (c) and B (c) depicts images of cells treated with Au-BSA nanoparticles alone. A (d) and B (d) show the cells treated with Au-BSA -TR nanoparticles. A (e) and B (e) show the cells treated with Au_{clust}-BSA.*

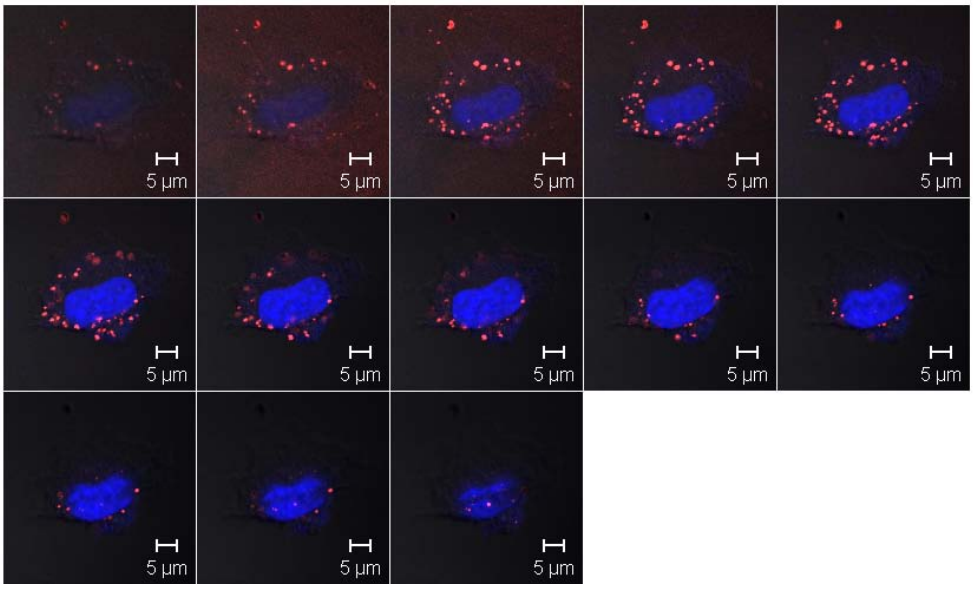

Figure 4.5: *Z stacking image of LN229 cells treated with Au-BSA.*

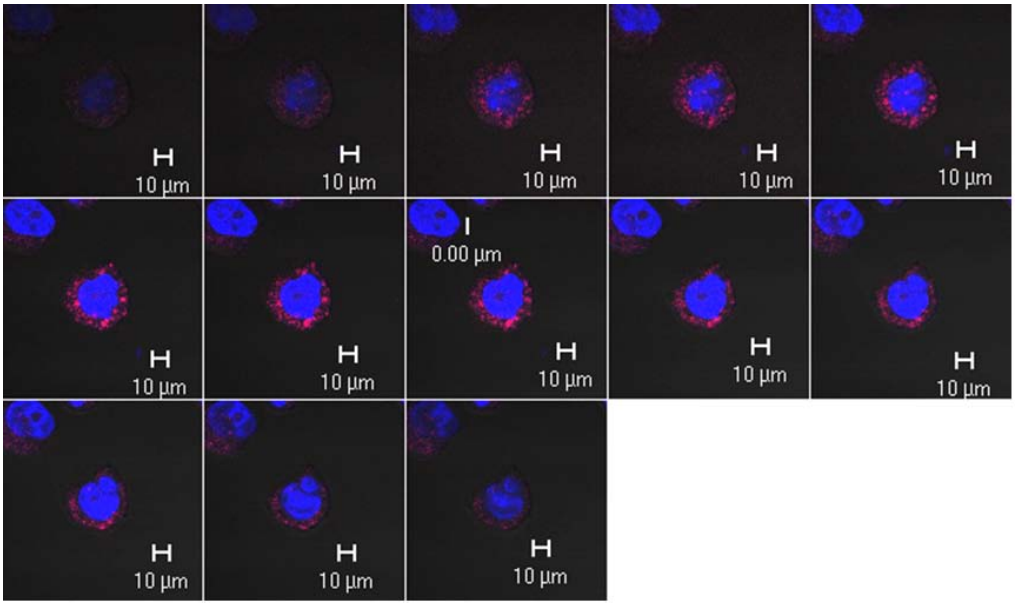

Figure 4.6: *Z stacking image of LN229 cells treated with Au_{clust}-BSA.*

nanoparticles into the NIH3T3 cells. However human glioma cell line show marked uptake of both the nanoparticles. We accredit this phenomenon to the nature of the cell type and the presence of BSA on the surfaces of nanoparticles. Cancer cells are highly proliferating and to meet their fast rate of replication they need enhanced supply of energy and nutrients. For this they develop enhanced permeability and retention (EPR) of macromolecules and they do this by developing leaky, defective blood vessels of tumor tissue which makes its vasculature permeable for macromolecules. In blood vessels of normal tissue, on the other hand, only small molecules can pass through the endothelial cells[12]. Not only this, the retention in the tumor tissue is also enhanced due to an impaired or absent lymphatic system. It has been shown that tumors are able to trap the plasma proteins and utilize their degradation products for proliferation[13]. Stehle *et al.* have proposed a hypothesis that albumin serves as a major energy and nutrition source for tumor growth and hence a reason for high albumin turnover in rodent tumors[14]. Similarly, in patients with rheumatoid arthritis, metabolism of synovial cells is highly up-regulated. Albumin could be a relevant source to meet the high demand for nitrogen and energy, and hence their enhanced uptake into these cells. For this, permeability of the blood-joint barrier for albumin in inflamed joints is markedly increased[15]. Since both the nanoparticles (Au-BSA and Au_{clust}-BSA) are BSA coated, cancerous cells might be

internalizing them with greater efficacy as compared to normal cells. NIH3T3 cells are normal fibroblast cells and lack these characteristics; hence uptake of nanoparticles by these cells could have been diminished or negligible.

4.4 Conclusion:

In this chapter, we have demonstrated that the cellular uptake of nanoparticles crucially depends upon the nature of cells. BSA capped nanoparticles or clusters were efficiently taken up by human glioma cells while no uptake was observed in normal fibroblast cells. Such enhanced uptake of BSA coated nanoparticles could have important implication in targeted drug delivery to cancerous cells using the BSA capped nanoparticles/clusters.

References:

1. Chithrani, B. D.; Ghazani, A. A.; Chan, W. C. W., Determining the size and shape dependence of gold nanoparticle uptake into mammalian cells. *Nano Lett* **2006,** 6, (4), 662-668.

2. Goodman, C. M.; McCusker, C. D.; Yilmaz, T.; Rotello, V. M., Toxicity of gold nanoparticles functionalized with cationic and anionic side chains. *Bioconjugate Chem* **2004,** 15, (4), 897-900.

3. Patra, H. K.; Banerjee, S.; Chaudhuri, U.; Lahiri, P.; Dasgupta, A. K., Cell selective response to gold nanoparticles. *Nanomedicine: Nanotechnology, Biology and Medicine* **2007,** 3, (2), 111-119.

4. Unfried, K.; Albrecht, C.; Klotz, L. O.; Von Mikecz, A.; Grether-Beck, S.; Schins, R. P. F., Cellular responses to nanoparticles: Target structures and mechanisms. *Nanotoxicology* **2007,** 1, (1), 52-71.

5. Arvizo, R. R.; Miranda, O. R.; Thompson, M. A.; Pabelick, C. M.; Bhattacharya, R.; Robertson, J. D.; Rotello, V. M.; Prakash, Y. S.; Mukherjee, P., Effect of nanoparticle surface charge at the plasma membrane and beyond. *Nano Lett* 10, (7), 2543-8.

6. Muhammed, M. A. H.; Shaw, A. K.; Pal, S. K.; Pradeep, T., Quantum Clusters of Gold Exhibiting FRET. *The Journal of Physical Chemistry C* **2008,** 112, (37), 14324-14330.

7. Muhammed, M. A. H.; Verma, P. K.; Pal, S. K.; Retnakumari, A.; Koyakutty, M.; Nair, S.; Pradeep, T., Luminescent Quantum Clusters of Gold in Bulk by Albumin-Induced Core Etching of Nanoparticles: Metal Ion Sensing, Metal-Enhanced Luminescence, and Biolabeling. *Chemistry-A European Journal*.

8. Demchenko, A. P.; Muhammed, M. A. H.; Pradeep, T., Luminescent Quantum Clusters of Gold as Bio-Labels. In *Advanced Fluorescence Reporters in Chemistry and Biology II*, Springer Berlin Heidelberg: Vol. 9, pp 333-353.

9. Lin, C. A. J.; Yang, T. Y.; Lee, C. H.; Huang, S. H.; Sperling, R. A.; Zanella, M.; Li, J. K.; Shen, J. L.; Wang, H. H.; Yeh, H. I., Synthesis, characterization, and bioconjugation of fluorescent gold nanoclusters toward biological labeling applications. *ACS nano* **2009,** 3, (2), 395-401.

10. Thomas, K. G.; Kamat, P. V., Chromophore-functionalized gold nanoparticles. *Acc. Chem. Res* **2003,** 36, (12), 888-898.

11. Eustis, S.; El-Sayed, M. A., Why gold nanoparticles are more precious than pretty gold: Noble metal surface plasmon resonance and its enhancement of the radiative and nonradiative properties of nanocrystals of different shapes. *Chemical Society Reviews* **2006,** 35, (3), 209-217.

12. Kratz, F., Albumin as a drug carrier: design of prodrugs, drug conjugates and nanoparticles. *Journal of Controlled Release* **2008,** 132, (3), 171-183.

13. Babson, A. L.; Winnick, T., Protein transfer in tumor-bearing rats. *Cancer Research* **1954,** 14, (8), 606.

14. Jacobson, G. B.; Watanabe, Y.; Valind, S.; Kuratsune, H.; Langstrom, B.; Stehle, G.; Sinn, H.; Wunder, A.; Schrenk, H. H.; Stewart, J. C. M., Plasma protein (albumin) catabolism by the tumor itself--implications for tumor metabolism and the genesis of cachexia. *Critical reviews in oncology/hematology* **1997,** 26, (2), 77-100.

15. Levick, J. R., Permeability of rheumatoid and normal human synovium to specific plasma proteins. *Arthritis & Rheumatism* **1981,** 24, (12), 1550-1560.

Chapter 5

BSA capped gold nanoparticles: an efficient drug delivering agent for the anticancer drug Methotrexate

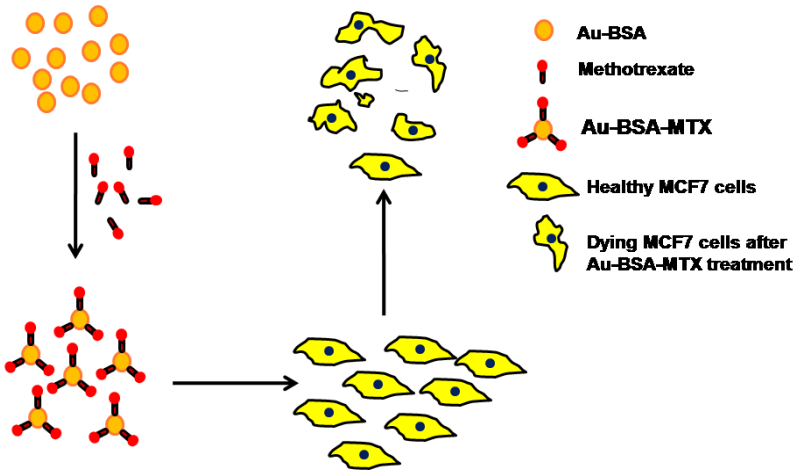

BSA capped gold nanoparticles were conjugated to methotrexate and their cytotoxicity against human breast cancer cell line MCF-7 was evaluated. The drug conjugated to BSA gold nanoparticles were found to evoke more toxicity to the cell lines than the equivalent concentration of drug alone. Drug loading was characterized by UV-vis spectroscopy, FTIR and TGA analysis. Cell death with Au-BSA-MTX was confirmed by MTT assay, Trypan blue viability counting, immunostaining, western analysis, DNA laddering assay, cell cycle analysis by FACS and TUNEL assay.

5.1 Introduction:

From the results presented in the previous chapters, we could confirm that Au-BSA nanoparticles meet the important requirements to serve as a good drug delivery agent. Thus we embarked on a study to load an anticancer drug methotrexate (MTX) on Au-BSA and tested its efficacy against human breast cancer cell line MCF-7. Based on the assumption that normal healthy cells do not actively divide, any substance that targets and blocks cell cycle will have a disproportionately severe effect on cancer cells in comparison to most healthy tissues[1]. MTX, an analogue of folic acid, is amongst the most widely used anticancer drug in a wide range of malignancies[2]. Folate receptors are over expressed in cancer cells[3]. The target for these receptors, folic acid is a small cofactor molecule that is an essential vitamin for human beings and is involved in the transfer of methyl group onto uracil to form thymine. During this process, folic acid molecule gets oxidized. Dihydrofolate reductase (DHFR) enzyme restores the oxidized folic acid to reduced form which in turn can undergo the new cycle of thymine synthesis. Anticancer drug MTX is a folic acid analogue and competitively inhibits DHFR. The affinity of MTX for DHFR is thousand fold greater than folic acid. When cells are treated with MTX, it competitively binds with DHFR and blocks its function. As a result, level of reduced folate decreases and hence syntheses of thymine and purine nucleotides stop. In such cases, uracil instead of thymine gets erroneously incorporated into the growing DNA chains. This leads into halting of DNA synthesis as repair enzymes cannot remove many faulty nucleotides efficiently and finally DNA fragmentation and apoptosis of cells occur[1]. In humans methotrexate appears to inhibit DNA synthesis to a greater extent than RNA synthesis, suggesting that inhibition of thymidylate synthesis is the most important mechanism of methotrexate cytotoxicity[2, 4]. Hence the drug is highly cell cycle dependent, acting primarily during DNA synthesis (S-phase). As a result, those tissues undergoing rapid cellular turnover with a high fraction of the cells in cycle are the most susceptible to the drug's cytocidal effects.

Breast cancer is the most common type of cancer and is the leading cause of cancer-related mortality worldwide in women. It is now the most common cancer in UK and in 2007 almost 45,700 women and 277 men were diagnosed with breast cancer. Female breast cancer incidence rates have increased by around 50 % over the

last twenty-five years. Breast cancer risk is strongly related to age, with 81 % of cases occurring in women aged 50 years and over and is the second most commonly diagnosed cancer in women under 35. In 2008 it was estimated that worldwide, 1.38 million women were diagnosed with breast cancer, accounting for around a tenth (10.9 %) of all new cancers and nearly a quarter (23 %) of all female cancer cases[5]. Breast cancer is controlled by surgery and radiotherapy, supported by adjuvant chemo- or hormono-therapies. However, current chemotherapies for breast cancer cells are limited due the emergence of drug resistance, non-specific effects, short term efficacy and toxicity on normal tissues[6]. Due to high resistance of breast cancer against chemotherapy, a highly efficient drug delivery system is required that can improve the tumor response and reduce the toxicity by improved targeting of drug to tumor cells and co-administration of drugs that prevent toxicity to normal but not to cancer cells. In this premise, nanoparticles are gaining interest as efficient drug delivery agent as they improve drug delivery to tumors without specific targeting by the so-called enhanced penetration and retention (EPR) effect, where the vessel leakiness and impaired lymphatic drainage of cancers causes accumulation of nanometer-sized particles[7].

Therefore, we chose to load the drug MTX on BSA capped gold nanoparticles and aimed to the study the anticancer effect of Au-BSA-MTX composite against breast cancer cell growth, proliferation and tried to delineate its mode of action leading to MCF-7 cell death.

5.2 Experimental details:

5.2.1Synthesis of gold nanoparticles by BSA:

The protocol of synthesis of gold nanoparticles by BSA is mentioned in section 2.2.1.ii

5.2.2 Synthesis, characterization and quantification of drug loaded Au-BSA:

For drug conjugation experiments, 1 µL of stock solution containing 25 mg/mL of Methotrexate (MTX) was added to 1 mL of $2X10^{-4}$ M Au-BSA and kept overnight for incubation at 4° C. Purification of Au-BSA-MTX from unbound MTX was done by centrifuging the solution at 10,000 rpm for 10 min followed by washings (thrice) with 10 mM phosphate buffer (pH= 7.1). Finally, the pellet was redispersed in 1 mL of

phosphate buffer such that the surface plasmon peak intensity of Au-BSA-MTX before and after the centrifugation was same and was characterized thoroughly by UV-vis spectroscopy, Zeta potential, FTIR and TGA analysis.

5.2.3 Cellular toxicity studies of Au-BSA, MTX and Au-BSA-MTX:

5.2.3.A *Cell line and growth medium:*

Human breast cancer cell line MCF-7 was procured from the Cell Repository of National Centre for Cell Science, Pune, India and cultured in Dulbecco's modified eagle's medium (DMEM) (Gibco BRL Carlsbad CA), supplemented with 1.5 gm/L sodium bicarbonate, 4 mM glutamine and 10% fetal bovine serum (Gibco, USA). The cultures were maintained in a humidified atmosphere of 5% CO_2 at 37 °C in an incubator.

5.2.3.B *In vitro cytotoxicity test:*

Cytotoxicity studies of Au-BSA-MTX and MTX were performed by seeding 3000 cells/well of MCF-7 cells in a 96 well plate. After plating of the cells, they were incubated for 24 h in order to allow them plate prior to the administration of samples. After 24 h of incubation, cell medium was replaced with 200 µL of solution containing fresh medium, Au-BSA, MTX and Au-BSA-MTX. Cells incubated with medium alone were taken as control. To determine the effect of blank nanoparticles on cell viability, cells were incubated with Au-BSA alone. After the addition of the entire test samples, cells were then further incubated for 72 h at 37 °C and 5 % CO_2 in a humidified environment to allow both time dependent and concentration dependent drug-induced cytotoxicity. At the end of each exposure, the toxicity level of each test samples was assessed by MTT assay[8] to determine the cytotoxicity of Au-BSA-MTX in comparison with free MTX and Au-BSA. After incubation of cells with test samples, MTT was added and incubated further for 4 h. After 4 h, medium was removed and 100 µL of DMSO was added to dissolve the formazan crystal resulting from the reduction of tetrazolium salt by metabolically active cells only. The absorbance of dissolved formazan crystals was measured at 570 nm. Since the absorbance directly indicates the number of viable cells, % viability was calculated directly from the absorbance values. All experiments were performed in triplicates.

5.2.3.C *Cell viability assay by Trypan Blue:*

Trypan blue is a diazo dye; a vital stain, used to selectively color dead cells. Live cells/tissues having intact plasma membrane will not take up the dye and hence will not get colored. When viewed under microscope, only dead cells will appear blue colored. Viability of cells can be calculated by the following formula: % viability = [(no. of viable cells)/ no. of dead + no. of viable cells)]. In this, cell suspension of the sample to be assayed was prepared and diluted in 1:1 ratio with 0.4 % Trypan blue solution. The diluted cell suspension was loaded on the counting chambers of hemocytometer and allowed to settle in the counting chamber. The number of stained cells was counted followed by total cell count. Percentage of stained cells and unstained cells were calculated and represented as dead and live cells respectively.

5.2.3.D *Immunostaining:*

Immunostaining studies were performed by seeding MCF-7 cells at low density on cover slips in a 24 well plate. After plating of the cells, they were allowed to attach to the cover slips and hence were incubated for 24 h prior to the administration of samples. After 24 h of incubation, cell medium was replaced with 500 µL of solution containing fresh medium, Au-BSA, MTX and Au-BSA-MTX for 48 h and then used for the immunostaining. Cells were first rinsed with PBS, fixed in absolute methanol for 10 minutes at -20 ºC and then left for rehydration in PBS for 1h followed by blocking in 5 % BSA. Then the cells on coverslips were incubated with first antibody diluted in 1XPBS (1:100) for 1 h and washed thrice with PBS. Secondary antibody (dilution 1:50 anti-mouse AlexaFlour594 conjugated, anti-rabbit AlexaFlour594 conjugated and anti-goat AlexaFlour594 conjugated) was added and the cells were incubated on the coverslip for 1 h, followed by 3 washes with PBS. 10 µL DAPI of 5 mg/mL stock was added and washing with PBS was done. Coverslips were mounted on glass slides by using 1 % antifade DABCO (1,4-diazabicyclo[2.2.2]octane) as mounting medium. The expression of the markers was analyzed by Laser Scanning Confocal Microscopy (LSCM).

5.2.3.E *Western blot analysis:*

MCF7 cells were cultured and given treatment with Au-BSA, MTX and Au-BSA-MTX for 48 h. Cells incubated with medium alone were taken as control. The treated cell plate was washed with chilled PBS and later collected by scraping the cells using a cell scraper. The cells were washed with ice-cold TBS twice and lysed in chilled

cytoskeleton extraction (CSE) buffer. To make cell lysate, cells were resuspended in CSE buffer and sonicated. Lysate was spun at 12000 rpm, 30 minutes at 4 °C to remove debris. After that, it was mixed with equal volume of 3X PAGE loading dye, boiled at 95 °C for 4 minutes. Samples prepared were then loaded on 15 % SDS-polyacrylamide gels. The proteins were transferred to PVDF membrane using semidry transfer, and western blotting was performed. For western blotting PVDF membranes were incubated with cleaved caspase-3 (Asp175) primary antibody in 1-2 % non-fat dry milk for 1.3-2 h. The cleaved caspase3 (Asp175) antibody detects endogenous levels of the large fragment (17/19 kD) of activated caspase-3 resulting from cleavage adjacent to Asp175. After incubation, washing with 1X TBST for three times was done followed by incubation with secondary antibodies at 1:15,000 dilutions. Further they were washed three times with 1X TBST and blots were developed using ECL plus western detection kit, following the manufacturer's instructions.

5.2.3.F *Quantification of gold in MCF-7 cells:*

Inductively coupled plasma (ICP) is an analytical technique used for the detection of elements in sample. Quantification of gold after exposing MCF-7 cell line to Au-BSA and Au-BSA-MTX in MCF-7 cell line was performed by ICP by seeding these cells in a 24 well plate. After plating of the cells, they were allowed to attach to 24 well plate and hence were incubated for 24 h prior to the administration of samples. After 24 h of incubation, cell medium was replaced with 500 µL of solution containing fresh medium, Au-BSA, MTX and Au-BSA-MTX. The cells were then further incubated for 3 h at 37 °C. After 3 h of incubation, cells were trypsinized and collected and washed thrice to remove nanoparticles on the surface of cells. These cells were then digested using 3N HCl and ICP analysis was performed on them.

5.2.3.G *Identification of apoptosis by flow cytometry analysis (FACS):*

For the analysis of apoptosis by FACS, 10^5 cells were seeded in 55 mm plates. After 24 h, 48 h and 72 h cells were trypsinized and collected in DMEM containing 10 % serum to neutralize the effect of trypsin. The cells were then collected by centrifugation at 1,500 rpm at room temperature for 5 min, washed with PBS and resuspended in PBS. To permeabilize the cells for PI, the cells were fixed by drop wise addition of 70 % ethanol with gently vortexing of the cell suspension. This solution was left on ice for 1 h or at 4 °C overnight. After incubation period, cells

were washed with PBS, followed by addition of 5 µL of RNase (10 µg/mL stock solution). This cell suspension was incubated at 37 °C for 1 h. After this, 5 µL of PI (2 mg/mL stock) was added 15 minutes prior to acquiring the sample and were analyzed on Flow Cytometer.

5.2.3.H*Terminal deoxynucleotidyl transferase-mediated dUTP nick-end labeling (TUNEL)* assay:

MCF-7 cells were seeded in 55 mm petri plate until 70 % confluent, followed by treatment with MTX for 24 h, 48 h and 72 h at the indicated doses. Cells were then washed with phosphate-buffered saline (PBS) and then fixed with 1 % (w/v) paraformaldehyde in PBS and incubated on ice for 15 minutes. Fixed cells were washed with PBS twice and finally resuspended in 500 µL of PBS. This cell suspension was added drop wise in 5 mL of ice-cold 70 % (v/v) ethanol and stored at -20 °C. Apoptotic cells were determined by using APO-BrdU^{TM} TUNEL Assay Kit (Molecular Probes).

5.2.3.I *DNA laddering experiment:*

The confluent cells were treated with Au-BSA, MTX and Au-BSA-MTX for 24 h and then media was removed. Cells were washed with 1X PBS. 1.5 mL of TEN9 buffer [50mM Tris-pH 9, 100 mM EDTA, 200 mM NaCl, 10 % SDS and 150 µL of Proteinase K (10mg/ml)] was added and incubated at 37 °C for overnight. The lysate was collected in centrifuge tubes and equal volume of phenol was added to it. After centrifugation at 12,000 rpm for 10 minutes, supernatant was collected. To it equal volume of Chloroform Isoamyl alcohol (24:1) was added to the tubes followed by vigorous shaking. The tubes were then centrifuged at 12,000 rpm for 10 minutes and supernatant was collected in fresh tubes. DNA was precipitated by adding 3 equal volumes of absolute ethanol to the supernatant and centrifugation at 8,000 rpm for 5 minute was done. Pellet containing DNA was washed with 70 % ethanol and centrifuged at 8,000 rpm for 5 minutes and allowed to dry for 15 minutes. DNA was then resuspended in T10E1 buffer (10 mM Tris-HCl, 1 mM EDTA pH-8.0). 2 µL of RNAse (1µg/µL) was added to 10 µg of DNA and kept at 37 °C for10 minutes. 5 µg of DNA was loaded using loading buffer (0.1 % bromophenol blue, 0.1 % xylene cyanol FF, 60 % Glycerol) and run on a 0.8 % agarose gel electrophoresis in 1X TAE buffer (pH-8) at 70 V for 2 h.

5.3 Results and Discussion:

BSA has long been used for improving the stability, non-immunogenicity, toxicity and pharmacokinetic profile of many therapeutic drugs, proteins and peptides[9]. In the present study we used BSA capped gold nanoparticles (Au-BSA) for drug delivery applications. BSA capping provides sufficient functional moieties exposed on the surface of gold nanoparticles to which common anticancer drug MTX can attach. MTX is an analogue of folic acid (FA) and the main difference between FA and MTX is that FA has a hydroxyl group at the 4-position of the pyridine ring (Figure 5.1 A), while in MTX an amine group is present at the same position (Figure 5.1 B). Due to the structural similarity, cells internalize MTX through similar transport systems as folates. Therefore, MTX can be used not only as a drug but also as a potential targeting ligand. Linking MTX to nanoparticles allows for efficient and selective cellular uptake, a property unique to nanoparticle carriers. This could lead to enhanced therapeutic efficacy for the same amount of drug used.

This section is divided into two parts; first part describes the synthesis and characterization of drug loaded nanoparticles and later part deals with its anticancer activity against breast cancer cell line.

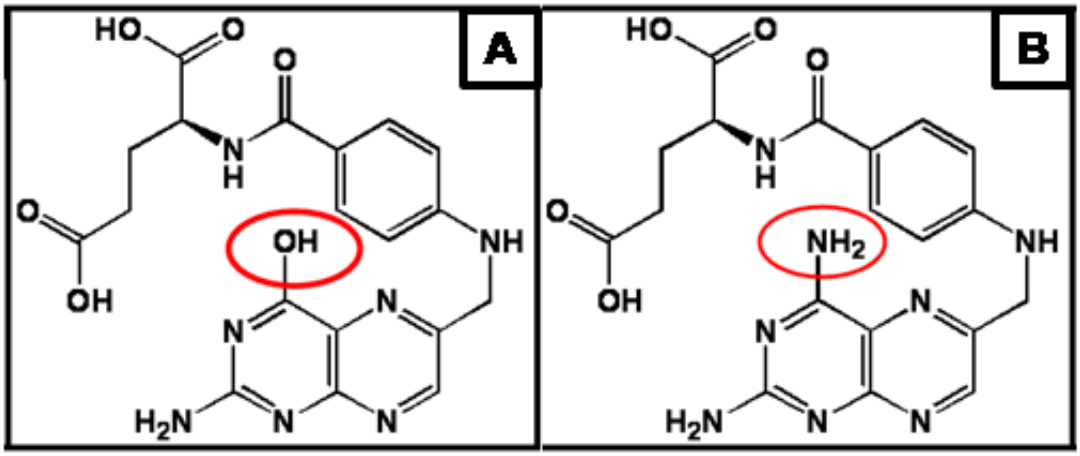

Figure 5.1: *Structure of* **(A)** *Folic acid and* **(B)** *Methotrexate.*

A) Characterization of Au-BSA and Au-BSA-MTX:

5.3.1 UV-vis absorption spectroscopy:

UV/vis absorption studies were done to monitor the MTX loading on Au-BSA. Au-BSA nanoparticles show characteristic absorption band at 527 nm (Curve 1, Figure 5.2). However, after conjugation with MTX, the surface plasmon peak shifted to 540 nm (Curve 2). This 13 nm shift in plasmon absorption peak could be due to a change in the local dielectric constant around Au-BSA nanoparticles as a result of MTX loading[10]. Absorption spectrum of pure MTX is shown in the inset of Figure 5.2.

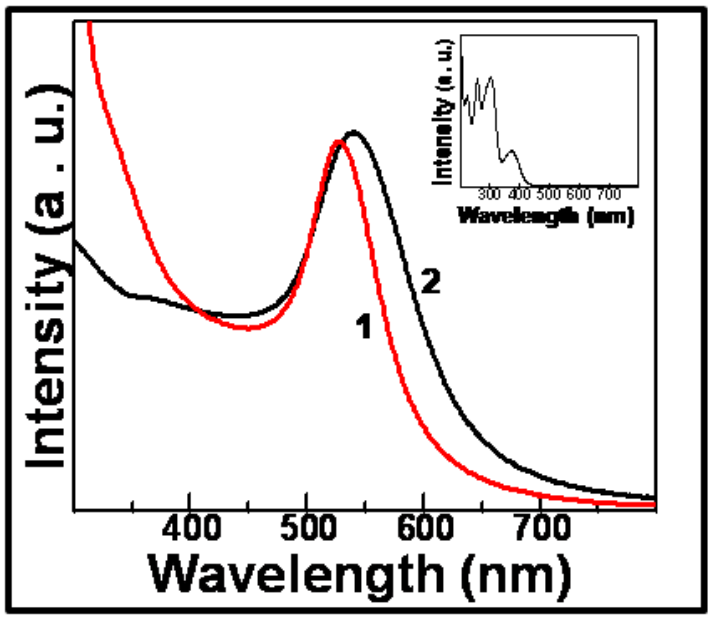

Figure 5.2: *UV/vis absorption curve of Au-BSA (curve 1) and Au-BSA-MTX (curve 2). Inset in the figure shows the absorption of pure MTX.*

5.3.2 Zeta Potential measurements:

The surface charge of Au-BSA before and after loading of MTX was determined by measurement of zeta potential. The average zeta potential of nanoparticles dispersion was determined as such without any dilution. At neutral pH, zeta potential values of Au-BSA was -28.7±6.7 mV which indicates that BSA capping imparts negative charge to gold nanoparticle surface and hence stability by electrostatic means. However, an increase in zeta potential value (-10.4±4.2 mV) was observed after MTX loading onto Au-BSA nanoparticles indicating the conjugation of MTX on Au-BSA. This may be attributed to the extra $–NH_2$ groups in MTX. Primary amines have a pKa in the range 9-11. So at neutral pH the $–NH_2$ group acquires a positive charge

which could lead to an overall reduction in the charge on the particle surface and hence could be a reason for the change in zeta potential values.

5.3.3 Agarose gel electrophoresis study:

Agarose gel electrophoresis was performed to further determine the charge present on Au-BSA-MTX. Figure 5.3 show the gel image where both Au-BSA and Au-BSA-MTX move towards the anode validating the presence of negative charge on the surface of nanoparticle systems. DNA loading dye having negative charge was used as a control for this experiment. Gel images show that Au-BSA-MTX has reduced mobility in comparison to Au-BSA which can be attributed to lower zeta potential value in comparison to Au-BSA.

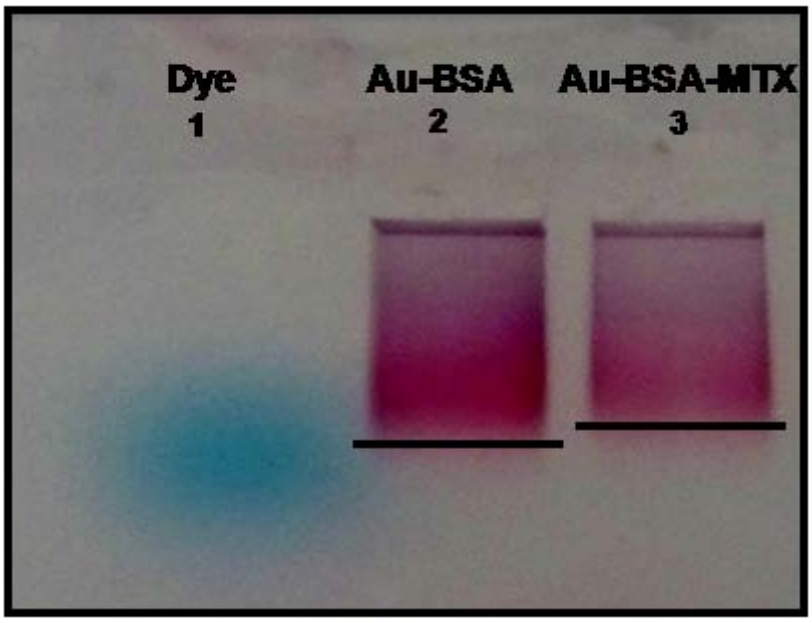

Figure 5.3: *Agarose gel electrophoresis of DNA loading dye (Lane 1), Au-BSA (Lane 2) and Au-BSA-MTX (Lane 3).*

5.3.4 Fourier Transform Infrared Spectroscopy (FTIR) measurements:

To further validate the loading of MTX on Au-BSA, an FTIR spectrum of MTX in pure solid form and in an adsorbed condition on Au-BSA was recorded (Figure 5.4 A). In pure BSA, 1659 cm^{-1} peak is ascribed to amide I and 1535 cm^{-1} peak is ascribed to amide II bonds respectively (curve 2). Their positions do not undergo any change in Au-BSA (curve 3). However after MTX loading and conjugation, a shift in amide I

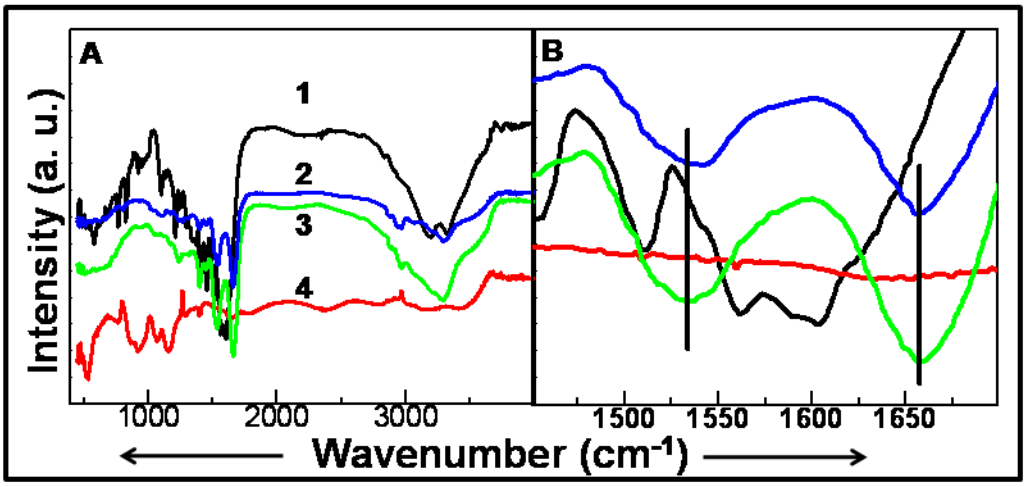

Figure 5.4: (A) *FTIR spectra of pure MTX (curve 1), pure BSA (curve 2), Au-BSA (curve 3) and Au-BSA-MTX (curve 4).* **(B)** *shows enlarged FTIR spectra of amide I and amide II bands.*

was observed while amide II peak disappears completely (Figure 5.4 B). Curve 1 represents the spectra recorded from pure MTX.

5.3.5 Thermogravimetric Analysis:

In order to quantify the amount of drug loaded on nanoparticle, thermogravimetric analysis of Au-BSA before and after MTX loading was performed. Curve 1 and curve 2 of Figure 5.5 show the weight loss in Au-BSA and Au-BSA-MTX respectively. From curve 1 it can be seen that weight loss in Au-BSA nanoparticles is approximately 30 % corresponding to the loss of BSA molecules attached to the nanoparticles. Approximately 50 % loss in weight is observed in MTX loaded Au-BSA nanoparticles as can be seen from curve 2. This corresponds to the combined loss of BSA and MTX molecules present on gold nanoparticles. Based on this result and considering the size of nanoparticles to be 15 nm, concentration of BSA and MTX are evaluated to be 2.6 X 10^{-22} moles and 1.8 X 10^{-20} moles per gold nanoparticle respectively.

B) Cellular toxicity studies of Au-BSA, MTX and Au-BSA-MTX:

5.3.6 Phase contrast images of MCF7cells:

Based on the fact that Au-BSA nanoparticles are highly cytocompatible and stable under varying pH and salt concentrations and are preferentially taken up by cancerous

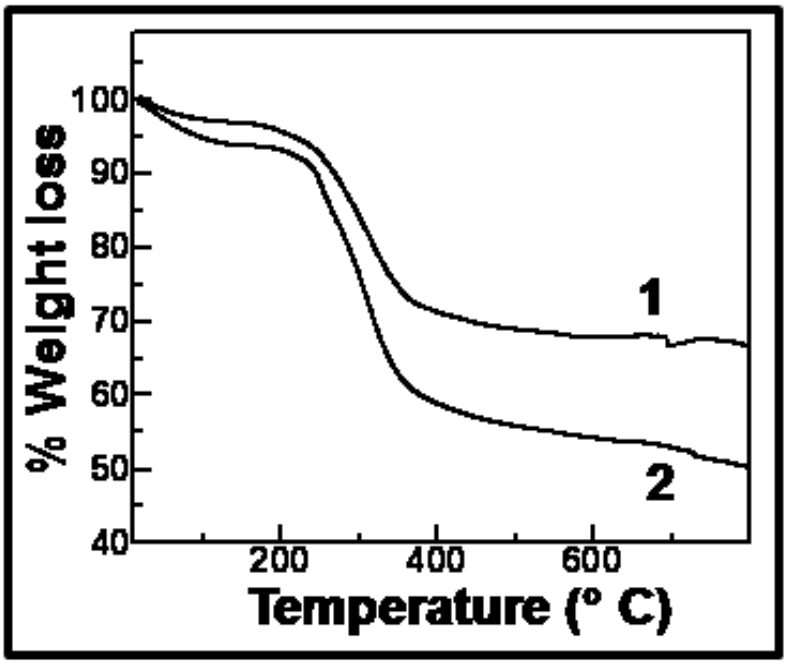

Figure 5.5: *TGA spectra showing weight loss in Au-BSA (curve 1) and Au-BSA-MTX (curve 2).*

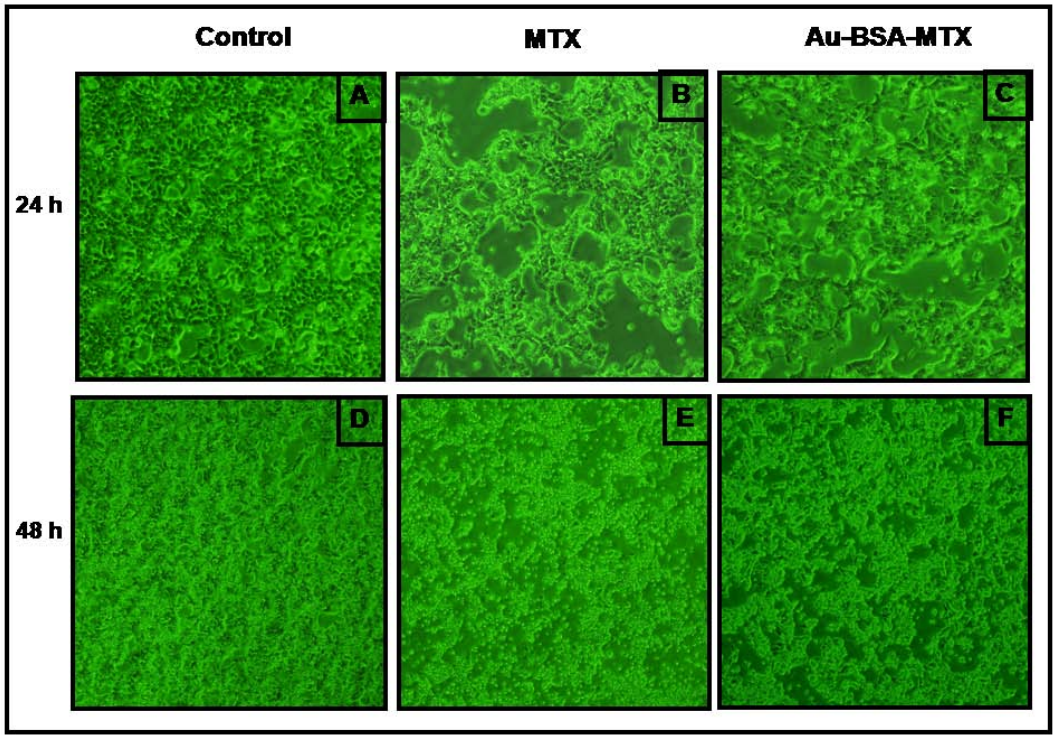

Figure 5.6: *Microscopic imaging of MCF7 treated with MTX and Au-MTX over a period of 24 h and 48 h in the presence of serum.*

cells than normal cells, we explored the potential of Au-BSA nanoparticles as a drug delivery carrier/agent. Exposure of cells to various toxic chemical agents or drugs leads to noticeable changes in the cell shape and morphology. Figure 5.6 A and D shows healthy MCF7 control cells over a period of 24 h and 48 h respectively. Figure 5.6 B and E shows the images of cells after treatment with bare MTX over a period of 24 h and 48 h. As can be seen from the images, due to drug action killing of cells was observed. Although the effect of the treatment was seen by 24 h, a more pronounced effect of the treatment is observed after 48 h. Similarly Figures 5.6 C and F show the effect of Au-BSA-MTX over a period of 24 and 48 h. In these figures it can be observed that the percentage of dead cells observed in Au-BSA-MTX treated cells at 48 h is visibly higher than that treated with only MTX. Many earlier investigations suggested that highly proliferating cells take up BSA as source of nutrients and energy[9]. We surmise that this may have lead to an enhanced uptake of Au-BSA nanoparticles and thus better drug delivery.

5.3.7 Trypan blue exclusion assay and Inductively coupled plasma (ICP) measurements:

This was further validated by Trypan blue exclusion assay and ICP analysis (Figure 5.7 A and B respectively). The Trypan blue dye exclusion assay shows that MTX had only 30 % live cell population; whereas Au-BSA-MTX had only 20 % live cell population. These results showed that Au-BSA-MTX was more efficient in killing MCF7 cells as compared to only drug. The same was confirmed by ICP analysis of MCF7 cells treated with MTX, Au-BSA and Au-BSA-MTX. ICP studies were performed to quantify the concentration of gold present in different cell lines treated with Au-BSA and Au-BSA-MTX. Standard curve for gold was made by using the known concentrations of gold. Finally, the concentration of gold present in cells treated with Au-BSA and Au-BSA-MTX were obtained from the standard graph. Figure 5.7 B shows an elevated uptake of gold in cells treated with Au-BSA-MTX as that compared to Au-BSA. This elevated uptake level and more efficient killing of cells by Au-BSA-MTX can be attributed to over expressed folate receptors in addition to the protein receptors present on MCF7 cells. Due to this, in comparison to free MTX, two mechanisms would be operative for the uptake of the MTX conjugated Au-BSA nanoparticles into the cancerous cells. One is the interaction of MTX with the

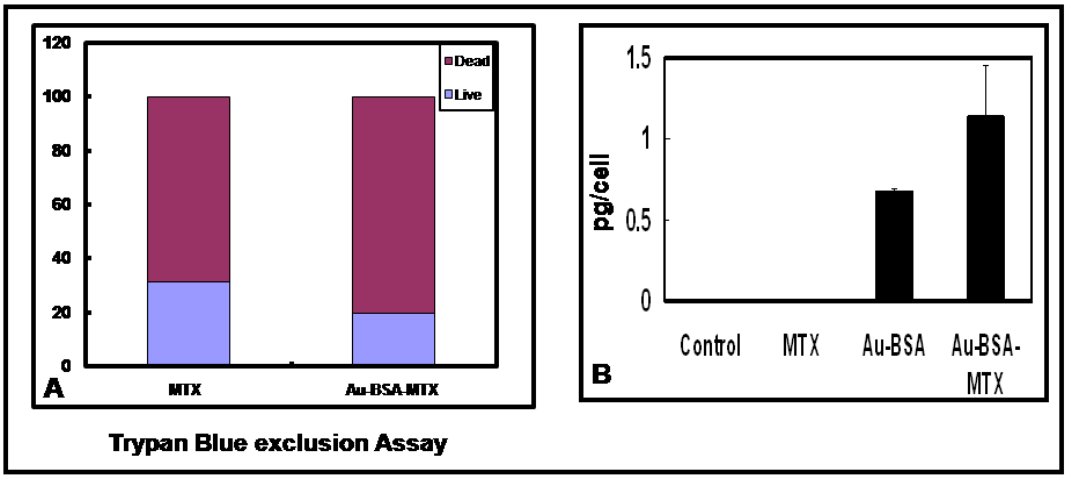

Figure 5.7: (A) *Trypan blue dye exclusion assay performed on MCF7 cells treated with MTX and Au-BSA-MTX in presence and absence of serum.* **(B)** *ICP analysis of MCF7 cells treated with MTX, Au-BSA and Au-BSA-MTX.*

folate receptors as a ligand followed by its uptake and another is interaction of BSA present on gold nanoparticles with the cell membrane proteins that facilitate the internalization of Au-BSA-MTX conjugate[10]. Such a synergistic effect would lead to an increased accumulation of MTX inside the cells resulting in a more pronounced effect.

5.3.8 MTT assay:

Pushing forward to determine the anticancer activity of free drug MTX and Au-BSA-MTX in a more quantitative way, MTT assay was performed on human breast cancer (MCF-7) cell line. MCF-7 cells in media were taken as controls that are assumed to have 100 % cell viability. Figure 5.8 summarizes the result obtained after 72 h of incubation of cells with different formulations, namely, Au-BSA, free MTX and Au-BSA-MTX. Au-BSA showed no effect on cell viability with respect to the increasing concentration even after 72 h of incubation confirming the biocompatibility of bare nanoparticles. However, decrease in the percent viability of cells treated with MTX and Au-BSA-MTX with increase in drug concentration was observed. It should be noted that at each concentration the drug loaded nanoparticles were taken such that the MTX concentration on them was similar to that of free drug, making a direct comparison possible. At the highest drug concentration of 1µg, a 20 % enhanced

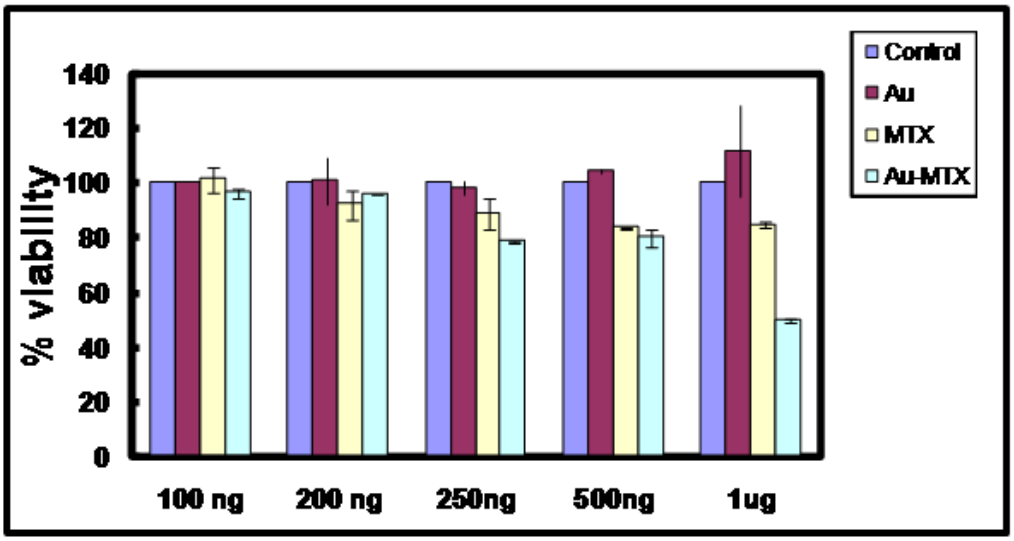

Figure 5.8: *Toxicity study of varying concentration of MTX and Au-BSA-MTX by MTT assay.*

killing of the cells treated with Au-BSA-MTX compared to free MTX was observed. Thus Au-BSA nanoparticles turned out to be more effective in killing the cancerous cells. Since results obtained with Au-BSA-MTX system were very encouraging, to get some more insights into the mechanism of action, we proceeded further to probe various biochemical aspects of the anticancer activity of Au-BSA-MTX.

5.3.9 Immunostaining of Ki-67 protein:

Ki-67 protein is a marker protein used to determine the growth fraction of a given cell population and expression of human Ki-67 is strictly associated with cell proliferation[11]. Ki-67 protein is present throughout the active phases of cell cycle (G_1, S, G_2) except the resting phase (G_0). MCF-7 cells treated with Au-BSA, MTX and Au-BSA-MTX were assessed for their proliferation rates using Ki-67 assay. Cells with media alone were taken as control. Proliferation rates were determined on the basis of average number of number of Ki67 positive cells in 10 fields over total number of cells in those respective fields. Control cells and Au-BSA treated cells show normal proliferation rates as can be seen from Figure 5.9 A and B. However, a decrease in number of Ki-67 positive cells was observed in MTX (Figure 5.9 C) and Au-BSA-MTX (Figure 5.9 D) treated cells. A closer examination of the images showed a difference in the staining pattern of Ki-67 protein in MTX and Au-BSA-

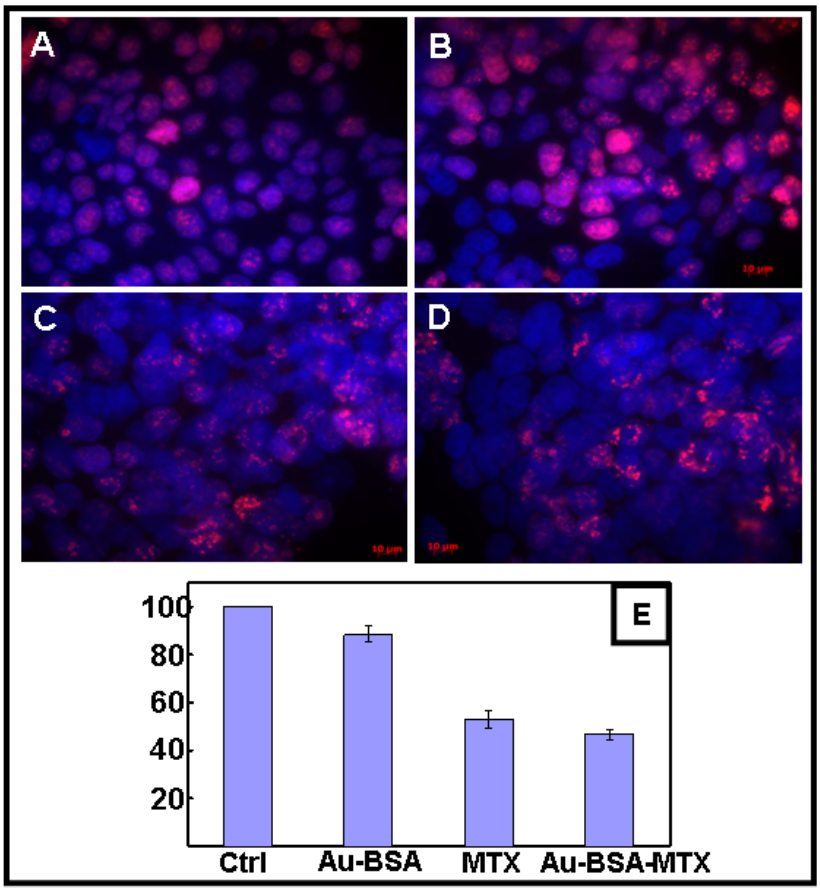

Figure 5.9: *Immunostaining of Ki-67 in MCF7 cells.* **(A)** *Control,* **(B)** *Au-BSA,* **(C)** *MTX and* **(D)** *Au-BSA-MTX treated MCF-7 cells.* **(E)** *Graph showing number of cells positive for Ki-67 proliferation marker protein after the treatment.*

MTX treated cells with respect to that of control cells and Au-BSA treated cells. In the control and Au-BSA treated cells, Ki-67 was found to stain nuclei uniformly whereas in pure MTX and Au-BSA-MTX instead of uniform nuclear staining of Ki-67, punctate staining was observed indicating disintegration of nuclear content. This difference in staining pattern and decrease in Ki-67 positive cells in MTX and Au-BSA-MTX can be attributed to the occurrence of drug induced nuclear fragmentation and apoptosis. Figure 5.9 E shows a graphical representation of Ki-67 positive cells in test as well as control cells. A clear decrease in the number of proliferating cells in comparison to control cells was observed after drug treatment.

5.3.10 Caspase-3 study:

We further tried to check whether cell death was occurring due to apoptosis or necrosis. The process of neoplastic transformation, progression and metastasis

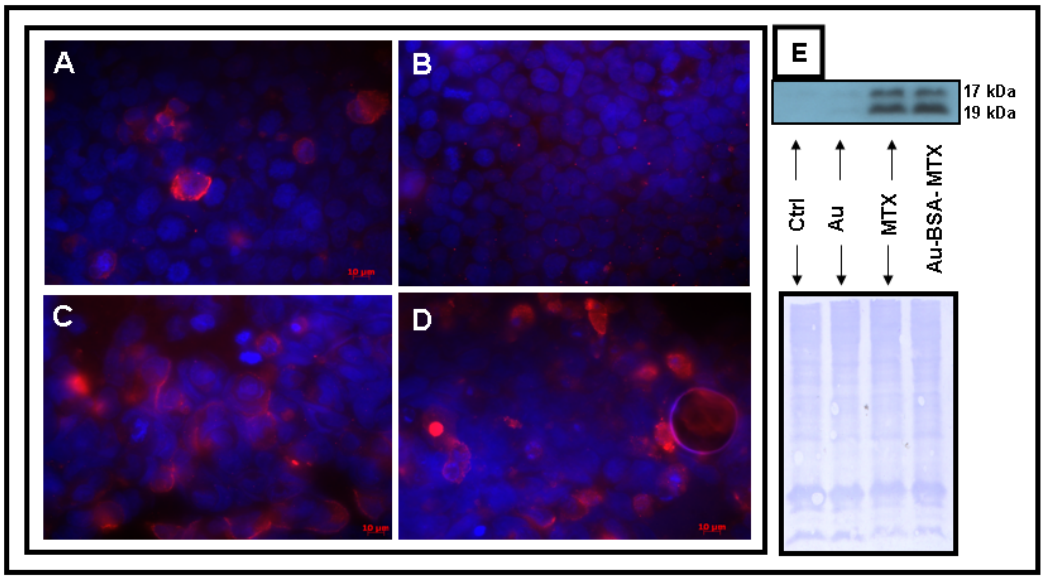

Figure 5.10: *Immunostaining of Caspase-3 in MCF7 cells.* **(A)** *Control,***(B)** *Au-BSA,* **(C)** *MTX and* **(D)** *Au-BSA-MTX treated MCF-7 cells.* **(E)** *Upper panel shows Western blot analysis for Caspase-3 and lower panel shows Coomassie Brilliant Blue staining for equal loading of proteins.*

involves alterations in apoptotic pathways[12]. On the other hand, many chemotherapeutic agents utilize apoptotic pathway for the induction of cancer cell death. However, resistance of cancer cells to standard chemotherapy seems to occur due to alterations in the apoptotic pathways. Therefore, understanding the role and mechanisms of apoptosis and its application for cancer treatment may lead to advancement in chemotherapy. Biochemical events involved in apoptotic pathway are very complex that involve a variety of different signaling pathways and results in a multitude of changes in the dying cell. Effectors of apoptosis are many and activation of one or more members of a family of cysteine proteases called caspases are involved in most of the apoptotic pathways of mammalian cells[12]. Caspases exert their action at several levels of signaling during apoptosis, ranging from responding to external factors at the transmembrane receptor to proteolytic breakdown of cellular components. Their proteolytic activity results ultimately in the demise of the cell and has led to caspases being called the central executioners of apoptosis. Among the group of 11 caspases identified to date in humans, Caspase-3 has been recognized as a central player in mediating apoptosis and is the most widely studied. Caspases are synthesized and exist mostly in the cytoplasm of viable cells as an inactive pro-

enzyme. Activation of caspase zymogens is an early event in the process of apoptosis[13, 14].

In order to deduce by which pathway apoptosis is induced, we probed Au-BSA, MTX and Au-BSA-MTX treated MCF7 cells with caspase-3 antibody. From Figure 5.10 it is observed that only few cells are positive for caspase-3 in control cells (Figure 5.10 A) and Au-BSA treated cells (Figure 5.10 B). While cells treated with MTX (Figure 5.10 C) and Au-BSA-MTX (Figure 5.10 D) showed a high number of caspase-3 positive cells. To further validate the same, we performed western blot analysis for caspase-3. Caspase-3 occurs as an inactive zymogen form under normal cell conditions and gets activated during apoptosis. Activation requires proteolytic processing of its inactive zymogen into activated 17 and 19 kDa fragments. Figure 5.10 E shows western blot analysis for caspase-3. MCF-7 cells treated with MTX and Au-BSA-MTX show two bands of 17 kDa and 19 kDa corresponding to activated caspase-3 proteins. Coomassie Brilliant Blue staining of the membrane was performed to determine the equal loading of proteins. These results show that cell death in MCF-7 cells when they are treated with pure MTX or Au-BSA-MTX was by the induction of caspase-3 mediated apoptosis and not due to necrosis.

5.3.11 DNA laddering study:

Death taking place via apoptosis was also confirmed by performing gel electrophoresis of DNA samples of cells treated with Au-BSA, MTX and Au-BSA-MTX. Untreated cells were taken as control. DNA cleavage during apoptosis occurs at sites between nucleosomes, protein-containing structures that occur in chromatin at ~200 bp intervals[15]. This DNA fragmentation was analyzed using agarose gel electrophoresis to demonstrate a "ladder" pattern at ~200 bp intervals. Necrosis, on the other hand, is characterized by random DNA fragmentation which forms a "smear" on agarose gels. Lane 1 of Figure 5.11 was loaded with 1kb ladder. Lane 2, 3, 4 and 5 were loaded with equal amount of DNA extracted from control MCF-7 cells, Au-BSA treatment, MTX treatment and Au-BSA-MTX respectively. Intact DNA band was observed in control and Au-BSA treated cells as no DNA fragmentation has occurred. However an apoptotic DNA fragmentation at an interval of 200 bp in MCF-7 cells treated with MTX and Au-BSA-MTX was seen which indicated induced apoptosis. A closer look shows that the DNA fragmentation observed in the sample of

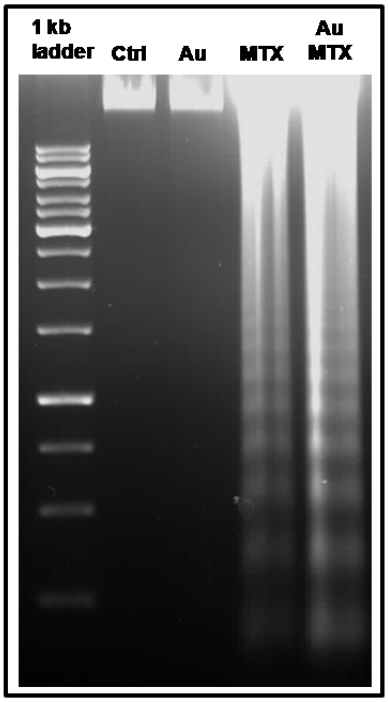

Figure 5.11: *Gel electrophoresis of DNA of MCF7 cells treated with Au-BSA, MTX and Au-BSA-MTX*

MCF-7 cells treated with Au-BSA-MTX is more pronounced as compared to MTX confirming more effective killing by Au-BSA-MTX.

5.3.12 Cell cycle analysis by FACS and TUNEL assay:

MTX is known to effect the cell cycle by preventing the progression of cells from G_1 to S phase of cell cycle and arrests cells in the late G_1-S boundary[16, 17]. Therefore in order to establish the mechanism of action of the MTX, cell cycle analysis of drug treated MCF-7 cells was performed using Flow Cytometry. The percentage number of cells in a particular stage of cell division is based on the amount of DNA present in the cell. Figure 5.12 A shows cell cycle analysis graph. Over the period of 6, 12 and 24 h, control cells and Au-BSA treated cells show an increase in percentage cell number in S+G_2M indicative of the cells moving to the next phase of cell division after G_0-G_1 phase. We observe that cells treated with Au-BSA behave in the same manner as control. The percentage numbers of cells present in G_0-G_1 phase in control and Au-BSA is almost near 50 %, after 24 h and 40 % in S+G_2M. In cells treated with MTX and Au-BSA-MTX almost 65 % of cells have been arrested in the late G1 phase due to which only around 22 % of cells have been able to be move on to S+G_2M

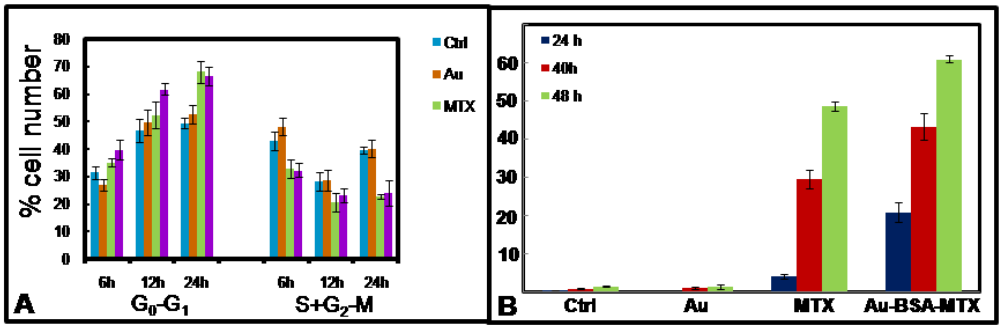

Figure 5.12: (A) *Cell cycle analysis of MCF-7 cells treated with Au-BSA, MTX and Au-BSA-MTX over a period of 6 h, 12h and 24h.* **(B)** *TUNEL assay performed on MCF-7over a period of 24 h, 40 h and 48 h.*

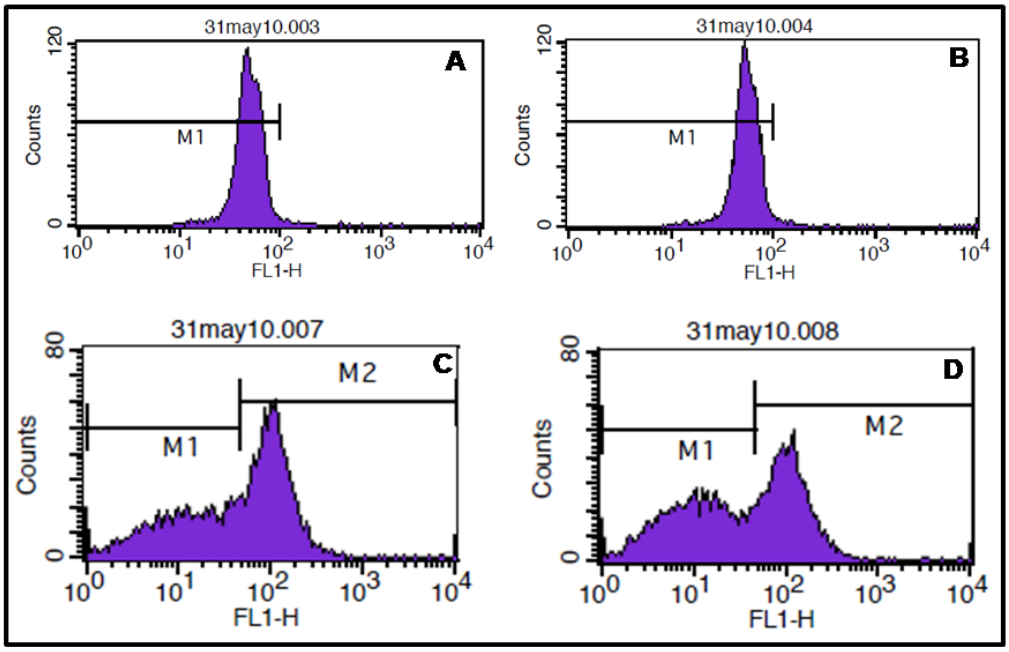

Figure 5.13: (A) *Representative images of TUNEL assay performed on MCF-7 cells at 48 h.* **(A)** *MCF-7 cells (control),* **(B)** *Au-BSA,* **(C)** *pure MTX and* **(D)** *Au-BSA-MTX.*

population. Thus the time dependent study of cell cycle in MCF-7 cells shows that the free drug and Au-BSA-MTX effectively show late G_1 to S phase arrest. TUNEL assay was performed to clearly separate the live cell population and apoptotic cell population. Apoptotic cells show BrdU incorporation and therefore are positive for anti-BrdU antibody[18, 19]. TUNEL assay also showed (Figure 5.12 B) that as the time proceeds, the percentage of apoptotic cell population increases in MTX and Au-BSA-

MTX treated cells. Interestingly, as can be seen from the graph, the percentage of apoptotic cell population is always higher in Au-BSA-MTX treated cells as compared to pure MTX treated cells. Compared to MTX alone, Au-BSA-MTX showed 16 %, 10 %, and 12 % higher apoptotic cell population at 24 h, 40 h and at 48 h of treatment respectively. Thus, the Au-BSA-MTX seems to work better and with greater efficiency at all times as compared to bare MTX drug alone. Figure 5.13 shows representative images of tunnel assay performed at 48 h. In summary this data indicates that drug and drug loaded nanoparticles induce G_1-S phase arrest and induce apoptosis in breast cancer cell line MCF-7.

5.4 Conclusion:

Breast cancer is the most common type of cancer occurring in women worldwide. Human breast cancer cells over express folate receptors. Methotrexate is a folic acid analogue and causes cell death by mediating cell cycle arrest and apoptosis. We have demonstrated successful loading of MTX on Au-BSA nanoparticles and assessed its concentration and time dependent anticancer activity on MCF-7 breast cancer cell line. MTT assay and Ki-67 proliferation studies showed that MTX induces inhibitory action on the growth of MCF-7 cell line. DNA gel electrophoresis, Flow cytometry and TUNEL assay studies showed that the MTX induced G_1-S phase arrest, DNA fragmentation and finally led to apoptosis. The apoptotic cell death is mediated by the induction of caspase-3 pathway.

References:

1. Goodsell, D. S., The molecular perspective: Methotrexate. *The Oncologist* **1999,** 4, (4), 340.

2. Bleyer, W. A., The clinical pharmacology of methotrexate. New applications of an old drug. *Cancer* **1978,** 41, (1), 36-51.

3. Kohler, N.; Sun, C.; Wang, J.; Zhang, M., Methotrexate-modified superparamagnetic nanoparticles and their intracellular uptake into human cancer cells. *Langmuir* **2005,** 21, (19), 8858-8864.

4. Hoffbrand, A. V.; Tripp, E., Unbalanced deoxyribonucleotide synthesis caused by methotrexate. *British Medical Journal* **1972,** 2, (5806), 140.

5. Ferlay, J.; Shin, H. R.; Bray, F.; Forman, D.; Mathers, C.; Parkin, D. M., GLOBOCAN 2008, Cancer Incidence and Mortality Worldwide: IARC CancerBase No. 10 [Internet]. In International Agency for Research on Cancer, Lyon, France.

6. Nizamutdinova, I. T.; Lee, G. W.; Son, K. H.; Jeon, S. J.; Kang, S. S.; Kim, Y. S.; Lee, J. H.; Seo, H. G.; Chang, K. C.; Kim, H. J., Tanshinone I effectively induces apoptosis in estrogen receptor-positive (MCF-7) and estrogen receptor-negative (MDA-MB-231) breast cancer cells. *International Journal of Oncology* **2008,** 33, (3), 485-491.

7. Maeda, H.; Wu, J.; Sawa, T.; Matsumura, Y.; Hori, K., Tumor vascular permeability and the EPR effect in macromolecular therapeutics: a review. *Journal of Controlled Release* **2000,** 65, (1-2), 271-284.

8. Mossmann, T., Rapid colorimetric assay for cellular growth and survival: application to proliferation and cytotoxicity assays, Immunol. *Methods* **1983,** 65, 55-58.

9. Kratz, F., Albumin as a drug carrier: design of prodrugs, drug conjugates and nanoparticles. *Journal of Controlled Release* **2008,** 132, (3), 171-183.

10. Chen, Y. H.; Tsai, C. Y.; Huang, P. Y.; Chang, M. Y.; Cheng, P. C.; Chou, C. H.; Chen, D. H.; Wang, C. R.; Shiau, A. L.; Wu, C. L., Methotrexate conjugated to gold nanoparticles inhibits tumor growth in a syngeneic lung tumor model. *Molecular Pharmaceutics* **2007,** 4, (5), 713-722.

11. Scholzen, T.; Gerdes, J., The Ki-67 protein: from the known and the unknown. *Journal of cellular physiology* **2000,** 182, (3), 311-322.

12. Bold, R. J.; Termuhlen, P. M.; McConkey, D. J., Apoptosis, cancer and cancer therapy. *Surgical Oncology-Oxford* **1997,** 6, (3), 133-142.

13. Mazumder, S.; Plesca, D.; Almasan, A., Caspase-3 activation is a critical determinant of genotoxic stress-induced apoptosis. *Methods Mol Biol* **2008,** 414, (1), 13-21.

14. Herr, I.; Debatin, K. M., Cellular stress response and apoptosis in cancer therapy. *Blood* **2001,** 98, (9), 2603.

15. Arends, M. J.; Morris, R. G.; Wyllie, A. H., Apoptosis. The role of the endonuclease. *The American journal of pathology* **1990,** 136, (3), 593.

16. Taylor, I. W.; Tattersall, M. H. N., Methotrexate cytotoxicity in cultured human leukemic cells studied by flow cytometry. *Cancer Research* **1981,** 41, (4), 1549.

17. Tsurusawa, M.; Niwa, M.; Katano, N.; Fujimoto, T., Flow cytometric analysis by bromodeoxyuridine/DNA assay of cell cycle perturbation of methotrexate-treated mouse L1210 leukemia cells. *Cancer Research* **1988,** 48, (15), 4288.

18. Li, J. C.; Kaminskas, E., Accumulation of DNA strand breaks and methotrexate cytotoxicity. *Proceedings of the National Academy of Sciences of the United States of America* **1984,** 81, (18), 5694.

19. Celtikci, B.; Lawrance, A. K.; Wu, Q.; Rozen, R., Methotrexate-induced apoptosis is enhanced by altered expression of methylenetetrahydrofolate reductase. *Anti-cancer drugs* **2009,** 20, (9), 787.

Chapter 6

In vivo toxicity assessment of BSA capped gold nanoparticles: Paving roads for future directions!!!

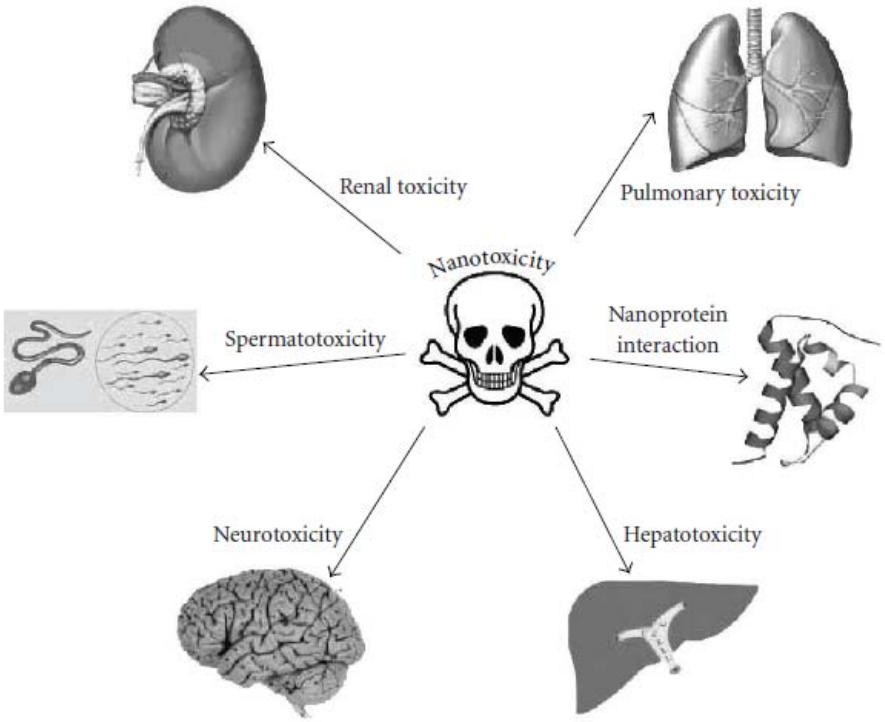

This chapter discusses the effect of BSA capped gold nanoparticles *in vivo* in Wistar rats. The results suggested no adverse behavioral, hematological, biochemical and histopathological changes being associated with the BSA capped gold nanoparticles at the investigated concentrations. Thus the use of BSA capped gold nanoparticles for drug delivery, bioimaging, etc. should be encouraged.

6.1 Introduction:

The development of nanoparticles for biomedical applications including medical imaging and drug delivery is currently undergoing a remarkable development[1-7]. The advantages of nanoparticle drug delivery systems are manifold: high stability, higher carrier carrying capacity, feasibility of incorporation of both hydrophilic and hydrophilic substances/molecules and compatibility with different administration routes (oral, intravenous, dermal, sub-cutaneous, intra-peritoneal and inhalation)[8, 9]. They can also be used for providing improved protection and reduced clearance for easily degraded or short half-life drugs, such as small peptides and nucleic acids, for a prolonged pharmacological effect[10, 11]. Using nanoparticles to deliver drug can also improve the tissue specificity due to selective uptake of nanoparticles in certain tissues especially tumor tissues. Tumor tissues have leaky endothelial wall which contribute significantly for the uptake of nanoparticles by a phenomenon known as "enhanced permeability and retention" (EPR) effect.

For nanomaterials to be truly useful in medicine, understanding their pharmacokinetics (PKs) and biodistribution — how and where the materials travel and accumulate — in living systems is essential. Chemical and physical properties of nanoparticles for e.g. size, surface charge and surface chemistry play important role in determining the PK and biodistribution[10, 12-17]. On the other hand, as a range of nanoparticles types and application increases, a detailed assessment of the factors that affects the biocompatibility and/or toxicity of nanoparticles are crucial for the safe development of the nanotechnology. Out of various nanoparticles system developed, gold nanoparticles are extraordinarily biocompatible and can serve as a promising candidate to address the size, shape and surface properties dependent biological responses to nanoparticles. Several publications have shown distributions of nanoparticles to multiple animal organs including liver, spleen, kidney, heart and brain. For instance, Hillyer and Albretcht have done a detailed quantitative and qualitative study of gastrointestinal uptake and tissue/organ distribution of 4, 10, 28 and 58 nm sized gold nanoparticles. They have found that maximum uptake of nanoparticles was of 4 nm gold nanoparticles after oral administration in mice[12]. Similarly, the biodistribution of various sized gold nanoparticles on intravenous administration in mice was investigated and revealed that 15, 50, 100 and 200 nm

mainly accumulated in liver, lung and spleen, whereas accumulation in various tissues of gold nanoparticle was a size dependent phenomenon. High amounts of 15 nm gold nanoparticles were found in all tissues including blood, liver, lung, spleen, kidney, and stomach and were able to pass the blood-brain barrier. On the other hand, little amount of 200 nm gold nanoparticles were found in blood, brain, stomach and pancreas[18]. Accordingly, in another study, rats intravenously injected with gold nanoparticles of different sizes (10, 50, 100 and 250 nm) show deposition of 10 nm gold nanoparticles in the various organs, whereas larger gold nanoparticles were detected only in blood, liver and spleen[13]. Studies of biodistribution of 1.4 nm and 18 nm gold nanoparticles that were administrated by intravenous injection or intratracheal instillation in rats showed that the 1.4 nm gold nanoparticles can get translocated through the air/blood barrier of the respiratory tract in significant amounts, whereas the 18 nm gold nanoparticles are almost completely trapped in the lungs. Moreover, evidences showed that the gold nanoparticles got modified during the translocation process and their biodistribution kinetics was different from that of intravenously injected 1.4 nm nanoparticles[19].

However, like two faces of a coin, gold nanoparticles too have a darker side. In a study by Chen *et al.*, toxicity of wide range of citrate-capped gold nanoparticles (3, 5, 8, 12, 17, 37, 50 and 100 nm) in mice was observed. They found that smallest sized (3 and 5 nm) and largest sized (50 and 100 nm) were not toxic while nanoparticles residing in the intermediate range (8-37 nm) toxic and showed lethal effects on mice inducing severe sickness, loss of appetite, weight loss, change in fur color and shorter average life span. Pathological examinations of the major organs of mice in diseased groups indicated an increase of Kupffer cells in liver and loss of structural integrity in the lungs and diffusion of white pulp in the spleen[8]. Interestingly, in the same study, the same nanoparticles were not toxic *in vitro* using HeLa cell lines. This study revealed a large discrepancy between the *in vitro* and *in vivo* results and hence highlights the notion that *in vitro* results should not be taken as a benchmark for the good predictions of their *in vivo* applications. In a similar study in mice by the same group, gold nanoparticles were found to induce antibody responses, indicating that factors other than cytotoxicity can complicate the *in vivo* applications of AuNPs[20]. Cho *et al.* have shown that on intravenous injection of 13

nm PEG-modified gold nanoparticles in rats leads to accumulation in liver and induce acute inflammation and apoptosis in it[21]. Similarly, in a study, 15 and 50 nm PEG coated gold nanoparticles altered the morphology of liver, spleen, kidney and lungs of rat after 24 h of injection[22].

Based on these observations, the interactions of nanomaterials with living systems should be studied for every system in detail and should not rely on extrapolations from previous studies. A systematic toxicity study must be carried out for each specific case under precise conditions, before imaging, diagnosis and therapeutic applications of gold nanoparticles can be carried out in human. As a part of this thesis work we have been able to project Au-BSA nanoparticles as a good candidate that meet most of the stipulations laid down for good drug delivery agents. However, we could also project Au-BSA-MTX as a potential drug formulations based on cell lines studies. The purpose of the work presented in this chapter was to evaluate the biological distribution and toxicity assessment of BSA capped gold nanoparticles upon oral administration in Wistar rats.

6.2 Experimental details:

6.2.1 Preparation of nanoparticles for oral administration:

Au-BSA nanoparticles were synthesized in bulk amount as described earlier (Chapter 2, section 2.2.1.ii). Further these were subjected to centrifugation to concentrate the nanoparticle solution to get 75 ppm, 150 ppm and 300 ppm concentration for oral dosing.

6.2.2 Sub-acute oral toxicity of BSA coated gold nanoparticles:

6.2.2.A *Study design:*

Toxicity studies were performed at Poona College of Pharmacy, Pune, India. Animal handling was performed according to Good Laboratory Practice. The sub-acute toxicity study was conducted as per OECD guideline no. 407 (OECD 407, 2001). The study protocol was approved by IAEC (Institutional Animal Ethical Committee) constituted as per guidelines of committee for the purpose of control and supervision of experiments on animals (CPCSEA), Government of India.

6.2.2.B *Test animals, housing and feeding condition:*

Wistar rats of either sex (140-180 g) were purchased from National Toxicology Centre, Pune, India. The animals were housed under standard conditions of temperature (24±1ºC), relative humidity (55±10%) and 12 h light/ dark cycles throughout the experiment. Animals had access to commercially available standard pellet diet and filtered water, *ad libitum*. Animals were acclimatized for one week prior to the initiation of treatment. During this acclimatization period, the health status of the rats was monitored daily.

6.2.2.C *Body weight of animals and food intake:*

Before administration of Au-BSA dispersion, the animals were weighed using a calibrated balance. The weight of the animals was recorded daily throughout the experimental period at fixed time. For recording the food consumption, weighed amount of standard rat food pellets (Pranav Agro Industries, Sangli, Maharashtra, India) was placed in the food tray of the cage. The unconsumed pellets were weighed and replaced with fresh pellets in each tray every day. The time of providing the feed was fixed throughout the study.

6.2.2.D *General observation:*

Throughout the study period, animals were observed in their cages daily for mortality and signs of any toxic effects. Effect of treatment on general health of the animals, body weight and behavior was also noted.

6.2.2.E *Dosing of gold nanoparticles to animals:*

Animals were randomly divided in four groups containing 5 male and 5 female rats per group. Three different doses were given to each group as shown in table 6.1. Distilled water was taken as a vehicle control. Vehicle control and Au-BSA were administered by oral route using a stainless steel feeding needle. Maximum permissible volume to be administered was limited to 2 mL. Au-BSA nanoparticles were redispersed in water and administered orally for 28 days at prefixed time daily.

6.2.2.F *Blood sampling and analysis:*

i) Haematology analysis:

At the end of the 28 day study period, the animals were fasted overnight. The following morning, each animal was anaesthetized using anaesthetic ether and blood

samples were collected from the retro orbital plexus of all the rats. Blood for haematology studies was collected into two sets of tubes. In one set of tubes, disodium EDTA (anti-coagulant) was present. A fully automatic hematology analyzer was used to measure the following parameters: Hematocrit (ht), haemoglobin (Hb), red blood corpuscles count (RBC), white blood corpuscles count (WBC) and differential leukocyte count (DLC). Erythrocyte sedimentation rate (ESR) was determined by Wintrobe's method.

Table 6.1: *Assignment of Wistar rats for 28 days oral toxicity studies.*

Group	***Test sample***	***Dose to animals***	***Male***	***Female***
A	Control	Vehicle (distilled water)	5	5
B	Low	75 ppm	5	5
C	Medium	150 ppm	5	5
D	High	300 ppm	5	5

ii) Biochemical analysis:

The serum was obtained by centrifugation of the whole blood at 3000 rpm for 15 min. Biochemical parameters viz, alkaline phosphatase (ALP), alanine aminotransferase (ALT), aspartate aminotransferase (AST), blood sugar level (BSL), creatinine, urea, total protein, albumin, bilirubin, cholesterol were assayed by semi automated clinical chemistry analyzer. The electrolytes (Na^+ and K^+) were analyzed using electrolyte analyzer.

6.2.2.G *Urine analysis:*

Urine samples were also collected at the end of the study period and analyzed for appearance, pH, glucose, protein, and blood.

6.2.2.H *Histopathological observations:*

The animal groups treated with Au-BSA and control were sacrificed at the end of study and the organs such as heart, kidney, liver, brain, lungs, stomach, intestines, pancreas, spleen, urinary bladder, testis, uterus and ovaries were rapidly dissected out,

washed in sterile phosphate buffered saline and carefully weighed on an analytical balance. The isolated organs were trimmed into small pieces and preserved in 10 % formalin for 24 h. The specimens were successively dehydrated with alcohol of 70, 80 and 100 % each for 1 h. Tissues were cleaned by treating with xylene each time for 1 h. Infiltration and impugnation was done by treating twice with paraffin wax each time for 1 h. Paraffin "L" shaped moulds were prepared. Specimens were cut in sections of 3-5 µm in thickness stained by hematoxyline-eosin. The sections were mounted by use of disterene phthalate xylene. Sections from all processed tissues of control and Au-BSA treated groups were examined under light microscope (Nikon coolpix camera mounted on a Nikon Eclipse 50i microscope, Japan).

6.2.2.I *Statistical analysis:*

Data of the body weight, food consumption, haematology and biochemistry values are presented as the mean ± SD. The P values were calculated in GraphPad Prism by one way ANOVA followed by Dunnett's test by comparing different groups (control group vs. treatment groups). The value of $P<0.05$ was considered to be statistically significant.

6.3 Results and Discussion:

Studies at organism level are more complex than a single cell; therefore extensive toxicological studies are required for the assessment of the safety of nanoparticles at the whole animal level, *in vivo*. These studies should include general health indicators such as behavioral abnormality, weight loss, percent of mortality and average life span[23]. Investigations should also include the nanoparticle intake, translocation to blood, biodistribution, accumulation, metabolism and excretion[19]. Till date, there is no systematic procedure that has given conclusive results about *in vivo* toxicity because different working groups have used different biosystems, a range of nanoparticle size and shape and diverse protective ligand shells. In spite of this perplexity, majority of toxicity studies favors "biocompatibility" of the gold nanoparticles. However, for any type of clinical application of gold nanoparticles, it is very important to know the biocompatibility and the fate of these nanoparticles. Therefore, the toxicity of the Au-BSA nanoparticles was investigated by carrying out sub-acute oral toxicity in Wistar rats.

In a 28 days sub-acute toxicity studies, rats were randomly assigned to four groups; one control and three test groups. In each group five males and five females were kept. Control group received water as a vehicle control while the three experimental groups received different concentrations of Au-BSA (75 ppm, 150 ppm and 300 ppm). The animals were observed daily for any signs of morbidity and mortality. Detailed physical examinations for signs of morbidity were conducted every week during the study period. It was observed that the animals fed with different concentrations of Au-BSA were healthy and no unusual changes in behavior or in locomotor activity, no ataxia and no signs of intoxication were observed during the study period of 28 days. No dose related changes in the motor activity were found. The eye examinations did not reveal any dose related eye abnormality. No mortality occurred during the study period.

Table 6.2: *Effect of Au-BSA nanoparticles on body weight of male rats during 28 days study period.*

Group	Animal Body Weight (g) Male		
	0^{th} day	**28^{th} day**	**Difference**
Control	136.75 ± 4.11	199.25 ± 17.35	62.5
Low (75 ppm)	144.75 ± 4.79	189.75 ± 5.38	45.0
Medium (150 ppm)	134.00 ± 10.55	182.00 ± 21.86	48.0
High (300 ppm)	150.75 ± 10.05	187.25 ± 24.13	36.5

Weight of the animals was monitored daily and all the animals showed normal weight gains during the study period. There was no statistically significant difference ($P>0.05$) in increase in body weight between the control group and experimental groups in both male and females (Table 6.2 and 6.3 respectively) indicating that different concentrations of Au-BSA did not alter the weight of animals. Monitoring of food intake of animals showed that at different concentrations of Au-BSA no effect

Table 6.3: *Effect of Au-BSA nanoparticles on body weight of female rats during 28 days study period.*

Group	Animal Body Weight (g) Female		
	0^{th} day	**28^{th} day**	**Difference**
Control	129.25 ± 6.5	158.00 ± 21.06	28.75
Low (75 ppm)	139.75 ± 5.6	180.25 ± 10.05	40.50
Medium (150 ppm)	124.25 ± 9.5	172.00 ± 14.63	47.75
High (300 ppm)	142.50 ± 5.5	176.25 ± 7.97	33.75

Table 6.4: *Effect of Au-BSA nanoparticles on food consumption of rats during 28 days study period.*

Group	Food Consumption (g/100 g of animal)			
	Male		Female	
	1^{st} day	**28^{th} day**	**1^{st} day**	**28^{th} day**
Control	12.44 ± 1.07	10.44 ± 1.34	12.06 ± 0.88	12.31 ± 0.69
Low (75 ppm)	12.5 ± 1.17	13.36 ± 0.78	11.88 ± 0.66	13.25 ± 0.79
Medium (150 ppm)	13.63 ± 0.78	11.19 ± 0.69	11.38 ± 1.13	11.38 ± 1.13
High (300 ppm)	12.50 ± 1.34	12.63 ± 0.78	12.63 ± 0.97	12.61 ± 0.65

on food consumption was observed as food consumption of the animals in the control and experimental groups was similar (Table 6.4).

One of the most common parameter to monitor while performing *in vivo* toxicity study is to examine the blood composition such as cell type and serum chemistry, after exposure to nanoparticles [24]. Here any change from the normal

Table 6.5: *Effect of Au-BSA nanoparticles on hematocrit level in rats after 28 days treatment.*

Group	Hematocrit (%) (Mean ± SD)	
	Male	**Female**
Control	44.7 ± 2.1	42.1 ± 1.1
Low (75 ppm)	43.1 ± 1.9	43.1 ± 1.4
Medium (150 ppm)	44.1 ± 1.9	35.4 ± 0.8
High (300 ppm)	41.7 ± 2.2	41.8 ± 1.8

Table 6.6: *Effect of Au-BSA nanoparticles on haemoglobin level in rats after 28 days treatment.*

Group	Haemoglobin (gm/dL) (Mean ± SD)	
	Male	**Female**
Control	15.1 ± 0.7	14.5 ± 0.6
Low (75 ppm)	14.6 ± 0.6	12.2 ± 0.2
Medium (150 ppm)	15.0 ± 0.6	15.2 ± 0.5
High (300 ppm)	14.4 ± 0.6	14.7 ± 0.6

condition (pre-exposure) i.e. either increase or decrease in blood constituents is considered to be due to toxicity of the nanoparticles on the animals. For haematological analysis, cell population, such as red and white blood cells or specific consideration of cells is considered during the studies. Haematological parameters viz; hematocrit (Table 6.5), haemoglobin concentration (Table 6.6), red blood corpuscles (RBC) count (Table 6.7), white blood corpuscles (WBC) count (Table 6.8) and differential leukocyte count (DLC) (Table 6.9 and 6.10) in both control and experimental groups were conducted. There was no significant difference ($P>0.05$)

Table 6.7: *Effect of Au-BSA nanoparticles on red blood corpuscles (RBC) count in rats after 28 days treatment.*

Group	RBC (million/cmm) (Mean ± SD)	
	Male	**Female**
Control	7.95 ± 0.27	7.29 ± 0.28
Low (75 ppm)	7.92 ± 0.55	6.23 ± 0.31
Medium (150 ppm)	7.98 ± 0.23	7.43 ± 0.70
High (300 ppm)	7.66 ± 0.46	7.49 ± 0.26

Table 6.8: *Effect of Au-BSA nanoparticles on white blood corpuscles (WBC) count in rats after 28 days treatment.*

Group	WBC (million/cmm) (Mean ± SD)	
	Male	**Female**
Control	11875 ± 2381	15575± 806
Low (75 ppm)	11625 ± 1630	9125 ± 1554
Medium (150 ppm)	8500 ± 3864	12200 ± 3581
High (300 ppm)	10275 ± 3801	9075 ± 2037

and all the values were found within the normal range with no difference between the control and experimental groups. Hematocrit value for female medium dose was decreased in comparison to the control but this was considered to be of no toxicological significance. White blood corpuscles count was also decreased in case of female low and high doses (75 ppm and 300 ppm respectively) in comparison to the control. However, the decreased level was considered to be of no toxicological

Table 6.9: *Effect of Au-BSA nanoparticles on differential leucocyte count (DLC) in male rats after 28 days treatment.*

Groups	Differential Leucocytes Count (%) (Mean ± SD) Male				
	Neutrophils	**Lymphocytes**	**Eosinophils**	**Monocytes**	**Basophils**
Control	19.0 ± 2.16	73.25 ± 2.5	2.75 ± 0.96	5.00 ± 0.8	0.00 ± 0.00
75 ppm	16.5 ± 5.20	76.25 ± 5.6	2.50 ± 1.29	4.75 ± 1.3	0.00 ± 0.00
150 ppm	13.5 ± 5.0	80.5 0± 5.3	1.75 ± 1.26	5.00 ± 0.8	0.00 ± 0.00
300 ppm	18.8 ± 6.19	74.00 ± 8.6	2.50 ± 1.29	4.25 ± 1.3	0.00 ± 0.00

Table 6.10: *Effect of A-BSA nanoparticles on differential leukocyte count (DLC) in female rats after 28 days treatment.*

Groups	Differential Leucocytes Count (%) (Mean ± SD) Female				
	Neutrophils	**Lymphocytes**	**Eosinophils**	**Monocytes**	**Basophils**
Control	22.75 ± 6.4	73.50 ± 1.2	2.35 ± 0.85	4.50 ± 1.3	0.00 ± 0.00
75 ppm	16.75 ± 1.7	76.25 ± 1.9	1.95 ± 1.15	5.25 ± 0.9	0.00 ± 0.00
150 ppm	11.25 ± 2.2	75.00 ± 0.8	1.75 ± 0.50	5.00 ± 0.8	0.00 ± 0.00
300 ppm	17.5 ± 3.1	73.50 ± 1.3	2.25 ± 1.15	3.50 ± 1.3	0.00 ± 0.00

significance (P>0.05). These results suggested that Au-BSA were non toxic as they did not affect the circulating red cells, nor hematopoiesis and leucopoiesis that could otherwise have caused haematological disorders[25]These results also indicated that the normal metabolism of the animals was not affected by the administration of Au-BSA nanoparticles to animals.

The biochemical tests such as basal sugar level analysis, urea analysis, creatinine level, total bilirubin and cholesterol level etc. were used for diagnosis of diseases of heart, liver, kidney, etc after Au-BSA nanoparticle treatment. The elevated levels indicate the occurrence of liver damage, ischemic heart disease, acute coronary syndromes, etc. Liver enzymes (aspartate aminotransferase (AST), alanine aminotransferase (ALT) and alkaline phosphatase (ALP)) are normally found within the cells of the liver and if the liver is injured or damaged, the liver enzymes levels increase due to the leaking of the enzymes in the blood. Serum ALT/AST has been used as an index to monitor liver pathology [26]. Serum ALP is a sensitive detector of intrahepatic and extrahepatic bile obstruction, presence of infiltrative diseases of the liver and all bone disease associated with osteoblastic activity (e.g., osteomalacia and rickets) [26].

Table 6.11: *Effect of Au-BSA nanoparticles on liver enzymes of male rats after 28 days treatment.*

Group	Liver Enzymes (Mean ± S.D.) Male		
	Aspartate aminotransferase (IU/L)	**Alanine aminotransferase (IU/L)**	**Alkaline phosphatase (IU/L)**
Control	250.25 ± 9.81	74.25 ± 9.82	600.50 ± 101.30
Low (75 ppm)	234.75 ± 16.11	62.50 ± 16.11	597.50 ± 262.90
Medium (150 ppm)	285.75 ± 9.47	73.50 ± 9.47	592.25 ± 156.40
High (300 ppm)	244.50 ± 4.92	80.75 ± 4.92	501.25 ± 54.35

Tests conducted for the presence of liver enzymes AST, ALT and ALP showed no significant difference (P>0.05) in control and experimental groups of both male and female rats (Table 6.11and 6.12). AST and ALT levels were decreased in case of low dose (75 ppm) in female rats. However, these decreased levels were considered to be of no toxicological significance in comparison to the respective

Table 6.12: *Effect of Au-BSA nanoparticles on liver enzymes of female rats after 28 days treatment.*

Group	Liver Enzymes (Mean ± S.D.) Female		
	Aspartate aminotransferase (IU/L)	**Alanine aminotransferase (IU/L)**	**Alkaline phosphatase (IU/L)**
Control	254.00 ± 31.19	82.25 ± 28.36	460.00 ± 110.00
Low (75 ppm)	185.00 ± 16.83	48.00 ± 5.75	381.25 ± 82.16
Medium (150 ppm)	271.00 ± 29.44	61.00 ± 7.26	466.50 ± 194.60
High (300 ppm)	231.25 ± 36.62	65.75 ± 11.87	362.50 ± 72.23

control group (P>0.05). This might suggest a non-toxic effect or absence of hepatocellular damage at the investigated concentration. Since no alteration in the level of ALP is observed it suggests no interference with the calcification and/or metabolic activities involving the liver.

Table 6.13: *Effect of Au-BSA nanoparticles on blood sugar level (BSL) in rats after 28 days treatment.*

Group	Blood Sugar Level (mg/dL) (Mean ± S.D.)	
	Male	**Female**
Control	70.50 ± 9.0	71.75 ± 11.6
Low (75 ppm)	68.00 ± 6.3	56.75 ± 18.6
Medium (150 ppmj)	67.25 ± 4.9	66.25 ± 4.3
High (300 ppm)	65.75 ± 3.9	66.75 ± 7.9

The levels of blood glucose were not significantly different (P>0.05) between the control and experimental groups of both male and female rats (Table 6.13).

Bilirubin is formed by the breakdown of hemoglobin in the liver, spleen and bone marrow [26]and an increase of it in tissue or serum leads to jaundice. A slight variation in bilirubin concentration is also an indicator of effects on hemoglobin metabolism. However, the level of plasma analytes, such as cholesterol and bilirubin determined showed no significant difference (P>0.05) between control and Au-BSA nanoparticles treated groups (Table 6.14).). Cholesterol levels were decreased in case of all the doses in male rats. However, these decreased levels were considered to be of no toxicological significance in comparison to the respective control group (P>0.05).

Table 6.14: *Effect of Au-BSA nanoparticles on bilirubin and cholesterol on rats after 28 days treatment.*

Groups	Male rats		Female rats	
	Bilirubin	Cholesterol	Bilirubin	Cholesterol
	(mg/dL) (Mean ± S.D.)			
Control	0.41 ± 0.07	69.25 ± 6.5	0.29 ± 0.06	62.00 ± 3.92
75 ppm	0.31 ± 0.06	55.75 ± 5.4	0.45 ± 0.04	58.50 ± 6.66
150 ppm	0.34 ± 0.08	55.00 ± 3.8	0.41 ± 0.05	63.00 ± 4.24
300 ppm	0.40 ± 0.05	46.25 ± 4.9	0.37 ± 0.11	51.75 ± 2.87

The levels of total protein and albumin were not significantly different (P>0.05) between the control and experimental groups of both male and female rats (Table 6.15). The kidney function tests (blood urea, creatinine, sodium and potassium) showed no significant difference (P>0.05) between the control and experimental groups of rats (Table 6.16 and 6.17). Feeding animals with different concentration of Au-BSA nanoparticles did not alter the functioning of the animal, indicating normal metabolism of the animals with respect to hematological and biochemical analysis.

Table 6.15: *Effect of Au-BSA nanoparticles on total protein and albumin on rats after 28 days treatment.*

Groups	Male rats		Female rats	
	Total Protein	Albumin	Total Protein	Albumin
	(mg/dL) (Mean ± S.D.)			
Control	8.22 ± 0.46	3.98 ± 0.48	7.85 ± 0.34	3.80 ± 0.29
75 ppm	8.22 ± 0.33	3.68 ± 0.22	7.25 ± 0.31	3.80 ± 0.32
150 ppm	7.42 ± 0.46	3.40 ± 0.37	8.38 ± 0.51	3.78 ± 0.25
300 ppm	7.55 ± 0.37	3.25 ± 0.26	7.93 ± 0.31	3.78 ± 0.17

Table 6.16*: Effect of Au-BSA nanoparticles on kidney function test of male rats after 28 days treatment.*

Groups	Kidney Function Test (Mean ± S.D.) Male			
	Urea (mg/dL)	Creatinine (mg/dL)	Na (mmol/L)	K (mmol/L)
Control	46.25 ± 3.50	0.48 ± 0.06	137.25 ± 2.99	4.98 ± 0.17
75 ppm	38.75 ± 4.11	0.41 ± 0.06	136.00 ± 2.94	4.85 ± 0.34
150 ppm	34.50 ± 2.65	0.49 ± 0.05	135.25 ± 0.96	5.25 ± 0.42
300 ppm	34.50 ± 3.42	0.47 ± 0.04	136.50 ± 3.11	5.05 ± 0.42

The urine samples of the male and female rats were collected over time. The pH of urine of both male and female rats in the control and the experimental group was alkaline. In case of protein analysis, traces of protein were found in the urine. It is known that occurrence of traces proteins is a normal finding in most of the animals. A higher concentration of proteins is considered abnormal which may be due to glomerular injury, defective tubular reabsorption etc. If the kidney functioning is

Table 6.17: *Effect of Au-BSA nanoparticles on kidney function test of female rats after 28 days treatment.*

Groups	Kidney Function Test (Mean ± S.D.) Female			
	Urea (mg/dL)	Creatinine (mg/dL)	Na (mmol/L)	K (mmol/L)
Control	33.75 ± 4.53	0.41± 0.03	138.00 ± 3.37	4.95 ± 0.17
75 ppm	39.50 ± 3.70	0.42 ± 0.07	139.00 ± 3.37	4.73 ± 0.28
150 ppm	46.50 ± 6.61	0.48 ± 0.05	137.00 ± 2.94	4.85 ± 0.26
300 ppm	39.00 ± 6.06	0.53 ± 0.05	136.75 ± 4.35	4.48 ± 0.26

normal, the glucose is reabsorbed by the renal tubules. No glucose was present in urine of both male and female rats of control and the experimental groups.

Another widely utilized *in vivo* test is the examination of histopathological changes that occurs in cells/tissues/organs after exposure to nanoparticles[24]. Histological examination was performed on tissues that have been fixed after sacrifice of the exposed animal and changes in the tissue and cell morphology were assessed using light microscopy. Some of the typical tissues examined after nanoparticles exposure include: liver, kidneys, spleen, lungs and heart[24, 27]. Histopathological studies were carried out to study the effect of Au-BSA nanoparticles on the vital organs. The individual organs were weighed and it was found that there was no significant difference ($P>0.05$) between the organ weight of control and treated groups (Table 6.18). The absence of any changes in various organs point out the fact that the Au-BSA nanoparticles did not induce any anomalous growth or inflammation of these organs which would otherwise have resulted in higher organ weight in the treated groups.

Table 6.18: *Effect of Au-BSA nanoparticles on organ weight of rats after 28 days treatment.*

Organs		Organ weight (g) (Mean ± S.D.)			
		Control	**75 ppm**	**150 ppm**	**300 ppm**
Heart		0.71 ± 0.04	0.72 ± 0.08	0.74 ± 0.13	0.71 ± 0.13
Kidney	**Left**	0.77 ± 0.09	0.73 ± 0.07	0.75± 0.12	0.73 ± 0.14
	Right	0.75 ± 0.09	0.80 ± 0.07	0.76 ± 0.10	0.75 ± 0.12
Liver		7.55 ± 0.43	6.96 ± 0.71	7.12 ± 0.61	7.73 ± 1.46
Lung (combined)		1.62 ± 0.46	1.80 ± 0.37	1.83 ± 0.23	1.65 ± 0.21
Pancreas		0.71 ± 0.14	0.92 ± 0.05	0.81 ± 0.27	0.64 ± 0.11
Spleen		1.16 ± 0.19	1.34 ± 0.34	1.08 ± 0.33	1.13 ± 0.34
Stomach		1.60 ± 0.08	1.62 ± 0.42	1.37 ± 0.17	1.60 ± 0.21
Intestine	**Large**	3.07 ± 0.33	3.11 ± 0.78	2.55 ± 0.62	2.30 ± 0.40
	Small	5.29 ± 0.62	5.57 ± 0.59	5.31 ± 1.16	6.19 ± 0.90
Brain		1.55 ± 0.24	1.73 ± 0.17	1.66 ± 0.24	1.47 ± 0.30
Urinary Bladder		0.12 ± 0.05	0.13 ± 0.03	0.12 ± 0.05	0.13 ± 0.11
Testis		1.17 ± 0.10	1.16 ± 0.12	1.29 ± 0.12	1.20 ± 0.07
Uterus		0.70 ± 0.12	0.61 ± 0.17	0.49 ± 0.25	0.54 ± 0.20
Ovaries		0.11 ± 0.02	0.10 ± 0.03	0.12 ± 0.02	0.11 ± 0.05

The histopathological findings of all the organs can be seen in Figure 6.1 to 6.11. Any structural changes in the organs are considered to be an indication for any sort of toxicity due to nanoparticles. The histopathology of all the organs are discussed below[28].The absence of any pathological change in organs point out the fact that the Au-BSA nanoparticles did not induce any toxicity in animals.

Heart: The section of the control heart showed normal myocardium. Same findings were observed for dose 50 ppm, 150 ppm and 300 ppm. No pigment deposits were seen in any groups. Thus there was no toxic effect of Au-BSA nanoparticles on the heart (Figure 6.1).

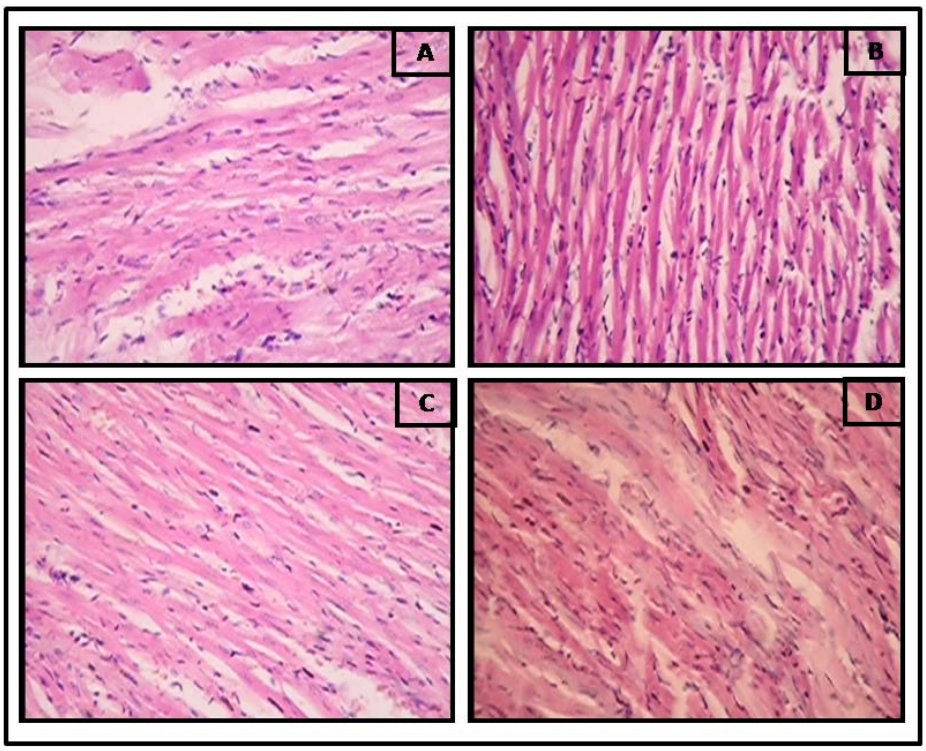

Figure 6.1: *Light photomicrograph of* ***heart*** *after 28 days of administration of Au-BSA nanoparticles by oral route at a dose of (a) control, (b) 75 ppm, (c) 150 ppm and (d) 300 ppm*

Kidney: The sections of the control rat showed normal renal cortex with normal appearing glomerular tubules and normal renal papilla. After the dose of Au-BSA nanoparticles, sections were showed renal cortex with normal appearing glomerular tubules and normal renal papilla. There were no pigment deposits in the tubules in the treated groups (Figure 6.2).

Liver: The sections of the control and the Au-BSA nanoparticles treated groups showed normal hepatic architecture. The hepatocytes in the control liver sample appeared normal and the portal tracts were also found to be normal. However, in all nanoparticles treated groups accumulation of nanoparticle was observed as reported in earlier literatures[12, 18, 22, 29]. Even then no inflammation was seen in the Au-BSA nanoparticles treated groups (Figure 6.3).

Lung: The sections from control animals showed normal alveolar architecture. No thickening of inter alveolar septa or cellular infiltrations were observed. The same histopathological findings were observed in Au-BSA nanoparticles treated groups (Figure 6.4).

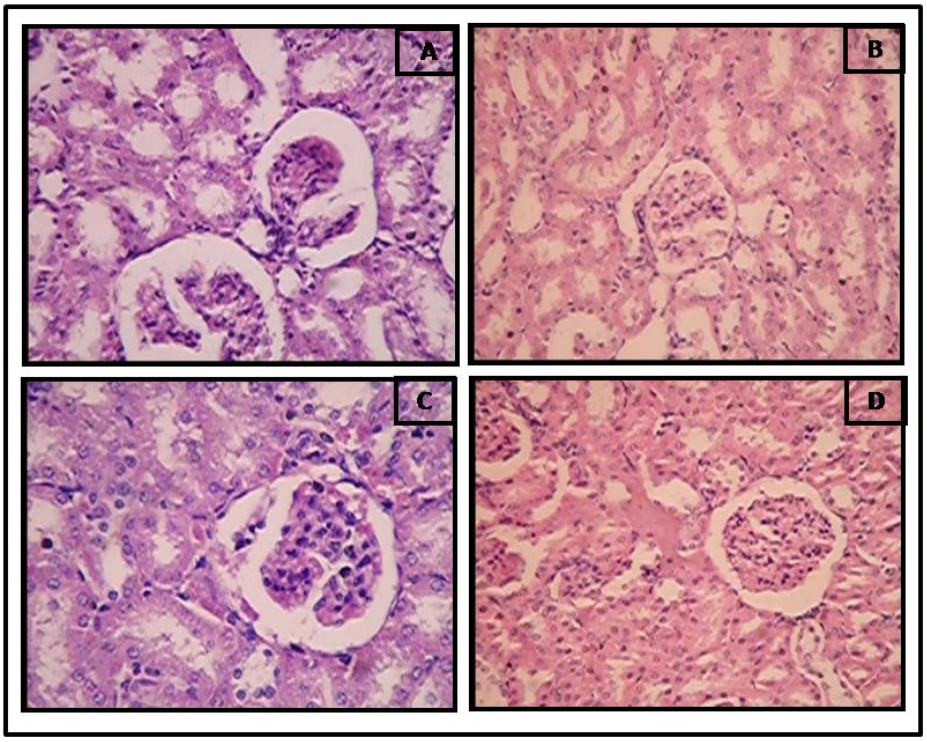

Figure 6.2: *Light photomicrograph of **kidney** after 28 days of administration of Au-BSA nanoparticles by oral route at a dose of (a) control, (b) 75 ppm, (c) 150 ppm and (d) 300 ppm.*

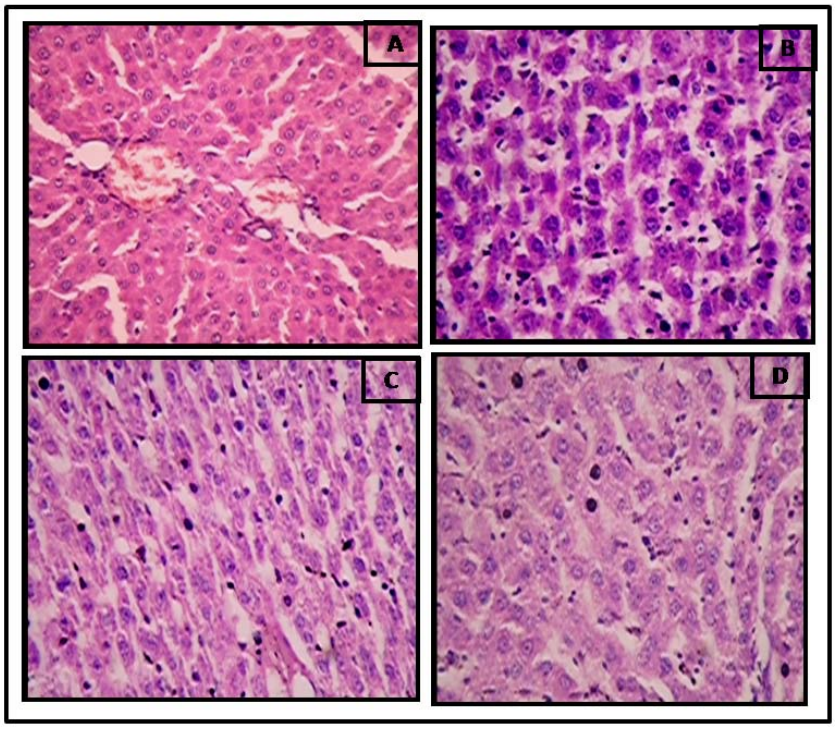

Figure 6.3: *Light photomicrograph of **liver** after 28 days of administration Au-BSA nanoparticles by oral route at a dose of (a) control, (b) 75 ppm, (c) 150 ppm and (d) 300 ppm.*

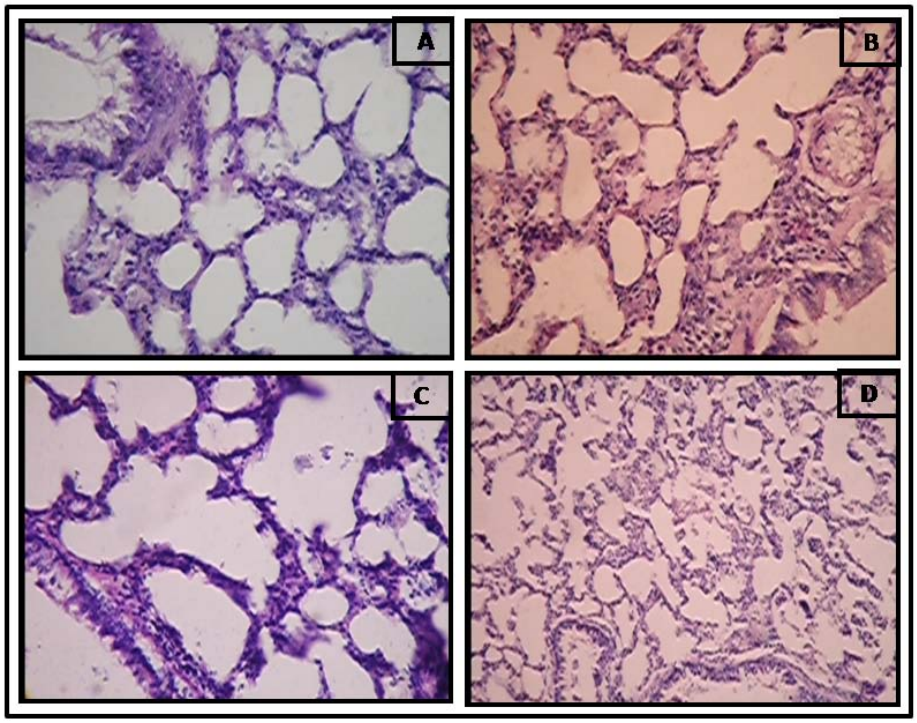

Figure 6.4: *Light photomicrograph of **lungs** after 28 days of administration of Au-BSA nanoparticles by oral route at a dose of (a) control, (b) 75 ppm, (c) 150 ppm and (d) 300 ppm*

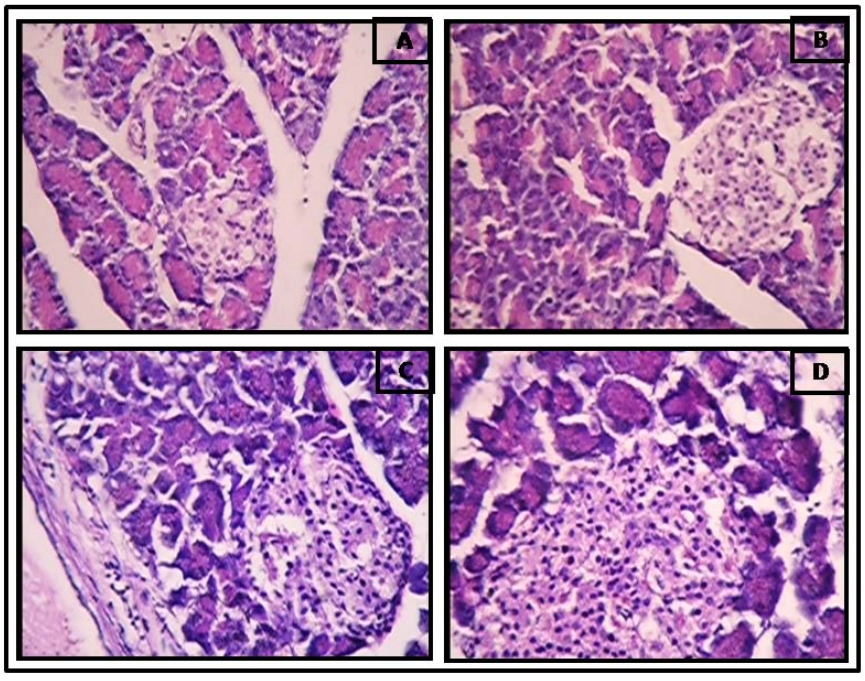

Figure 6.5: *Light photomicrograph of **pancreas** after 28 days of administration of Au-BSA nanoparticles by oral route at a dose of (a) control, (b) 75 ppm, (c) 150 ppm and (d) 300 ppm*

Pancreas: The sections from the control and the Au-BSA nanoparticles treated groups showed normal pancreatic architecture. Pancreatic cells were observed normal in all AuNPs treated groups (Figure 6.5).

Spleen: The two major functional zones of the spleen are the hematogenous red pulp and the lymphoid white pulp. The section from the control showed normal splenic architecture with normal red and white pulp. Same histopathology was observed with the Au-BSA nanoparticles treated groups (Figure 6.6)

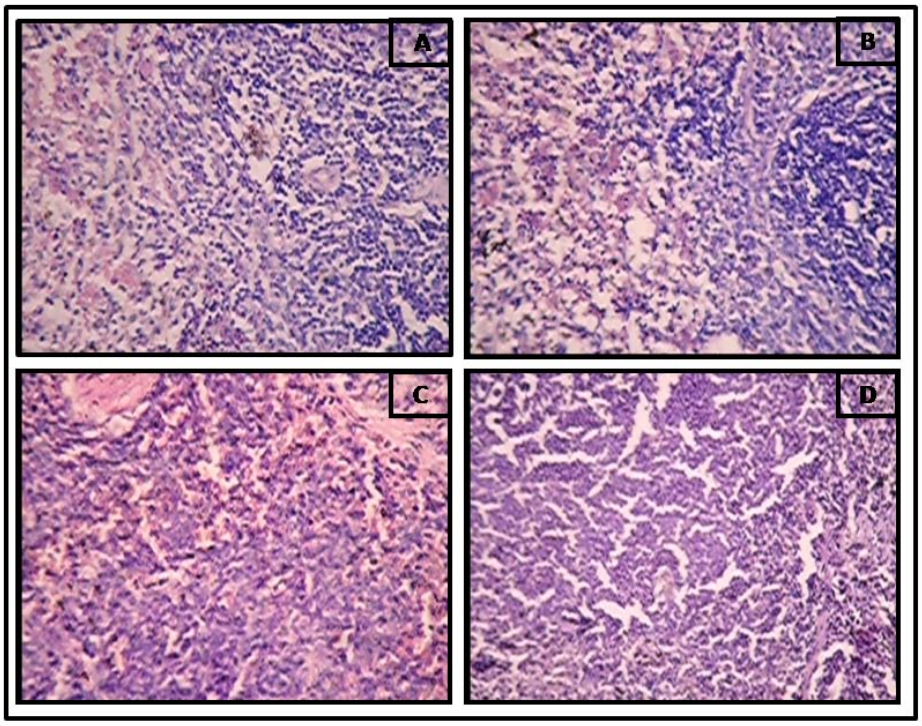

Figure 6.6: *Light photomicrograph of* ***spleen*** *after 28 days of administration of Au-BSA nanoparticles by oral route at a dose of (a) control, (b) 75 ppm, (c) 150 ppm and (d) 300 ppm*

Stomach: The most conspicuous tissue feature of the stomach is the thick glandular mucosa, packed with gastric glands which secrete digestive enzymes and acid. There were no pathological changes in the mucosal lining of the control as well as the Au-BSA nanoparticles treated groups. No inflammation was observed in the treated groups (Figure 6.7).

Intestines: There were no pathological changes in the mucosal lining of the small as well as large intestine in the control group. In the Au-BSA nanoparticles treated

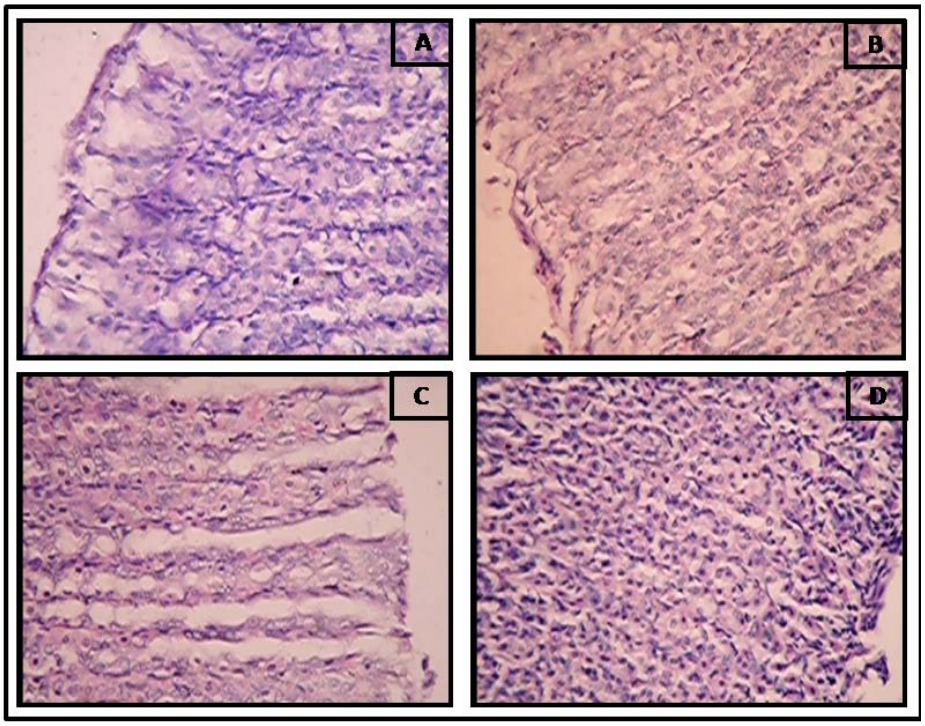

Figure 6.7: *Light photomicrograph of **stomach** after 28 days of administration of Au-BSA nanoparticles by oral route at a dose of (a) control, (b) 75 ppm, (c) 150 ppm and (d) 300 ppm*

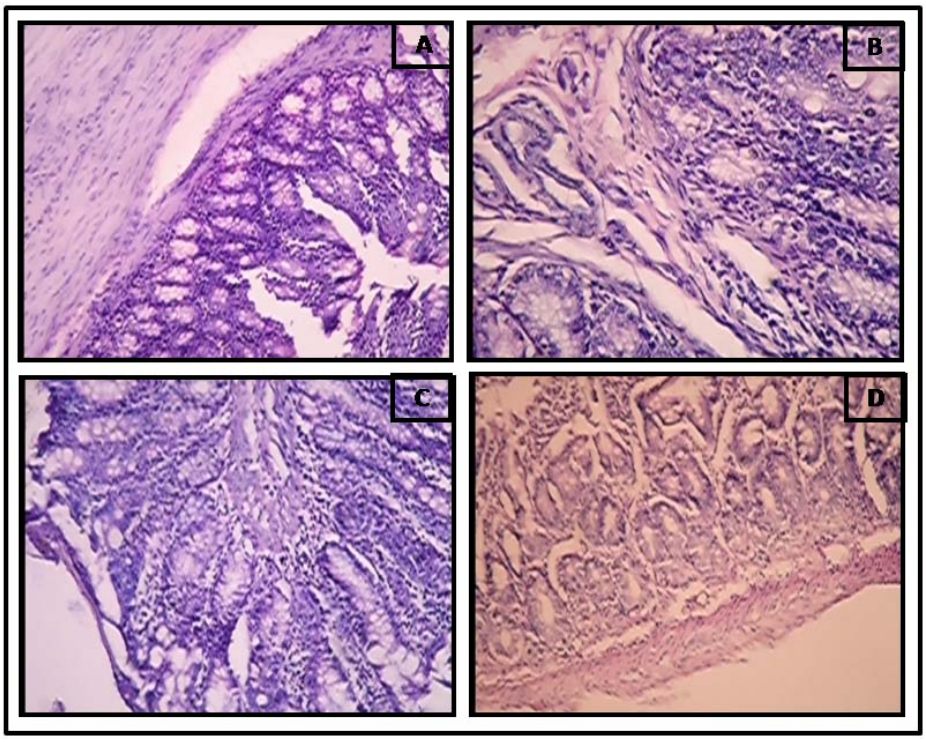

Figure 6.8: *Light photomicrograph of **intestine** after 28 days of administration of Au-BSA nanoparticles by oral route at a dose of (a) control, (b) 75 ppm, (c) 150 ppm and (d) 300 ppm*

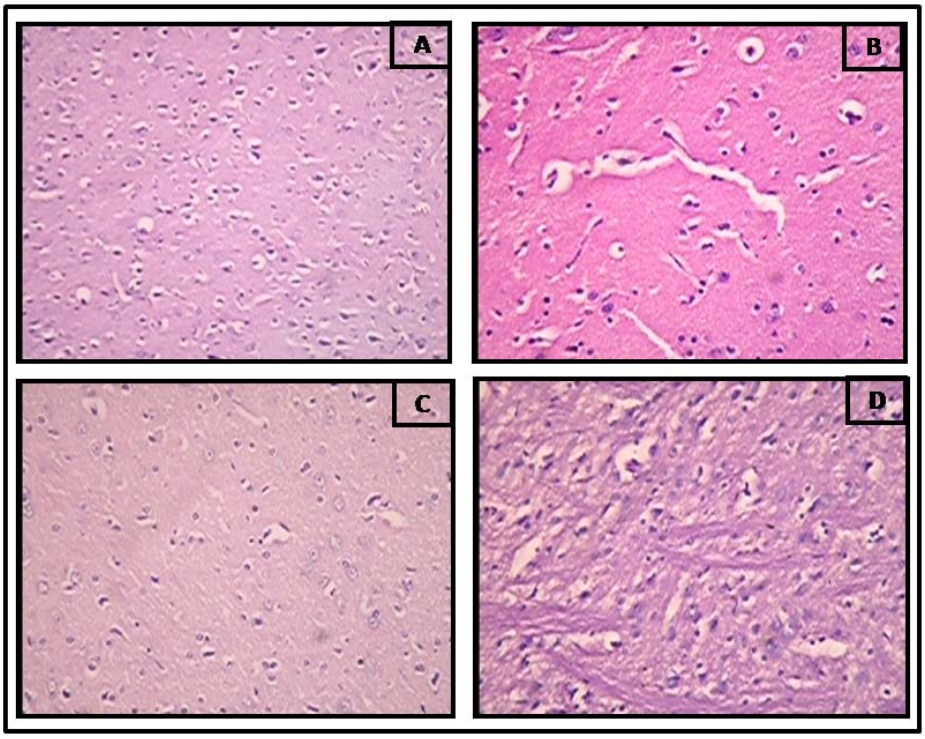

Figure 6.9: *Light photomicrograph of **brain** after 28 days of administration of Au-BSA nanoparticles by oral route at a dose of (a) control, (b) 75 ppm, (c) 150 ppm and (d) 300 ppm*

groups (50, 150, 300 ppm), no change was observed confirming no treatment related toxicity due to Au-BSA nanoparticles (Figure 6.8).

Brain: The Au-BSA nanoparticles treated sections from the brain showed normal neuronal as well as glial elements. No morphological alteration was noted in the brain samples (control and Au-BSA) treated animals (Figure 6.9).

Testis: The testis sections of the Au-BSA nanoparticles treated groups showed normal shape and size of seminiferous tubules with active spermatogenesis and maturation. The interstitium was normal. There was no pathological change observed in the Au-BSA nanoparticles treated group (Figure 6.10).

Ovaries: Histological examination of ovaries in the control and treated groups revealed different stages of follicular development. No abnormalities were observed in germinal epithelium, stages of follicular development, maturation and corpus luteum (Figure 6.11).

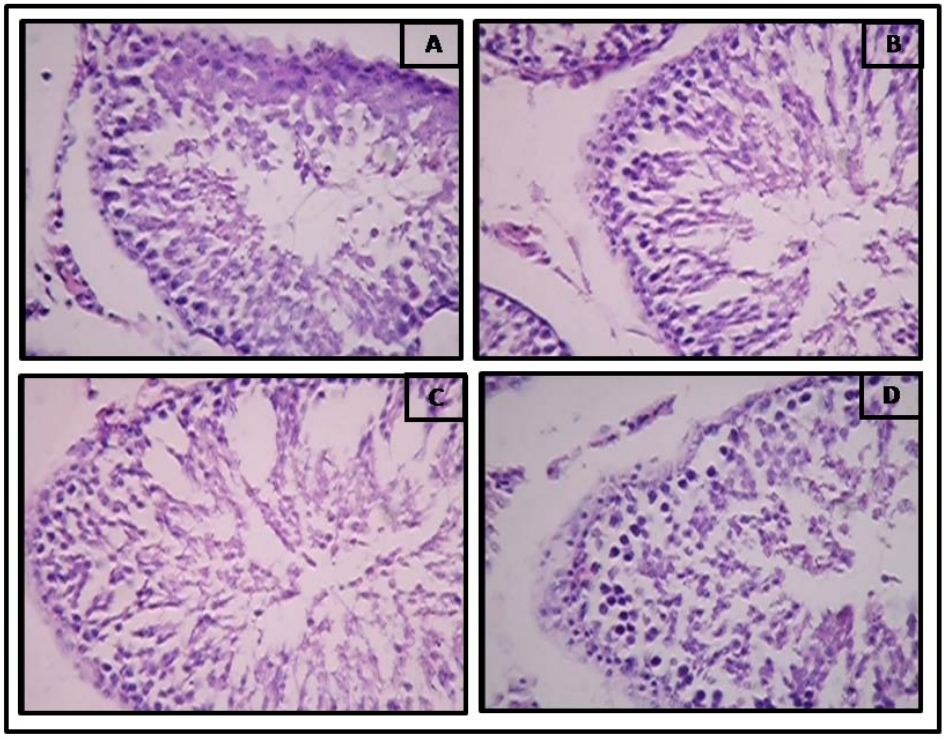

Figure 6.10: *Light photomicrograph of **testes** after 28 days of administration of Au-BSA nanoparticles by oral route at a dose of (a) control, (b) 75 ppm, (c) 150 ppm and (d) 300 ppm*

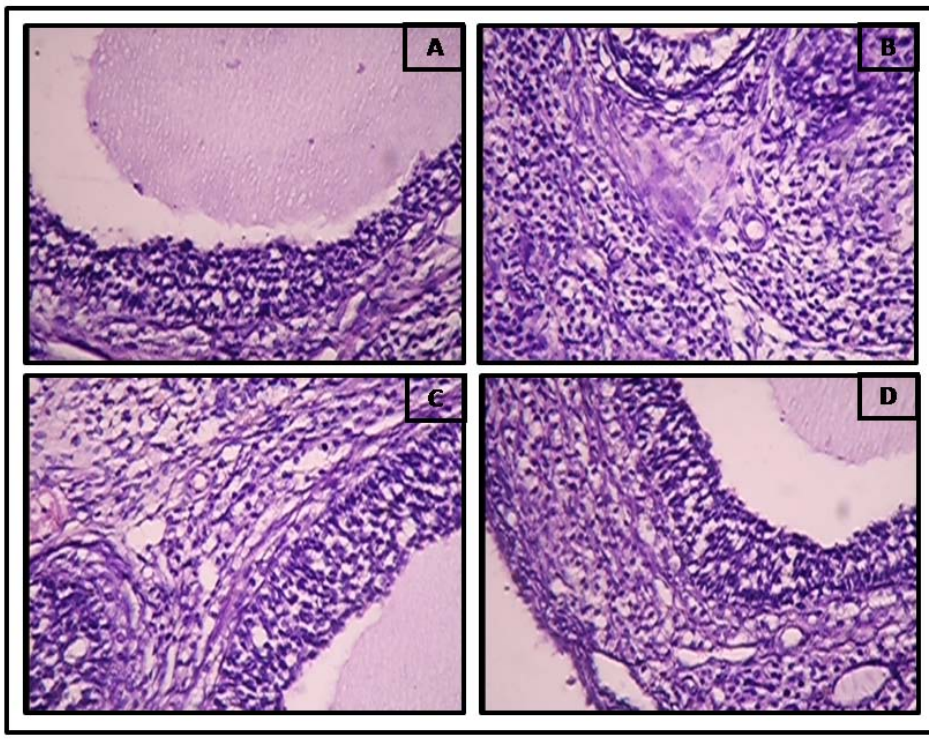

Figure 6.11: *Light photomicrograph of **ovary** after 28 days of administration of Au-BSA nanoparticles by oral route at a dose of (a) control, (b) 75 ppm, (c) 150 ppm and (d) 300 ppm*

6.4 Conclusion:

In our efforts to determine the possible use of BSA capped gold nanoparticles as carriers for drug delivery we have successfully evaluated the sub-acute oral toxicity of BSA capped gold nanoparticles. Animals treated with Au-BSA nanoparticles showed normal weight gain and food consumption during the study period. Au-BSA nanoparticles did not induce adverse alterations in biochemical and hematological parameters. Histopathological studies were performed to study the effect of Au-BSA on vital organs. There was no pathological difference in the control and Au-BSA treated group. However deposition of Au-BSA nanoparticles without any toxic effect was observed in the liver of all the nanoparticles administered groups. Our findings reveal that BSA reduced and capped gold nanoparticles did not cause any toxicity for a period of 28 day study period. Therefore BSA capped gold nanoparticles show promising potential for the safe use as a drug delivery system.

References:

1. Boisselier, E.; Astruc, D., Gold nanoparticles in nanomedicine: preparations, imaging, diagnostics, therapies and toxicity. *Chemical Society Reviews* **2009,** 38, (6), 1759-1782.

2. Niemeyer, C. M., Nanoparticles, proteins, and nucleic acids: biotechnology meets materials science. *Angewandte Chemie International Edition* **2001,** 40, (22), 4128-4158.

3. Salata, O. V., Applications of nanoparticles in biology and medicine. *Journal of Nanobiotechnology* **2004,** 2, (1), 3.

4. De, M.; Ghosh, P. S.; Rotello, V. M., Applications of nanoparticles in biology. *Advanced Materials* **2008,** 20, (22), 4225-4241.

5. Murphy, C. J.; Gole, A. M.; Stone, J. W.; Sisco, P. N.; Alkilany, A. M.; Goldsmith, E. C.; Baxter, S. C., Gold nanoparticles in biology: beyond toxicity to cellular imaging. *Acc. Chem. Res* **2008,** 41, (12), 1721-1730.

6. Alivisatos, P., The use of nanocrystals in biological detection. *Nature Biotechnology* **2003,** 22, (1), 47-52.

7. Rosi, N. L.; Mirkin, C. A., Nanostructures in biodiagnostics. *Chem. Rev* **2005,** 105, (4), 1547-1562.

8. Chen, Y. S.; Hung, Y. C.; Liau, I.; Huang, G. S., Assessment of the in vivo toxicity of gold nanoparticles. *Nanoscale Research Letters* **2009,** 4, (8), 858-864.

9. El-Ansary, A.; Al-Daihan, S., On the toxicity of therapeutically used nanoparticles: an overview. *Journal of Toxicology* **2009,** 2009.

10. Li, S. D.; Huang, L., Pharmacokinetics and biodistribution of nanoparticles. *Molecular pharmaceutics* **2008,** 5, (4), 496-504.

11. Kratz, F., Albumin as a drug carrier: design of prodrugs, drug conjugates and nanoparticles. *Journal of Controlled Release* **2008,** 132, (3), 171-183.

12. Hillyer, J. F.; Albrecht, R. M., Gastrointestinal persorption and tissue distribution of differently sized colloidal gold nanoparticles. *Journal of pharmaceutical sciences* **2001,** 90, (12), 1927-1936.

13. De Jong, W. H.; Hagens, W. I.; Krystek, P.; Burger, M. C.; Sips, A.; Geertsma, R. E., Particle size-dependent organ distribution of gold nanoparticles after intravenous administration. *Biomaterials* **2008,** 29, (12), 1912-1919.

14. Hoet, P. H. M.; Brüske-Hohlfeld, I.; Salata, O. V., Nanoparticles – known and unknown health risks. *Journal of Nanobiotechnology* **2004,** 2, (1), 12.

15. Dobrovolskaia, M. A.; Aggarwal, P.; Hall, J. B.; McNeil, S. E., Preclinical studies to understand nanoparticle interaction with the immune system and its potential effects on nanoparticle biodistribution. *Molecular pharmaceutics* **2008,** 5, (4), 487-495.

16. Alexis, F.; Pridgen, E.; Molnar, L. K.; Farokhzad, O. C., Factors affecting the clearance and biodistribution of polymeric nanoparticles. *Molecular pharmaceutics* **2008,** 5, (4), 505-515.

17. Balogh, L.; Nigavekar, S. S.; Nair, B. M.; Lesniak, W.; Zhang, C.; Sung, L. Y.; Kariapper, M. S. T.; El-Jawahri, A.; Llanes, M.; Bolton, B., Significant effect of size on the in vivo biodistribution of gold composite nanodevices in mouse tumor models. *Nanomedicine: Nanotechnology, Biology and Medicine* **2007,** 3, (4), 281-296.

18. Sonavane, G.; Tomoda, K.; Sano, A.; Ohshima, H.; Terada, H.; Makino, K., In vitro permeation of gold nanoparticles through rat skin and rat intestine: Effect of particle size. *Colloids and Surfaces B: Biointerfaces* **2008,** 65, (1), 1-10.

19. Semmler-Behnke, M.; Kreyling, W. G.; Lipka, J.; Fertsch, S.; Wenk, A.; Takenaka, S.; Schmid, G.; Brandau, W., Biodistribution of 1.4-and 18-nm gold particles in rats. *Small* **2008,** 4, (12), 2108-2111.

20. Huang, G. S.; Chen, Y. S.; Yeh, H. W., Measuring the flexibility of immunoglobulin by gold nanoparticles. *Nano Lett* **2006,** 6, (11), 2467-2471.

21. Cho, W.-S.; Cho, M.; Jeong, J.; Choi, M.; Cho, H.-Y.; Han, B. S.; Kim, S. H.; Kim, H. O.; Lim, Y. T.; Chung, B. H.; Jeong, J., Acute toxicity and pharmacokinetics of 13 nm-sized PEG-coated gold nanoparticles. *Toxicology and Applied Pharmacology* **2009,** 236, (1), 16-24.

22. Terentyuk, G. S.; Maslyakova, G. N.; Suleymanova, L. V.; Khlebtsov, B. N.; Kogan, B. Y.; Akchurin, G. G.; Shantrocha, A. V.; Maksimova, I. L.; Khlebtsov, N. G.; Tuchin, V. V., Circulation and distribution of gold nanoparticles and induced alterations of tissue morphology at intravenous particle delivery. *Journal of Biophotonics* **2009,** 2, (5), 292-302.

23. Alkilany, A.; Murphy, C., Toxicity and cellular uptake of gold nanoparticles: what we have learned so far? *Journal of Nanoparticle Research* 12, (7), 2313-2333.

24. Marquis, B. J.; Love, S. A.; Braun, K. L.; Haynes, C. L., Analytical methods to assess nanoparticle toxicity. *The Analyst* **2009,** 134, (3), 425-439.

25. Nisha, A.; Muthukumar, S. P.; Venkateswaran, G., Safety evaluation of arachidonic acid rich Mortierella alpina biomass in albino rats--A subchronic study. *Regulatory Toxicology and Pharmacology* **2009,** 53, (3), 186-194.

26. Edem, D. O.; Usoh, I. F., Biochemical changes in Wistar rats on oral doses of mistletoe (Loranthus micranthus). *American Journal of Pharmacology and Toxicology* **2009,** 4, (3), 94-97.

27. Patra, C. R.; Abdel Moneim, S. S.; Wang, E.; Dutta, S.; Patra, S.; Eshed, M.; Mukherjee, P.; Gedanken, A.; Shah, V. H.; Mukhopadhyay, D., In vivo toxicity studies of europium hydroxide nanorods in mice. *Toxicology and Applied Pharmacology* **2009,** 240, (1), 88-98.

28. Atlas, C., Functional Histology. A Text and Colour Atlas. *British Medical Journal* **1980,** 56, (654), 300.

29. Sonavane, G.; Tomoda, K.; Makino, K., Biodistribution of colloidal gold nanoparticles after intravenous administration: Effect of particle size. *Colloids and Surfaces B: Biointerfaces* **2008,** 66, (2), 274-280.

Chapter 7

CONCLUSIONS

This chapter contains conclusions of the salient features of the work described in this thesis and the scope for future potential developments in this field.

7.1 Summary of the thesis:

The work described in this thesis focuses on the development of a stable and biocompatible nanoparticle system that can be successfully used as a drug delivery agent. For this, we have chosen a protein, Bovine serum albumin, as a reducing and capping agent for the synthesis of nanoparticles. The synthetic mechanism is addressed by carrying out detailed UV-vis, fluorescence and cyclic voltammetry studies. Realizing the fact that a drug delivery system should be water soluble, highly stable against varying pH and salt concentrations, biocompatible and should cause minimum/negligible toxicity to normal healthy cells, these issues were addressed too.

Applications of nanoparticles in cancer therapy require them to be preferentially taken up by the cancer cells. To address this issue we have loaded a fluorophore molecule, texas red to the gold nanoparticles and performed the uptake studies. We obtained selective uptake of nanoparticles by glioma cells than normal fibroblast cells. Extension to this finding we loaded an anticancer drug Methotrexate to gold nanoparticles and checked its anticancer activity against breast cancer cell lines. The drug conjugated to BSA gold nanoparticles was found to evoke more toxicity to the cell lines than the equivalent concentration of drug alone. This nanoparticle system was further taken to demonstrate its applicability for drug delivery application *in vivo*. The biodistribution and toxicity studies establish that BSA reduced gold nanoparticles produced no treatment related toxicity in rats following oral administration.

7.2 Scope of future work:

Our studies showed that BSA capped gold nanoparticles are highly stable and can be easily functionalized to load any ligand on them. Taking advantage of this characteristic, this work can be extended by loading nanoparticles with drug molecule and performing an *in vivo* toxicity assessment of the drug molecule.

Annexure-I

LIST OF PUBLICATIONS

- A Green Synthetic Approach for the preparation of Silver Nanoparticle Dispersions and Hydrogels using Gellan Gum as a Capping and Reducing agent: Cellular Uptake and Cytotoxicity Studies. Sheetal Dhar, **Priyanka Murawala**, Anjali Shiras, Varsha Pokharkar, and B. L. V. Prasad. **(Communicated)**
- Role of Capping Molecule: BSA Mediated Specific Uptake of Gold Nanoparticles and Gold Clusters by Cancerous Cells over Normal Cells. **Priyanka Murawala,** A. Tirmale, A. Shiras, T. Pradeep and B. L. V. Prasad. **(Manuscript under preparation)**
- BSA capped Gold Nanoparticles: Effective carrier of anticancer drug Methotrexate and its application on MCF-7 breast cancer cells. **Priyanka Murawala**, A. Tirmale, A. Shiras, and B. L. V. Prasad. **(Manuscript under preparation)**
- *In situ* synthesis of water dispersible bovine serum capped gold and silver nanoparticles and their cytocompatibility studies. **Priyanka Murawala**, S. M. Phadnis, R. R. Bhonde, and B. L. V. Prasad, **Colloids and Surfaces B: Biointerfaces** (2009) 73, 224-228.